Photon emission and quantum transport in nanoplasmonic cavities

Quentin Schaeverbeke

Thesis presented for the degree of Doctor of Philosophy

From Université de Bordeaux
and Universidad del País Vasco

Ecole doctorale Sciences Physiques et de l'Ingénieur - UBX
Lasers, Matière, Nanosciences
Escuela de Máster y Doctorado - UPV/EHU
Fisica de materiales

Photon emission and quantum transport in nanoplasmonic cavities

Quentin SCHAEVERBEKE

Under the supervision of:

Fabio PISTOLESI
Thomas FREDERIKSEN
Rémi AVRILLER

Defended in September 2020 before the jury:

Dvira SEGAL	University of Toronto	Referee
Benoît DOUÇOT	Sorbonne Université	Referee
Guillaume SCHULL	Université de Strasbourg	Examiner
Javier AIZPURUA	Universidad del País Vasco	Examiner
Jérôme CAYSSOL	Université de Bordeaux	Jury president

Abstract

English

The study of light–matter interaction has drawn through the years more and more interest. With the improvement of the techniques used for building electromagnetic cavities, it is now possible to couple cavities with nanocircuits merging the fields of quantum optics and nanoelectronics. Not only that, but some experiments also reported the possibility to use a scanning tunneling microscope as a plasmonic cavity coupled with electronic transport.

In this thesis a theoretical framework is proposed, based on mesoscopic quantum electrodynamics, for studying the coupling between electronic transport in a molecular junction and the electromagnetic field of a cavity. This thesis focuses on the sequential tunneling regime for the electrons and use density matrix approach. This allows to derive the master equation as well as a computational scheme to compute electronic current and the photon statistic when it is not possible to obtain analytical results.

First, a single–level model for the molecule in the junction is studied. Indeed the electronic current induces a fluctuation of the charge on the molecule that couples with the electromagnetic field in the cavity. The investigations on this system are done in the experimentally relevant limit of large damping rate κ for the cavity mode and arbitrary strong light–matter coupling strength. This model shows the equivalence between the electron–photon coupling for a single level and the electron–phonon coupling that has long been studied in nanoelectronics known as the Franck–Condon principle. The current–voltage characteristics show steps, each separated by the energy of a photon, as the electron tunneling dissipate some energy in the cavity mode. In this work a formula has been derived for the electronic current taking into account the damping of the cavity. This allows to show that the width of the current's steps are controlled by κ rather than the temperature. The single-level junction shows interesting light–emission regimes. At large bias voltage this theory predicts strong photon bunching of the order κ/Γ where Γ is the electronic tunneling rate. However, at the first inelastic threshold the theory predicts current–driven non–classical light emission from the single–level junction. Finally the investigation of the effect of a strong external drive of the cavity on the electronic current shows a quantization of the current that is linked to the Franck–Condon effect.

Finally the theory is applied to a double–level model for the molecular junction inspired by quantum optics. In this scenario, the cavity mode couples to the electronic transition between the two states of the molecule. The effect of the charge fluctuations for each single electronic level is neglected. Therefore the coupling is a dipolar coupling in this case. The focus is mainly on the weak coupling regime. The electronic current shows the Rabi splitting due to the hybridization of the cavity mode and the molecule. Electronic tunneling can occur into these hybridized states and is responsible for light emission in the cavity in a

single tunneling process. Light antibunching is seen in the weak coupling regime since our model predicts that only single photon emission is possible during a tunneling event in this case. Though the intermediate coupling regime is only briefly treated, the strong coupling regime is shown to be similar to two independent single level.

Keywords: quantum transport, nanophotonics, plasmonics

Spanish

El estudio de las interacciones entre luz y materia ha atraído un interés creciente a lo largo de los años. La mejora de las técnicas de fabricación de las cavidades electromagnéticas permite hoy conjugar las cavidades con nanocircuitos, combinando así los campos de la óptica cuántica y de la nanoelectrónica. Se añade a eso la posibilidad de usar un microscopio con efecto túnel a modo de cavidad plasmónica combinada con el transporte electrónico que fue demostrado en numerosas experiencias.

Esa tesis propone un cuadro teórico basado en la electrodinámica mesoscópica, permitiendo el estudio de la combinación del transporte electrónico dentro de una unión molecular con el campo electromagnético de una cavidad. El foco se centra en el régimen túnel secuencial de los electrones, a cual está apto el uso de la matriz densidad para los cálculos. Ese régimen permite establecer ecuaciones claves que rigen el desarrollo temporal de la matriz densidad, tal como un esquema de cálculo numérico de la corriente electrónica y de la estadística de los fotones en la cavidad cuando no es posible obtener un resultado analítico.

Primero se estudia un modelo de un solo nivel electrónico para la molécula. En efecto, la existencia de una corriente electrónica significa que la carga en la molécula fluctúa y esa fluctuación se combina con el campo electromagnético de la cavidad. El estudio de ese sistema se hace en el limite, experimentalmente pertinente, del ratio alto de la amortiguación κ del modo de la cavidad y del acoplo luz–materia arbitrariamente alto. Ese modelo demuestra la equivalencia del acoplo electrón–fotón para un nivel electrónico y el acoplo electrón–fonón que se ha estudiado desde hace mucho tiempo en el campo de la nanoelectrónica bajo el nombre del principio de Franck–Condon. La característica corriente–tensión del circuito hace aparecer una evolución de escalones, cada uno separado por la energía de un fotón. Eso corresponde a una disipación de energía por parte de los electrones al modo de la cavidad durante el proceso de transporte. En ese trabajo se derivó una ecuación para la corriente electrónica que toma en cuenta el efecto de la amortiguación de la cavidad. Esto demuestra que la anchura de los saltos en la corriente está controlada por κ más que por la temperatura. El modelo de un solo nivel muestra también regímenes inesperados de emisión de luz. En el límite de voltaje alto entre los electrodos de la unión molecular, la teoría predice una agrupación («bunching») de los fotones emitidos dentro de la cavidad. La correlación entre dos fotones emitidos alcanza un valor del orden de κ/Γ donde Γ es el ratio de tunelamiento de los electrones. Sin embargo, en el primer umbral de transferencia inelástica esa teoría

predice una emisión de luz no-clásica provocada por la corriente electrónica. Por fin, el estudio del impacto de una fuerte excitación externa del modo de la cavidad muestra también una cuantización de la corriente relacionada al efecto Franck–Condon.

Finalmente, la teoría desarrollada en esta tesis está aplicada también a una unión molecular de dos niveles electrónicos inspirada de la óptica cuántica. En ese escenario el modo de la cavidad está acoplado con la transición electrónica entre dos orbitales moleculares. El efecto de fluctuaciones de carga en cada orbital no se tiene en cuenta. Entonces en ese marco el acoplo es solo dipolar. Se centra la atención principalmente en el régimen del acoplo débil. La corriente electrónica muestra la huella de oscilaciones de Rabi como resultado de la hibridación del modo de la cavidad con la molécula. El transporte de electrones se puede ocurrir mediante estos estados híbridos. Entonces el traslado de un único electrón es responsable de la emisión de un fotón en la cavidad. Se observa el desagrupamiento («anti-bunching») de la luz emitida. Aunque el régimen de acoplo intermedio es solamente tratado en breve, el régimen de acoplo fuerte muestra que es muy similar a la combinación de dos niveles electrónicos independientes acoplado al modo de la cavidad.

Palabras claves: transporte cuántico, nanofotónica, plasmónica

French

L'étude de l'interaction entre la lumière et la matière n'a cessé de susciter un intérêt croissant au fil des années. L'amélioration des techniques de fabrication des cavités électromagnétiques permet aujourd'hui de coupler ces cavités à des nanocircuits, se faisant, combinant les champs de l'optique quantique et de la nanoélectronique. À cela s'ajoute enfin la démonstration expérimentale de la possibilité d'utiliser un microscope à effet tunnel comme cavité plasmonique couplée au transport électronique.

Cette thèse propose un cadre théorique basé sur l'électrodynamique quantique en cavité, permettant l'étude du couplage entre le transport électronique dans une jonction moléculaire et le champ électromagnétique d'une cavité. L'attention est portée sur le régime de transfert tunnel séquentiel des électrons, auquel est adapté l'utilisation les calculs basés sur l'usage de la matrice densité. Ce régime permet d'établir les equations maîtresses régissant l'évolution temporelle de la matrice densité, ainsi qu'un schéma de calcul numérique du courant électronique et des propriétés statistiques des photons dans la cavité quand il n'est pas possible d'obtenir un résultat analytique.

Dans un premier temps, l'attention est portée sur un modele de jonction moléculaire à une orbitale. En effet, l'existence d'un courant électronique signifie que la charge de la molécule fluctue et cette fluctuation se couple au champ électromagnétique de la cavité. L'étude de ce premier système est faite dans le régime, expérimentalement pertinent, de fort taux d'amortissement $\kappa \geq k_B T$ du mode de la cavité et de couplage lumière–matière arbitrairement élevé. Ce modèle met en évidence l'équivalence du couplage électron–photon et du cou-

plage électron–phonon pour un unique niveau électronique. Ce couplage électron–phonon est étudié depuis longtemps en nanoélectronique sous le nom de principe Franck–Condon. La caractéristique courant–tension du circuit fait apparaitre une évolution par paliers ou seuils inelastiques, chacun séparé par l'énergie d'un photon. Ce phénomène correspond à une dissipation d'énergie, par émission de photons dans la cavité, médiée par le courant électronique. Pour cette étude, une formule du courant électronique prenant en compte l'effet de l'amortissement de la cavité (facteur de qualité $Q \approx 10$) a été dérivée. Cela a permis de montrer que la largeur des sauts du courant est contrôlée par κ plutôt que la température. Ce modèle démontre la possibilité d'obtenir divers régimes d'émission de lumière par passage de courant au sein de la jonction. Pour une importante différence de potentiel entre les électrodes de la jonction, cette théorie prédît un important groupement («bunching») des photons émis dans la cavité. La fonction de corrélation de deux photons à temps égaux $g^{(2)}(0)$ atteint alors une valeur de l'ordre de κ/Γ, où Γ est le taux de transfert tunnel des électrons. En revanche, au premier seuil de transfert inélastique des électrons, cette théorie prédît une émission de lumière non–classique provoquée par le courant électronique moléculaire à un niveau (la jonction se comporte alors comme une source à un photon). Enfin, nous avons montré qu'en présence d'une source de voltage dépendant du temps appliqué à la cavité, le courant dc présente des paliers analogues à ceux obtenus dans le régime Franck–Condon.

La théorie développée dans cette thèse est ensuite appliquée à une jonction moléculaire à deux niveaux électroniques. Dans ce scénario, le mode de la cavité se couple à la transition électronique entre les deux orbitales moléculaires. L'effet des fluctuations des charges de chaque orbitale est négligé. Dans ce cadre, nous avons étudié le cas d'un couplage cavité-molécule de type dipolaire électrique. L'attention est portée principalement sur le régime de couplage faible entre le dipole de la molécule et le mode de la cavité. Le courant électronique montre l'empreinte des oscillations de Rabi provenant de l'hybridation du mode de la cavité et de la molécule. Le transfert d'électrons peut se produire au travers des états hybridés. On observe alors que le transfert d'un unique électron est responsable de l'émission d'un photon dans la cavité. Les photons émis dans la cavité sont ainsi dégroupés («anti-bunching»). Bien que le régime de couplage modéré soit seulement brièvement traité, le régime de couplage fort, quant à lui, se montre très similaire au couplage de deux niveaux électroniques indépendants avec le mode de la cavité.

Mots-clefs: transport quantique, nano-photonique, plasmonique

Acknowledgements

I would like to thank my supervisors Rémi Avriller, Thomas Frederiksen and Fabio Pistolesi for the opportunity they gave recruiting me, for their patience and discussions.

I also would like to thank Guillaume Schull for his attempt to gather experimentalists and theoreticians in the topic of STM light emission. For being very open to discussions, to share his knowledge and finally for his advice and comments about our work.

I thank the members of the jury for their attentive reading, interesting remarks and very insightful discussions.

Thank you.

Contents

Chapter 1

Introduction

1.1 Light–matter interaction

We have known since the 19th century that electrons are sensitive to electromagnetic fields. It is the Lorentz force that is responsible for electronic motion. It was also demonstrated that light is electromagnetic waves and therefore electrons and light were shown to interact in the photovoltaic effect discovered by E. Becquerel in 1839 [1]. Another example of light-matter interaction was shown by R. Hertz in 1887 in the photoelectric effect, where he showed that electrons can be extracted from a metal under light irradiation. Since then more examples of light-matter interactions have been demonstrated in chemistry with photocatalysis [2], in biological phenomena such as photosynthesis [3] or retinal photoreception [4].

Light–matter interactions have found some technological uses with the design of solar cells using the photovoltaic effect [5] or lasers for example [6]. Physicists have put a lot of efforts in understanding light-matter interactions from a fundamental point of view as well as the use that can be made of it in engineering. In fact the photoelectric effect described by R. Hertz found a theoretical explanation in 1905 in the famous work of A. Einstein [7]. This is a corner stone in the understanding of the nature of light since A. Einstein made use of the principle of quantification previously used by M. Planck to explain the black-body spectrum. Hence the notion of light particles, later on called photons, was introduced. This discovery led to the development of quantum mechanics and the study the quantum nature of light lead to the field known today as quantum optics.

1.2 Cavity Quantum Electrodynamics

In order to study light–matter interaction between an atom or a molecule and an electric field, physicists placed the object to study between two conducting plates. This is what is called a cavity. As the cavity gives some boundaries that limits the volume in which the electric field exists, this results in a discrete spectrum of the field. The study of the phenomena linked to the discretization of the cavity's modes is called Cavity

Quantum Electrodynamics (cavity-QED).

There are three types of phenomena involved in cavity QED. The modification of the spontaneous emission rate of an atom resonant with a cavity mode known as Purcell effect. The modification of the atom's energy levels known as Lamb shift. And finally, the oscillatory energy exchange between the atom and a cavity mode showing a pure quantum behaviour known as Rabi oscillations. The first two phenomena mentioned can be observed in the weak coupling regime but the Rabi oscillations require and define the strong coupling regime, that is when the coupling intensity overcomes the dissipation rates in the system. In other words, from the experimental point of view, the strong coupling regime is achieved when the Rabi oscillations are measurable.

The Purcell effect was the first of the three to be observed [8] and its observation started the field of cavity QED. It corresponds to the enhancement of the atomic spontaneous light emission rate by the factor $f = 3Q\lambda^3/4\pi^2 n^3 V$ when placed in a cavity, where λ is the wavelength, Q the quality factor of the cavity, n the refractive index and V the mode volume of the cavity. As the light emission rate of the atom is proportional to the density of modes of the electric field, the fact that the cavity's geometry concentrates a mode in its volume can result in the enhancement of the light emission rate of the atom when the cavity and the atomic transition are tuned. The enhancement factor is roughly given by the quality factor Q of the cavity. On the contrary, if the cavity and the atomic transition are not tuned, the light emission is suppressed since there is no mode available for the atom to relax its energy.

The shift of the atomic energies has been studied from a theoretical point of view [9–11] but very few experiments have been realised [12] as the measurements are limited to a particular contribution resulting from a single wave vector $\mathbf{k}$ in a planar geometry. Finally, the Rabi oscillations [13] have been studied theoretically using the Jaynes–Cummings model [14] and demonstrated in various experiments [15–18].

The Rabi oscillations are the manifestation of the interaction between the dipolar momentum of a two-level quantum dot μ and the electric field of the cavity which gives a coupling strength $\Lambda = \mu E_{zpm}$, where E_{zpm} is the zero point motion of the electromagnetic field. When Λ overcomes the dissipation of the cavity or the atom spontaneous emission rate, the Rabi oscillations can be measured by observing the splitted peak in the optical spectrum of the cavity. This defines the strong coupling regime. Several experiments have used the strong couplings between atoms and the electric field of a cavity [19–21] allowing to explore the quantum nature of light and matter, but only few have managed to strongly couple a single atom to the cavity field. This was done for the first time building the micromaser [22]. A particular interest of the micromaser is its ability to generate sub-Poissonian distribution of photons and therefore purely quantum fields in the cavity.

Recently, the capability to fabricate a source of photons with specified statistics has received great interest. This is mainly due to quantum cryptography requiring the design of single photon sources and therefore

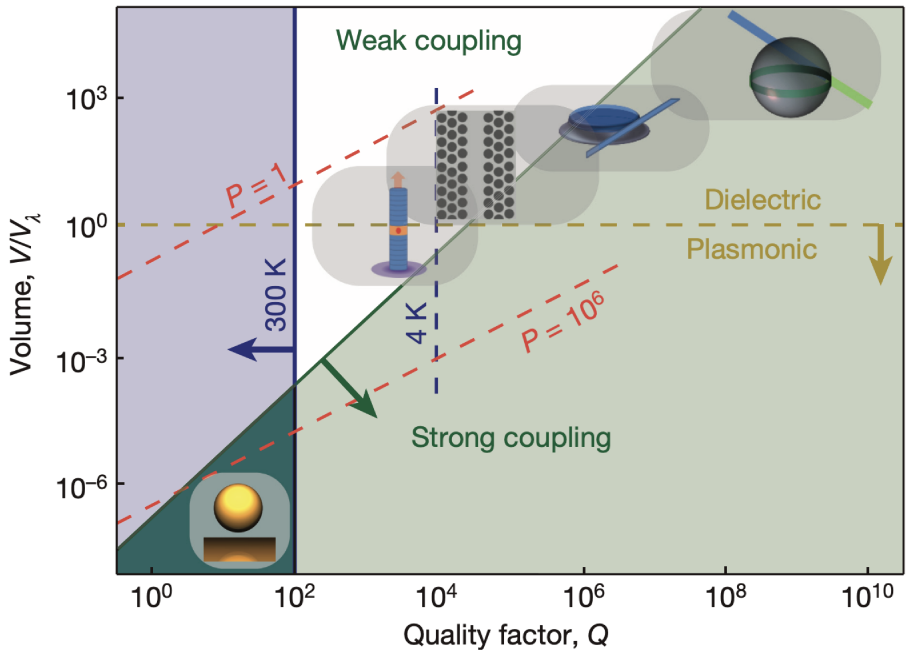

Figure 1.1: Coupling regime achieved for various type of cavities. The mode effective volume V/V_λ ($V_\lambda \sim (\lambda/n)^3$) is plotted against the cavity quality factor Q. The green region shows the strong coupling regime. The icons depicts some types of cavities, from right to left: whispering gallery spheres, microdisks, photonic crystals, micropillars and gold nanoparticles. Extracted from Ref. [29].

a lot of efforts have been put in the design of cavities strongly coupled to a single quantum dot. In their efforts to design strongly coupled cavities, physicists have explored various setups and geometries. To name a few examples cavities have been engineered using whispering gallery spheres [23], microdisks [24], photonic crystals [25] or micropillars [26,27]. The various types of cavities and their corresponding parameter regimes (effective volume against quality factor) are shown in Fig. 1.1. However getting to the strong coupling regime for a single quantum dot have remained a challenge [28].

From the nature of the coupling $\Lambda = \mu E_{zpm}$ we see that the coupling strength depends on two quantities. First the dot dipolar momentum, which is intrinsic to the molecule or atom we are considering and does not come from the specific design of the electromagnetic cavity. The second quantity of interest is the field zero-point quantum fluctuation's intensity. The field intensity corresponds to how well the cavity concentrate the electric field and this depends on the wavelength of the field and the volume of the cavity since $E_{zpm} = \sqrt{\hbar\omega_c/\mathcal{V}\epsilon_0}$, where ω_c is the cavity frequency, ϵ_0 the vacuum electric permittivity and $\mathcal{V}$ is the volume of the cavity. There are three limitations to the reduction of the size of the cavity. The first one is the difficulty to build the cavity due to technical limitations. The second one is that the smaller the cavity becomes, the bigger the loss rate κ gets and therefore it becomes harder to measure the

Rabi oscillations since they are perturbed by the cavity's electromagnetic environment. Finally optical cavities are limited to a size of hundreds of nanometers since the wavelength we want to select is given by the distance between the boundaries of the cavity.

1.3 Mesoscopic Quantum Electrodynamics

Strong coupling with a single quantum dot has mostly been realised for microcavities [13, 30–33]. At the same time nanoelectronics has also known progresses allowing for the fabrication of a wide variety of nanocircuits and the understanding of electron's dynamics. This led to the design of quantum dots with a discrete energy spectrum comparable to artificial atoms. Physicists were able to show, studying the electronic current, how the strong confinement of the electrons in a nanojunction leads to current quantization analogous to what was observed for a waveguide [34–36]. A few examples of quantum dots have been realised with carbon nanotubes [37], semiconducting nanowires [38] or self-assembled quantum dots [39].

At first the nanocircuits build for nanoelectronics experiments were studied based on dc current measurement, but it was quickly realised that the response of the circuit to microwave excitation was interesting for fundamental purpose but also for the engineering of quantum information devices. Therefore physicists start to study photo-assisted tunneling of electrons [40]. The fabrication of nanocircuits and the control of the electronic current offered by nanoelectronics give the missing tool for the fabrication of a single photon source. Indeed there are two major ingredients to gather for the use of a single photon source in quantum information. The ability to generate a small number of photons that was shown by strongly interacting microwave cavities with a quantum dots, and the ability to control the photon source which should be given by nanoelectronics. Hence nanoelectronics and quantum optics have merged in a field called Mesoscopic QED. Since then nanocircuits embedded in microwave cavities have been used to further study electronic transport thanks to photonic spectroscopic tools and to mimic Cavity-QED by trying to engineer ways to strongly coupled an artificial two level system to a microwave cavity. This includes carbon nanotubes [41–45], quantum dots using the coupling to the charge degree of freedom [46–49], and Josephson junctions [50–52].

1.4 Plasmonic cavities

We have seen so far that strong coupling between the cavity electromagnetic field and a two level system was achievable in microwave cavities with a real atom [13, 30–33] or using a nanocircuit [41–52] such as a double quantum dot junction for example. However, theoretically, if we manage to reduce the size of the cavity, we also increase the coupling and we could hope to overcome the increase of the loss rate. This has

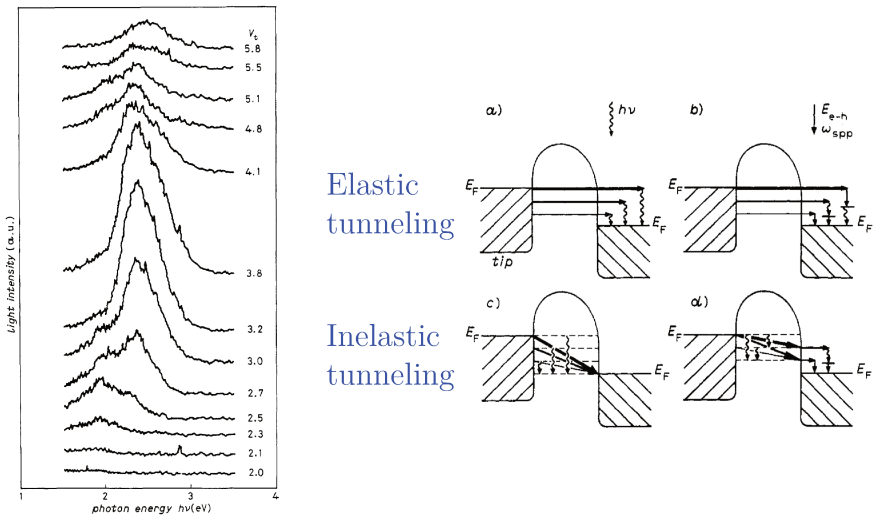

Figure 1.2: First light emission measurement from an STM junction. (a), (b) Schematic representation of the elastic tunneling processes in the STM junction. (c), (d) Schematic representation of the inelastic tunneling processes in the STM junction responsible for light emission. Reproduced from Ref. [53].

been another path that was explored to reach strong coupling. In fact instead of using standard optical cavities, the idea to use metallic nanostructures and surface plasmons to mimic the behaviour of a standard cavity at sub-wavelength scales emerged.

Plasmons are collective oscillation of electrons at an interface [54]. They allow for a very intense concentration of an electric field at the nanoscale at optical wavelengths and therefore overcome the diffraction limit as well as the need for a very controlled cavity (large Q and small temperature). However until recently strong coupling was only achieved thanks to superradiance due to a collective excitation of identical quantum emitters inside the cavity. Plasmonic cavities have been designed using gold particles [55] or silver nanorods and nanoprisms [56, 57] as plasmonic cavitities in interaction with J-aggregate as quantum emitters, showing the possibility to use plasmon polaritons even at room temperature to achieve strong coupling. More recently some experiments have even showed single molecule strong coupling using gold nanoparticles [29] or silver bowtie structure [58] as plasmonic cavities. Therefore showing how plasmonic cavities are promising for the design of quantum information devices. However in the case of plasmonic cavities at this point remains the question on how to control the light emission for their use as single photon sources for example. Considering their size, one could think that electronic transport can be considered between the metallic particles constituting the cavity. Interestingly, in parallel to the development of nanophotonics and plasmonic cavities, physicists have shown light emission from Scanning Tunneling Microscope (STM) experiments. The first report of light emission in an STM experiment was shown in 1989 by Gimzewski [53]. Fig. 1.2 shows reproduction of the first light

emission measurement done in [53]. Of course the STM tip and substrate being metallic structures, surface plasmons can propagate at their surfaces and we understand the STM junction acts as a plasmonic cavity in which the electronic current can be at the origin of the light emission. Further experiments have been realised using STM junction as plasmonic cavities in interaction with a molecule [59–70]. Fig. 1.3 shows a few examples of experiments extracted from the literature coupling molecules to the plasmonic field of an STM junction.

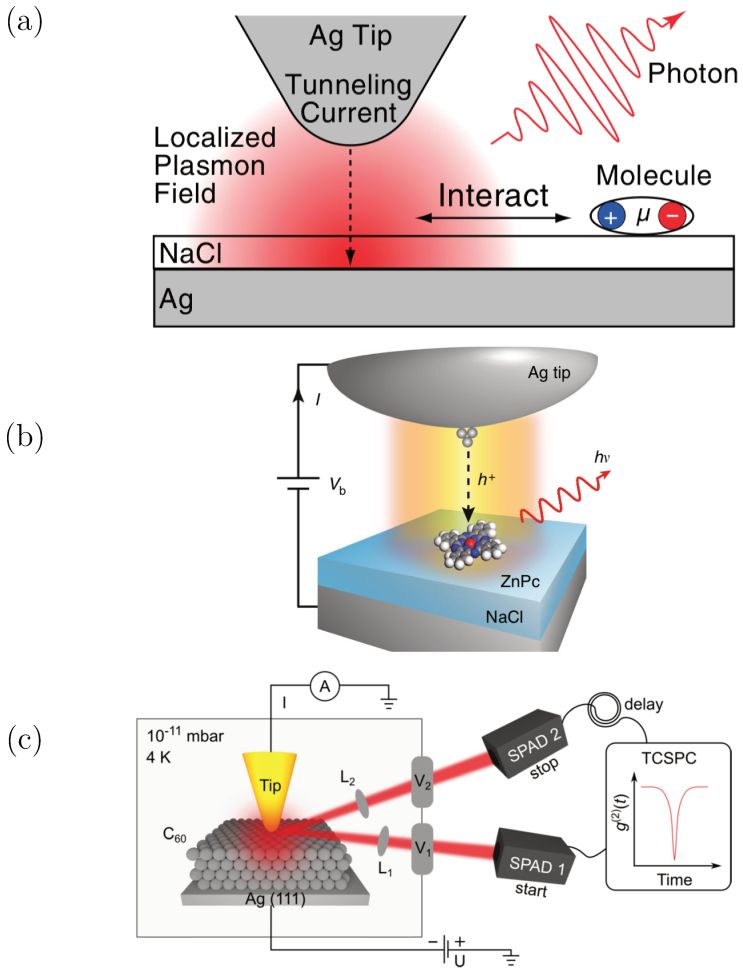

Figure 1.3: Examples of molecular coupling with the plasmonic field from an STM junction. (a) A plasmonic field is generated in the STM junction and a molecule outside of the junction interacts with the field. Reproduced from [71]. (b) Light emission from a single molecule in an STM junction. Reproduced from [72]. (c) Light emission from layers of C_{60} in an STM junction. Reproduced from Ref. [73].

An interesting feature with these techniques is that the high spatial resolution of the STM allows to study the variation of the light emission depending on the part of the molecule that is probed by the STM tip. Also, these techniques allow to mix current measurement with optical measurement. To this day the exact process of light emission is still

under discussion when an emitter is placed in the STM junction in this community and theoretical studies are still lacking though single photon emission was already shown to be possible [64, 72].

1.5 Outline of the thesis

The first objective of this thesis is to find a theoretical model for electronic transport through a two molecular orbitals coupled to the field of an electromagnetic cavity. Since the Jaynes–Cummings model used in quantum optics does not account for charge fluctuation of the molecule. Of course one has to extend the Hilbert space to take into account the state in which the molecule as a double occupancy or no occupancy at all [74,75]. However this is not enough since it neglects a crucial coupling term that called the monopolar coupling in the following. This coupling exists even for a single molecular orbital. Hence in chapter 2 the derivation of the Hamiltonian is discussed focusing on the interaction terms that arise between the electric field and the molecular orbitals.

As mentioned above, the electronic transport modifies how the molecule and the field of the electromagnetic cavity interact. First the current in a molecular junction in which only a single electronic level is involved is studied in chapter 3. In this chapter the theoretical framework for the derivation of the current and other physical quantities is introduced. This work is based on master and rate equations approach using the Born-Markov approximation. This relies on the weak tunneling rates between the electronic leads and the molecule, however the coupling between the molecular orbitals and the cavity's field is treated nonperturbatively. An important advantage of this theoretical approach is that it allows to treat correctly the strong damping of the plasmonic mode of the cavity and its effect on the electronic current.

As it will be shown, light can be emitted thanks to the coupling to a single electronic level molecular junction. In chapter 4 the different regimes of emitted light depending on the parameters of the system are explored. Mainly the coupling strength. The second-order correlation function of the emitted light shows that the single level molecular junction can act as a single photon source and analytical predictions using the rate equation approach are found.

This results are to be compared with the case of the two electronic level molecular junction in chapter 5.

Finally, a summary and an outlook are presented in chapter 6

Chapter 2

Discussion on the model Hamiltonian

The interaction between a molecule or an atom and an electric field has been studied for a very long time [19, 20, 76]. Classical as well as purely quantum approaches have been used. In this work we are interested in a pure quantum approach. Compared to a semi-classical approach, the purely quantum one is known to describe well the spontaneous as well as stimulated emission of an excited molecule and also allows for the interpretation in term of photons [14, 20]. So far, the interaction between an atom and an electric field is well known in fields such as cavity-QED, leading for example to the well known Jaynes–Cummings Hamiltonian [14, 77]. But, as light emitted from a scanning tunneling microscope (STM) was observed [78], came the idea to study the coupling between a molecular junction and the electric field of a cavity. In the STM setup, the molecular junction is made of the STM and a molecule placed between the STM tip and a substrate, and it interacts with the electric field that exists between the STM tip and the substrate [64–70], mimicking cavity QED experiments. So far, some processes have been proposed to explain the light emission [28, 68, 79–82], however a clear consensus is still missing in this field. In this chapter we introduce the Hamiltonian describing the coupling between a molecule, electronic leads and an electric field, discuss the various type of interaction involved and the importance of each terms regarding one another.

2.1 Model Hamiltonian of the electron–photon interaction

The following derivation of the Hamiltonian is based on the work of A. Cottet, T. Kontos and B. Doucot [83]. The system to be described consists in a molecule inside an STM junction. This molecule interacts with the electric field inside the junction and the tip and the substrate acting as electronic leads. The nanocircuit, where electron tunneling occurs, is modelled by a set of charges $\mathcal{Q}$. These charges interact with the electromagnetic field of the cavity $\{E, B\}$, where E is the electric field

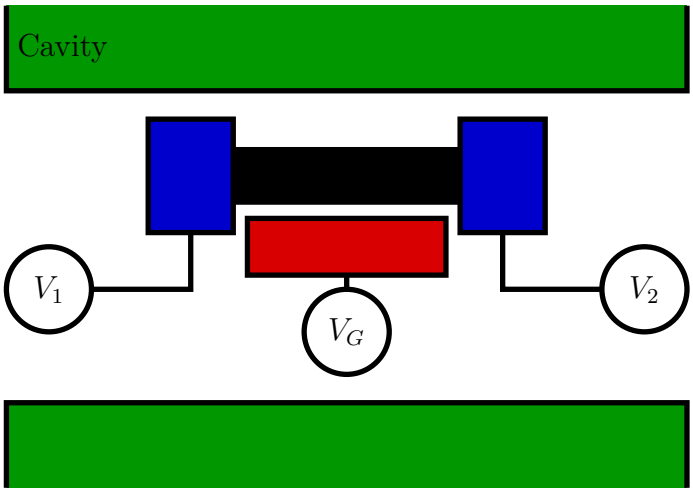

Figure 2.1: Generic scheme of a nanocircuit made of a nanoconductor (black) connected to fermionic reservoirs (blue) and electrostatic gates (red) inside a cavity (green).

and B is the magnetic field. The cavity, gate electrodes, and effective plasmonic reservoirs are taken into account as a set of boundary conditions whether the charge Q or the potential V is kept fixed. These ensembles are called $\mathcal{F}$ and $\mathcal{B}$, respectively. They are represented by green or blue elements in Fig. 2.1.

The STM junction is a special case of the typical system considered by Cottet et al [83]. Since the cavity is composed by the electronic reservoirs, its charge is not constant and it is, therefore, an element of $\mathcal{B}$. We call α a particle in $\mathcal{Q}$, so that the charge distribution in the circuit can be written $\rho(r,t) = \sum_\alpha e_\alpha \delta(r - r_\alpha)$ and the current distribution $j = \sum_\alpha e_\alpha \dot{r}_\alpha \delta(r - r_\alpha)$, where r is a position in space and e_α is the charge of α.

A field F is decomposed following the Hodge decomposition into a part with no rotational $F_\perp$, a part with no divergence $F_\parallel$ and a part with no rotational nor divergence F_{harm}, so that $F = F_\perp + F_\parallel + F_{\text{harm}}$. We also call U and A the scalar potential and vector fields such that $E = -\nabla U - \partial_t A$ and $B = \nabla \times A$. From Maxwell's equations in the Coulomb gauge $\nabla \cdot A = 0$, we find that

$$\nabla \cdot E_\parallel = \rho/\epsilon_0, \tag{2.1}$$

which translate onto U as

$$\Delta U = \rho/\epsilon_0. \tag{2.2}$$

We decompose this Laplace equation into two static problems. One corresponding to an homogeneous problem that describes the empty cavity,

$$\Delta \phi_{\text{harm}}(r) = 0, \tag{2.3}$$

with the boundary conditions

$$\int_{S_i} \nabla \phi_{\text{harm}}(r) \cdot n_i d^2 r = -Q_i, i \in \mathcal{F}, \tag{2.4}$$

$$\phi_{\text{harm}}(r) = V_i, \quad i \in \mathcal{B}, \tag{2.5}$$

where S_i is the surface of the object i, n_i is the outgoing unit length vector perpendicular to S_i. The second static problem in the decomposition corresponds to the description of the charge distribution of the circuit inside the cavity. It reads

$$\Delta G(r, r') = -\delta(r - r')/\epsilon_0, \tag{2.6}$$

with the boundary conditions

$$\int_{S_i} \nabla_r G(r, r').n_i d^2 r = 0, i \in \mathcal{F} \tag{2.7}$$

$$G_(r, r') = 0, i \in \mathcal{B} \quad \text{and} \quad r \in S_i. \tag{2.8}$$

This ensures that

$$E_{\text{harm}}(r) = -\nabla \phi_{\text{harm}} \tag{2.9}$$

$$E_{\parallel}(r, t) = -\nabla U_{\parallel} = -\int \nabla_r G(r, r')\rho(r', t)d^3 r'. \tag{2.10}$$

This leaves us with $E_\perp$ and B being determined by the potential vector A

$$E_\perp = -\partial_t A \tag{2.11}$$

$$B = \nabla \times A, \tag{2.12}$$

where A follows propagation equation

$$\Delta A - \frac{1}{c^2}\partial_t^2 A = -\mu_0 j_\perp. \tag{2.13}$$

The quantized Hamiltonian resulting from this field is [83]

$$H = H_{\text{A}} + \frac{1}{2}\sum_\alpha e_\alpha U_{\parallel}(q_\alpha) + \sum_\alpha e_\alpha \phi_{\text{harm}}(q_\alpha), \tag{2.14}$$

where $p_\alpha = m_\alpha \dot{q}_\alpha + e_\alpha A(q_\alpha)$ is the conjugate variable of q_α and $\Pi(r, t) = -\epsilon_0 E_\perp(r, t)$ is the conjugate variable of $A(r, t)$, and

$$H_{\text{A}} = \sum_\alpha \frac{1}{2m_\alpha}[p_\alpha - e_\alpha A(q_\alpha)]^2 + \frac{1}{2}\int \left(\frac{1}{\epsilon_0}|\Pi_\perp(r)|^2 + \frac{1}{\mu_0}|\nabla \times A(r)|^2\right) d^3 r, \tag{2.15}$$

is the Hamiltonian of an atom coupled to an electromagnetic field. Hence, compared to H_{A}, H has two supplementary terms; the third term in Eq. (2.14), containing the harmonic potential ϕ_{harm}, accounts for the effect of the electrostatic gates while the second term, containing the longitudinal potential $U_\parallel$, accounts for the Coulomb interaction between the tunneling electrons. The fourth term is treated in a standard way by separating the longitudinal part from the transverse part. This gives in one hand a Coulomb interaction Hamiltonian and in the other hand a radiation Hamiltonian H_R containing the modes of the cavity. In the following we will consider a single cavity mode, so that $H_R = \omega_c a^\dagger a$ with $a^\dagger$ the creation operator. The vector potential A is written in terms of

the cavity mode $A(r) = i\mathcal{A}(r)(a - a^\dagger)$. We can use the field operator of the tunneling charges ψ to write the Hamiltonian Eq. (2.14)

$$H = \int \psi^\dagger(r) h_{\mathcal{Q}}(r) \psi(r) d^3r + H_{Coul} + \omega_c a^\dagger a \tag{2.16}$$

Where

$$h_{\mathcal{Q}}(r) = \frac{1}{2m}(eA(r) - i\nabla)^2 - e\phi_{\text{harm}}(r) - eV_{conf}(r) \tag{2.17}$$

and

$$H_{Coul} = \frac{e^2}{2} \int \psi^\dagger(r)\psi^\dagger(r')G(r,r')\psi(r')\psi(r)d^3r'd^3r. \tag{2.18}$$

Here e is the (positive) electron charge and m its mass. While H_{Coul} corresponds to the second term in the Hamiltonian Eq. (2.14), the potential V_{conf} corresponds to the confinement potential arising from the last term in Eq. (2.14) treated as a mean field. Now we would like to write this Hamiltonian in a charge representation using second quantization and remove the term A^2 from the Hamiltonian. In order to perform this transformation, it was proposed in Ref. [83] to introduce a pseudopotential $V_\perp(a + a^\dagger)$ defined for r inside the nanocircuit.

$$V_\perp(r) = \omega_c \int_{C(r_0,r)} \mathcal{A}(r').dr', \tag{2.19}$$

where r_0 is a point in the nanocircuit and C a continuous path connecting two points. $V_\perp$ can be interpreted as the work performed by the cavity electric field when a charge is transported along a path C connecting the point r to the reference point r_0. As long as that magnetic effects are negligible, meaning that $\nabla \times \mathcal{A}$ can be ignored, the choice of C and r_0 should not have much effects. In this limit it should be noted that $\nabla V_\perp(r) \simeq \omega_c \mathcal{A}$. We define now the unitary transformation

$$U = \exp\left\{ \frac{e(a - a^\dagger)}{\omega_c} \int V_\perp(r)\psi^\dagger(r)\psi(r)d^3r \right\}. \tag{2.20}$$

While this transformation has no effect on H_{Coul}, it introduces a term $\mathcal{V}(a + a^\dagger) + \mathcal{V}^2/\omega_c$, where

$$\mathcal{V} = -e \int \psi^\dagger(r)\psi(r)V_\perp(r)d^3r, \tag{2.21}$$

and it removes the term A^2 from $h_{\mathcal{Q}}$, leading to

$$\tilde{h}_{\mathcal{Q}}(r) = -\frac{\Delta}{2m} - e\phi_{\text{harm}}(r) - eV_{\text{conf}}(r). \tag{2.22}$$

We thereby find that the transformed Hamiltonian is

$$\tilde{H} = \int \psi^\dagger(r)\tilde{h}_{\mathcal{Q}}(r)\psi(r)d^3r + H_{\text{Coul}} + \omega_c a^\dagger a + \mathcal{V}(a + a^\dagger) + \mathcal{V}^2/\omega_c. \tag{2.23}$$

Hence, we find a linear coupling between the photons and the tunneling electrons, given by $\mathcal{V}(a+a^\dagger)$. At this point, if one assumes that the vector potential A does not vary over the length of the nanocircuit $A(r) \simeq A$ one obtains the dipole approximation usually used in cavity-QED. One can expand the pseudopotential keeping only the linear dependence on r: $V_\perp(r) = \omega_c A \cdot r(a + a^\dagger)$. However, this approximation does not hold for plasmonic cavities since the electric field is known to have strong variations at the scale of the circuit [70].

2.2 Electronic transport description

As we specified earlier, our aim is to describe the tunneling of the electrons through the nanocircuit. To do so, we need to express the Hamiltonian in the charge representation. We call $\mathcal{O}$ the ensemble of objects constituting the nanocircuit and j an orbital of one object. Hence, we describe each part of the nanocircuit as a collection of creation (annihilation) operator $c^\dagger_{o,j}(c_{o,j})$, such that $\{c^\dagger_{o,j}, c_{o',j'}\} = \delta_{o,o'}\delta_{j,j'}$. The different orbitals in an object are orthogonal, while the overlap between two orbitals of two different objects can exist although we consider the case where this overlap is weak. The tunneling Hamiltonian without the cavity reads [84]

$$H_T = \sum_{o,j} \varepsilon_{o,j} c^\dagger_{o,j} c_{o,j} + \sum_{o\neq o',j,j'} (t_{oj,o'j'} c^\dagger_{o,j} c_{o',j'} + H.c.), \tag{2.24}$$

where $\varepsilon_{o,j}$ is the energy of the orbital j on object o and $t_{oj,o'j'}$ is the tunnel coupling between orbitals j and j' on objects o and o'. From this representation of the tunneling charges, we write the field operators as

$$\psi(r) = \sum_{o,j} \varphi_{o,j}(r) c_{o,j}, \tag{2.25}$$

where $\varphi_{o,j}$ is the wave function of the orbital j of o and is mainly localised on o. Thus, introducing the field operator's expression Eq. (2.25) into the Hamiltonian Eq. (2.23) gives

$$H = H_T + \omega_c a^\dagger a + H^T_{\text{Coul}} + h_{int}(a + a^\dagger), \tag{2.26}$$

where

$$h_{int} = \sum_{o,o',j,j'} \Lambda_{oj,o'j'} c^\dagger_{o,j} c_{o',j'} \tag{2.27}$$

The term $\mathcal{V}^2/\omega_c$ has disappeared since it only introduces a renormalization of the electronic energy levels $\varepsilon_{o,j}$, the tunneling rates $t_{oj,o'j'}$ and the Coulomb interaction H^T_{Coul}.

2.3 Electron–photon coupling

The electron–photon coupling intensity is given by

$$\Lambda_{oj,o'j'} = -e \int V_\perp(r) \varphi^*_{o,j}(r) \varphi_{o',j'}(r) d^3r. \tag{2.28}$$

We can separate the couplings into two types of couplings. The first one is when $o = o'$ and $j = j'$. It is the coupling to the charge that is absent in the Jaynes–Cummings model. In this case the coupling depends on the pseudopotential and the modulus squared of the wave function

$$\Lambda_{o,j} = -e \int V_\perp(r) |\varphi_{o,j}(r)|^2 d^3r. \tag{2.29}$$

This term is particularly relevant in the case of electronic transport as it does not appear in quantum optics model due to the fact that the charge

in the atom/molecule is constant. When o is a quantum dot inside the cavity, this term describes the interaction between the charge fluctuations of the dot and the electric field of the cavity. If we assume that the empty quantum dot is neutral, then adding a charge on it amounts to adding a charged particle into the cavity which should interact with the electric field of the cavity. Otherwise, when o is an electronic lead, this term correspond to the coupling of a fermionic reservoir to the cavity field. This account for the processes by which an electron in a lead can relax some energy in the cavity plasmon mode, emitting a photon, or on the contrary a plasmon mode can decay in a fermionic reservoir, absorbing a photon.

We separate these two contribution into $\Lambda_{\mathcal{D},j}$ for the dots and $\Lambda_{\mathcal{R},j}$ for the fermionic reservoirs. While this first term can be interpreted as a shift of the energy level (this will be explained in more details later) of the dots or the fermionic reservoirs, the other coupling appearing in Eq. (2.28) is a term mixing the orbitals of two different objects of the nanocircuit

$$\Lambda_{oj,o'j'} = -e \int V_{\perp}(r)\varphi^{*}_{o,j}(r)\varphi_{o',j'}(r)d^3r, \tag{2.30}$$

for $o \neq o'$. This term depends on the overlap between two wave functions and the pseudopotential $V_{\perp}$. It accounts for the modulation of the tunneling between two parts of the nanocircuit by the electromagnetic field of the cavity. This last term can describe the excitation of the plasmonic mode by the tunneling current between two fermionic reservoirs or between the dot and a reservoir. This term is particularly relevant in experiments studying the light emitted by an STM like the one presented in Ref. [67]. In this experiment, represented schematically in Fig. 2.3 the authors show that a molecule interacts with the electric field. A transition occurs between its HOMO and LUMO states when the current in the STM is turned on. The current in the junction couples to the plasmon through terms of the form $-j \cdot A$. This coupling is responsible for plasmon emission. The plasmonic field is, in turn, able to induce HOMO-LUMO transitions in the molecule.

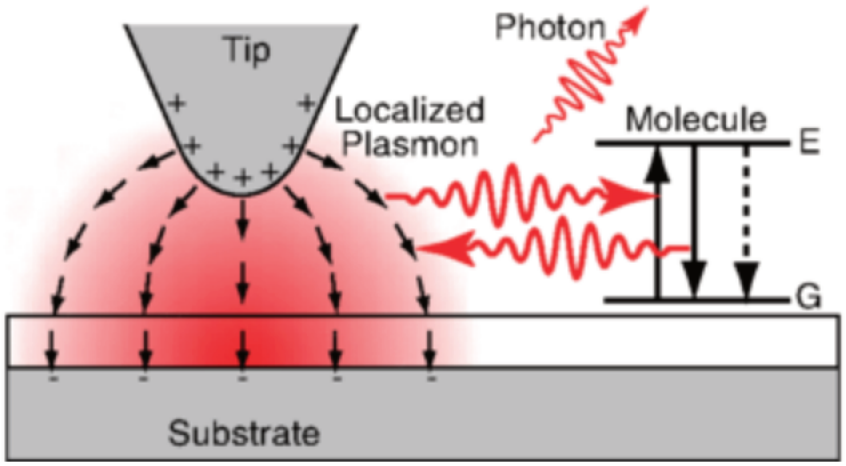

Figure 2.2: Representation of the interaction between the plasmonic field generated in a STM and the HOMO-LUMO transition of a molecule. Extracted from Ref. [67].

The intensity of the interaction is strongly dependent on the distance between the molecule and the tip and in Ref. [67] they show how the emitted light spectrum is modified by moving the molecule. A theoretical framework has been developed by Kaasbjerg and Nitzan in Ref. [80] in which a term $I(a + a^\dagger)$ appears in the Hamiltonian corresponding to the standard interaction $-\vec{j} \cdot \vec{A}$ between the electronic current and the cavity mode. This term mixes the orbitals of two electronic reservoirs of the tunnel junction and is still found in the interaction Hamiltonian Eq. (2.27). This term in the Hamiltonian also contributes to the damping of the cavity and contains terms allowing the exchange of a photon when an electronic transition occurs in a dot. Basically it is in this last term that we will find the between the HOMO-LUMO transition and the electric field of the cavity that is responsible for the Rabi oscillations and appears in the Jaynes–Cummings model. As this corresponds to the interaction between a dipolar momentum and the electromagnetic field, we call it dipolar coupling.

2.4 Origin of the pseudopotential

So far we have expressed the coupling term as being proportional to Eq. (2.28). In this expression intervenes the pseudopotential $V_\perp$ that is, as any potential, only defined up to a constant. The value of the constant is given by the origin r_0 for the path $\mathcal{C}$ in Eq. (2.28). This means that as we have defined the coupling so far, it is also defined up to a constant and does not have a unique value. Of course the physics does not depend on this constant since we can show that adding to the pseudopotential $V_\perp$ a constant C only introduces a shift of the equilibrium position of cavity mode without changing the physics

$$\mathcal{V}' = -e \int [V_\perp(r) + C]\psi^\dagger(r)\psi(r)d^3r = \mathcal{V} + CN, \tag{2.31}$$

where N is the total number of charges in the system. Hence shifting the pseudopotential by a constant C adds a term $CN(a^\dagger + a)$ to the Hamiltonian. This term can be removed by the unitary transformation $U = e^{CN(a-a^\dagger)}$ which shifts the cavity operators by the quantity CN.

We now discuss which origin we choose for the pseudopotential in order to define the coupling terms $\Lambda_{oj,o'j'}$. This amounts to choosing an element of the circuit for which the coupling strength will be taken to be 0. In fact we have defined earlier $\mathcal{B}$ as being the ensemble of the elements in the circuit on which the voltage is fixed. This typically will include the electrodes. For the elements in $\mathcal{B}$ the voltage is fixed as a boundary condition given in Eq. (2.5). Therefore the static component of the field, given by ϕ_{harm} already includes the potential's origin, and the other components of the field $E_\perp$ and $E_\parallel$ should not introduce any other potential difference between any points of the elements of $\mathcal{B}$. This means that for all the elements of $\mathcal{B}$, $V_\parallel + V_\perp$ should always be equal to 0. Since from the boundary conditions for the elements in $\mathcal{B}$ in Eq. (2.8), the parallel component of the electric field have no contribution, we must have that $V_\perp$ is the same for all elements in $\mathcal{B}$ and can be taken to be 0.

As a conclusion the interaction term $\Lambda_{\alpha j}$ for all the leads α does not depend on the lead α and can always be chosen to be 0. This fixes a "natural" reference to the interaction terms in h_{int}. Another way to say that is that we define Λ_{lead} as being the coupling term to the charge in the leads and we define $\tilde{\Lambda}_{oj} = \Lambda_{o,j} - \Lambda_{lead}$ as the coupling strength for an object o that is not in $\mathcal{B}$. Therefore, for a term coupling the charge to the field, meaning $o, j = o', j'$, the coupling strength is the work for bringing the charge from a lead to the dot in the junction. In the following we will set $\Lambda_{lead} = 0$, so that $\tilde{\Lambda}_{oj} = \Lambda_{o,j}$.

2.5 Comparison between charge and dipolar coupling

We propose in this section a rough comparison between the coupling of the charge on one electronic level on a quantum dot and the coupling between the transitions of a charge between two electronic levels of the dot. We will refer to those two coupling as a monopolar coupling Λ_m when only one level is involved and to a dipolar coupling $\Lambda_{i,j}$ when two levels are involved. Let us start with some estimation of those couplings based on their physical interpretations. As we explained in the previous section, the monopolar coupling can be interpreted as the potential interaction between a charged particle and an electric field. This has the form

$$\Lambda_m = q \cdot V_m, \tag{2.32}$$

where q is the charge of the particle and V_m is the potential of the electric field. As the electric field is the gradient of the potential V_m, we approximate V_m as

$$V_m \simeq L E_{zpm}, \tag{2.33}$$

considering that the electric field does not vary over the distance L, where L is the typical length over which the tunneling event occurs and E_{zpm} are the zero-point quantum vacuum fluctuations of the cavity electric field.

If we look back at the model we derived earlier we can find a similar result. Indeed, neglecting the pseudopotential's $V_\perp$ variations in the cavity, we approximate the monopolar coupling as

$$\Lambda_m \simeq -eV_\perp(r_m) \simeq eLE_{zpm}, \tag{2.34}$$

where r_m is the location of the molecule. We recover exactly the estimation we made based on our interpretation of Λ_m. Considering the energy density of the field, we find the order of magnitude of Λ_m

$$u = \frac{\epsilon_0}{2}E^2 + \frac{1}{2\mu_0}B^2 = \frac{\omega_c}{\mathcal{V}}, \tag{2.35}$$

where $\mathcal{V}$ is the cavity's volume. Then we find the order of magnitude of the field

$$E_{zpm} \sim \sqrt{\frac{\omega_c}{\mathcal{V}\epsilon_0}}. \tag{2.36}$$

The dipolar interaction is the interaction between a dipolar momentum and an electric field. The energy of this interaction is

$$\Lambda_{i,j} = -\mu_{i,j}E_{zpm}, \tag{2.37}$$

where $\mu_{i,j} = -ed$ is the dipolar momentum between the two levels considered and d is the size of the dipole. Hence, we find that the ratio between the monopolar and the dipolar approximation should be of the order of

$$\frac{\Lambda_m}{\Lambda_{i,j}} \sim \frac{L}{d}. \tag{2.38}$$

As we expect $L > d$, this leads to a monopolar coupling stronger than the dipolar one. However, if we were to use the approximation $V_\perp$ constant in this case, we would find $\Lambda_{i,j} = 0$ as the two orbitals should be orthogonal.

2.6 Examples

In this section we show three examples of calculations of the coupling strength that are relevant with usual cases studied in the literature.

2.6.1 Point-like approximation

As we mentioned earlier, in most of the work that has been done so far in Cavity-QED, the quantum emitters have been considered in the point dipole approximation. When the cavity's dimensions are very large compared to the emitter's size this, is not an issue to consider that the electric field around the emitter is almost constant. However, for nanocavities, the emitter has a size that is close to the dimensions of the cavity and

therefore some recent works have questioned the point-dipole approximation for plasmonic cavities [85].

Through assuming that the point-dipole approximation holds (that we call in our case the point-like approximation), we want in this section to evaluate the corresponding coupling strength that should actually be an upper approximation of the real coupling strength. Considering the emitter to be point-like means that the extent of its wave functions is negligible compared to the scale over which the electric field varies and therefore the wave functions in the expression of the coupling strength in Eq. (2.28) behave has delta distributions. The coupling strength for a molecular orbital is then

$$\Lambda_{d,i} = -eV_{\perp}(r_0), \tag{2.39}$$

where d denotes the quantum dot, i one of its orbital and r_0 its location in the cavity. Here we assumed that $V_{\perp}$ is 0 in the leads so for a STM experiment, this means that $V_{\perp}$ at the boundaries of the cavity is vanishing and therefore the coupling is $\Lambda_{d,i} = 0$ when the dot is at the boundaries of the cavity. A way to show that is to consider the cavity as a box of length L. At $x = 0$ and $x = L$ are placed two perfectly reflecting surfaces and at $y = 0, L$ and $z = 0, L$ two perfectly conducting metals.

We can show from Maxwell's equations that a transverse magnetic field (TM) in such a geometry as the form

$$\begin{cases} E_x = E_{x0} \cos\left(\frac{n\pi x}{L}\right) \sin\left(\frac{m\pi y}{L}\right) \sin\left(\frac{p\pi z}{L}\right) \\ E_y = E_{y0} \sin\left(\frac{n\pi x}{L}\right) \cos\left(\frac{m\pi y}{L}\right) \sin\left(\frac{p\pi z}{L}\right) \\ E_z = E_{z0} \sin\left(\frac{n\pi x}{L}\right) \sin\left(\frac{m\pi y}{L}\right) \cos\left(\frac{p\pi z}{L}\right) \end{cases} \tag{2.40}$$

Using the definition of $V_{\perp}$ in Eq. (2.19), we choose $r_0 = 0$ so that the reference is at the surface of a lead and we choose the contour $\mathcal{C}$ as simple as possible in Cartesian coordinate as a path going along the z-axis then parallel to the y-axis and finally parallel to the x-axis. Hence

$$V_{\perp}(r) = \int_0^x E_x(x', y, z)dx' + \int_0^y E_y(0, y', z)dy' + \int_0^z E_z(0, 0, z')dz'. \tag{2.41}$$

Then we find the expression of the potential $V_{\perp}$ as a function of the position of the dot inside the cavity

$$V_{\perp}(x, y, z) = \frac{E_{x0}L}{n\pi} \sin\left(\frac{n\pi x}{L}\right) \sin\left(\frac{m\pi y}{L}\right) \sin\left(\frac{p\pi z}{L}\right). \tag{2.42}$$

Fig. 2.3 shows the evolution of the coupling strength along the x direction. We see that if the dot is on a boundary of the cavity then the coupling strength becomes 0, whereas when the dot is in the middle of the cavity the coupling strength reaches its maximum value as the potential also reach its own maximum value. We also recognize in Eq. (2.42) that the coupling strength is in that case given by the product $E_{zpm}L$.

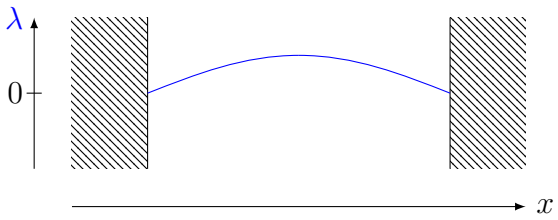

Figure 2.3: Intensity of the coupling λ along the x direction inside the cavity.

2.6.2 Homogeneous electric field

We now show the calculation of the coupling terms in a homogeneous field. This could apply to the microwave domain for which the cavity is very large compared to the nanocircuit inside

$$\vec{E} = \vec{E}_0 = \omega_c \vec{A}_0. \tag{2.43}$$

The pseudopotential resulting from such an electric field is

$$V_\perp(\vec{r}) = \int_{\mathcal{C}(\vec{r}_0,\vec{r})} \vec{E}_0(\vec{r}').d\vec{r}'. \tag{2.44}$$

We set the origin at r_0 so that $\vec{r}_0 = \vec{0}$ and define $\mathcal{C}(\vec{r},\vec{r}') = \vec{r}' - \vec{r}$.

For such a path $V_\perp$ have a simple expression in spherical coordinates

$$V_\perp(\vec{r}) = \vec{E}_0 \cdot \vec{r}. \tag{2.45}$$

It is interesting to note here that changing our reference point would only add a constant term in $V_\perp$ and only result in shifting the energy levels of the tunneling region and also renormalise the Coulomb interaction term. From the expression of $V_\perp$, we find the interaction terms

$$\Lambda_{oj,o'j'} = -e \int \vec{E}_0.\vec{r}\varphi^*_{o,j}(\vec{r})\varphi_{o,j}(\vec{r})d^3r. \tag{2.46}$$

To evaluate these terms, we use the hydrogen atom wave functions. Let's first consider a monopolar term and the orbital $1s$ of the hydrogen atom. We will consider the atom to be in the middle of the cavity. We call φ_{1s} the wave function of the orbital $1s$ of the hydrogen atom.

$$\varphi_{1s}(r) = \frac{1}{\sqrt{\pi a_0^3}} e^{-r/a_0}, \tag{2.47}$$

Where a_0 is the Bohr radius. As both the pseudopotential and the wave function have a spherical symmetry, we find no coupling between this orbital and the cavity electric field since for all vector $\vec{r}$ that will have a contribution, the vector $-\vec{r}$ will have the opposite contribution. In fact any orbital that present a central symmetry won't couple to the charge, then we conclude that the hydrogen atom or any atomic orbital won't couple to the electric field of the cavity through its charge. For the dipolar coupling we don't have the same restriction.

Let us consider the coupling between orbitals $1s$ and $2py$ of the hydrogen atom so that the product of the wave function does not have a central symmetry. The wave function for orbital $2py$ is

$$\varphi_{2py}(r) = \frac{1}{4\sqrt{2\pi}a_0^{5/2}}\cos(\theta)re^{-r/2a_0}, \tag{2.48}$$

Hence, the coupling corresponding to the dipolar momentum between these two orbitals is

$$\Lambda_{1s,2py} = -e\pi\frac{32\sqrt{2}}{81}a_0. \tag{2.49}$$

So far we have only discussed the case where the origin for the potential is at the center of the atom. Introducing an origin r_0 to the potential (or the wave function, which is equivalent and corresponds to moving the atom from the origin of the potential) we only add to the coupling the term

$$\Lambda^0_{oj,o'j'} = -e\vec{E}_0.\vec{r}_0\int \phi^*_{o,j}(\vec{r})\phi_{o'j'}(\vec{r})d^3r. \tag{2.50}$$

Therefore, applying this formula on every component of the coupling, we find a constant term proportional to the total number of charges in the system $-e\vec{E}_0.\vec{r}_0N(a+a^\dagger)$. This term corresponds to a shift of the cavity mode and can be removed by the unitary transformation $U = e^{-e\vec{E}_0.\vec{r}_0N(a-a^\dagger)}$. In conclusion the physics is not changed by moving the atom inside the cavity in this case assuming that we remain in a region where the electric field can be considered constant.

2.6.3 Plate capacitor

As another example we show the plate capacitor which would be a very simple model of cavity in which we can take into account the space variation of the electric field. Our cavity is made of two metallic plates at fixed voltages V_1 and V_2. As we suppose that the plates are very large in the x and y direction compare to their width and to the distance between them we will consider them as infinite planes orthogonal to the z-axis, see Fig. 2.4.

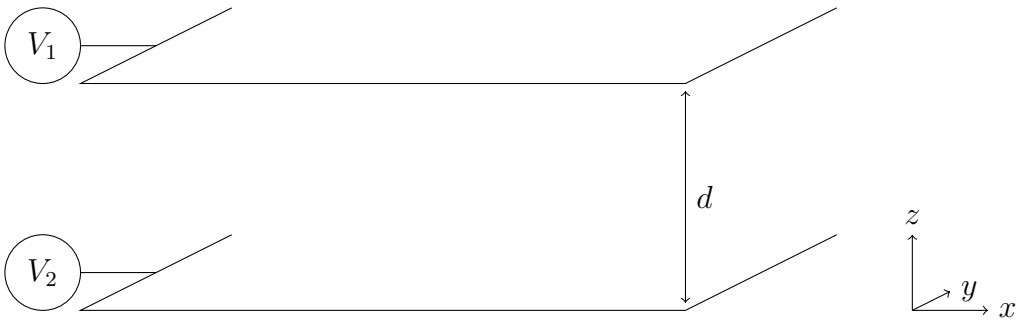

Figure 2.4: Plate capacitor.

From the Maxwell's equation and the Coulomb gauge condition we

find that

$$\begin{cases} \Delta E - \frac{1}{c^2}\partial_t^2 E = 0 \\ \Delta B - \frac{1}{c^2}\partial_t^2 B = 0 \\ \Delta V = 0 \\ \nabla \cdot A = 0 \end{cases} \tag{2.51}$$

We set the lower plate to be at $z = 0$, using the boundary conditions on the potential V and the translational invariance on the (x, y) plan,

$$V(z) = \frac{V_1 - V_2}{d} z + V_2. \tag{2.52}$$

From the potential V we deduce that the electric field is

$$E = \frac{V_2 - V_1}{d} e_z + E_{ac}(r, t), \tag{2.53}$$

where E_{ac} is solution of Eq. (2.51) and of the Maxwell's equations. As the electric field propagates freely in the (x, y)-plan, we assume plane wave solution for the (x, y) variation of E_{ac}

$$E_{ac}(r, t) = E_{ac}(z) e^{ik_\parallel \cdot r_\parallel - i\omega t}, \tag{2.54}$$

where $r_\parallel$ and $k_\parallel$ have no z component. From the boundary conditions

$$n \times E = 0 \tag{2.55}$$

$$n \cdot B = 0, \tag{2.56}$$

where n is unit a vector orthogonal to the plates, we know that the electric field has no (x, y) component at $z = 0$ and $z = d$. From Eq. (2.51) and Eq. (2.55) one can show that the fields can be decomposed into the TM and TE solutions. The TM fields have no component in the direction parallel to $k_\parallel$ for the magnetic field and the TE fields have no component in the direction parallel to $k_\parallel$ for the electric field. We chose a set of axis so that $k_\parallel = k \cdot e_x$ where e_x is a unit vector. Then we write a TE field as

$$E = E_y \sin\left(\frac{n\pi}{d} z\right) e^{ikx - i\omega t} e_y, \tag{2.57}$$

where e_y is a unit vector and a TM field as

$$B = B_y \cos\left(\frac{n\pi}{d} z\right) e^{ikx - i\omega t} e_y. \tag{2.58}$$

It follows from Eq. (2.58) that the TM-electric field is

$$E = -\frac{in\pi c^2}{\omega} B_y \sin\left(\frac{n\pi}{d} z\right) e^{ikx - i\omega t} e_x - \frac{\omega}{k} B_y \cos\left(\frac{n\pi}{d} z\right) e^{ikx - i\omega t} e_z. \tag{2.59}$$

Considering a TM field we find a potential vector

$$A = -\frac{iE_z}{\omega} \cos\left(\frac{n\pi}{d} z\right) e^{ikx - i\omega t} e_z, \tag{2.60}$$

where $E_z = -\omega B_y/k$. To compute the pseudopotential $V_\perp$ we first choose a path to connect two points in the nanocircuit. Let's choose a path that first extend along ρ, where ρ is the radius in cylindrical coordinates, then z, as shown in Fig. 2.5.

Figure 2.5: Continuous path C between r and r' in the (ρ, z)-plan.

The pseudopotential is found using Eq. (2.19)

$$V_\perp(r) = E_z \frac{d}{n\pi} \sin\left(\frac{n\pi}{d} z\right) e^{ikx} + V_0. \tag{2.61}$$

We see from Eq. (2.61) that if the field has no component along the z-axis there is no coupling. In the following we disregard the constant V_0. If we look at the coupling between an orbital $1s$ of the hydrogen atom and the electric we find

$$\Lambda_{1s} = -\frac{eE_z d}{n\pi^2 a_0^3} \int \sin\left(\frac{n\pi}{d}(\rho\cos\phi + z_0)\right) \rho^2 \sin\phi e^{-\frac{2\rho}{a_0} + ik\rho\cos\theta\sin\phi} d\rho d\theta d\phi, \tag{2.62}$$

where z_0 is the z coordinate of the center of the molecular orbital.

$$\Lambda_{1s} = -\frac{2eE_z d}{n\pi a_0^3} \sin\left(\frac{n\pi}{d} z_0\right) \int \cos\left(\frac{n\pi}{d}\rho\cos\phi\right) \rho^2 \sin\phi e^{-\frac{2\rho}{a_0} + ik\rho\cos\theta\sin\phi} d\rho d\theta d\phi, \tag{2.63}$$

Chapter 3

Electronic transport in a plasmonic cavity for a single level dot

As we explained in chapter 1, we are particularly interested in the description of an STM setup as depicted in Fig. 3.1. In those experiments the cavity is made of the apex of the STM and the substrate. The molecule or an atom is embedded inside the STM junction. Therefore, our nanocircuit includes the dot and the STM tip and substrate.

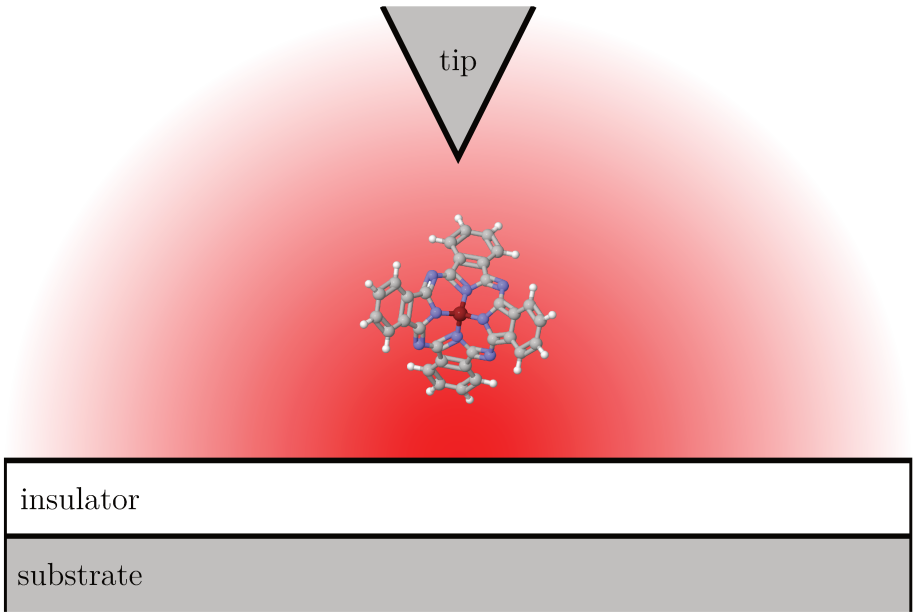

Figure 3.1: Representation of an STM cavity interaction with a molecule.

If we look at the coupling between the electrons on the dot and the electric field of the cavity in Eq. (2.27), we see a term proportional to the charge and a term proportional to a transition between two electronic levels of the dot. It is in the second term in Eq. (2.27) that we will find the dipolar interaction that has been long studied in quantum optics with models such as the Jaynes–Cummings model [14]. The first term is specific to the case of electronic transport as if the charge on the dot were

fixed, then we would reduce the Hilbert space accordingly and this term would be a constant and could be removed from the Hamiltonian through a unitary transformation. Also, this term is similar to the coupling of the charge with vibration modes of a molecule that as been studied in quantum transport in the well-known Franck-Condon physics [82,86–89]. Thus, we expect that this coupling could result in the emission of photons when the bias voltage between the STM tip and the substrate allows for it.

Hence, there are four reasons for studying a single-level dot model. The first one is that it is the simplest case we can think of and therefore, it should be a very nice theoretical framework. The second one is that it is experimentally relevant as the bias voltage applied in STM experiments is of the order of 2 eV at most. Therefore, in some cases, the bias voltage is smaller than the gap energy between two orbitals of the dot. This means that only one electronic level is involved in electronic transport and unless the molecule is excited by an external source of radiation, the dipolar coupling cannot lead to emission. Hence, only the monopolar coupling can contribute. Also, in limiting the system to a single electronic level, it allows us to isolate the effects of the charge-coupling, we can then add on top the other coupling as we well understand the effects of the first one. And finally this coupling is in general disregarded in quantum optics and plasmonic. However, we will show in the following that this coupling can result in photon emission and, depending on the parameters the light emitted, can show non-classical features, such as anti-bunching and sub-Poissonian distribution. This makes this kind of systems relevant for designing single-photon sources.

3.1 Hamiltonian for the single level-dot

The first step here is to write the Hamiltonian in a suitable representation. To do so, we first try to simplify as much as we can the expression of the interaction. From Eq. (2.26) we find three interaction terms. The first one is the interaction between the dot's charge and the electric field

$$H_S^{\text{int}} = \Lambda_d d^\dagger d(a + a^\dagger). \tag{3.1}$$

Of course we assume that we are not in a case where this term is zero as it will be our main focus. The second term is the interaction between the fermionic reservoirs' charges and the field

$$H_R^{\text{int}} = \sum_{\alpha k} \Lambda_{\alpha k} c_{\alpha k}^\dagger c_{\alpha k}(a + a^\dagger). \tag{3.2}$$

In our setup the field cannot penetrate far into the electrodes, so this term can be neglected. Also, near the Fermi energy the properties of the wave function can be considered constant so $\Lambda_{\alpha k} = \Lambda_\alpha$. Actually we can choose the potential so that this interaction term is zero by setting the origin of the potential at the electrodes, since we have shown in the previous chapter that the potential should be constant in the electrodes and the same for any electrodes.

Another way to understand this is by considering to subtract $\Lambda_B = \Lambda_\alpha$ everywhere in the coupling terms Λ_i, the sum of all the terms proportional to Λ_α will give a term proportional to the total number of charges and to the electric field as

$$\Lambda_\alpha \sum_{o,j} c^\dagger_{o,j} c_{o,j} (a + a^\dagger) = \Lambda_\alpha (a + a^\dagger). \tag{3.3}$$

Such a term can be eliminated of the Hamiltonian by the unitary transformation $U = e^{\Lambda_\alpha (a - a^\dagger)/\omega_c}$. Next, we have the interaction between a tunneling charge and the field

$$(\Lambda_{\alpha k,d} c^\dagger_{\alpha k} d + H.c.)(a + a^\dagger). \tag{3.4}$$

From the definition of the coupling, we can estimate the coupling $\Lambda_{\alpha k,d}$ as a tunneling amplitude times the coupling to the charge at most

$$\Lambda_{\alpha k,d} = t_{\alpha k} \Lambda_d / E_F, \tag{3.5}$$

where E_F is the Fermi energy at which the electrons tunnel between the leads and the dot. Typically for metallic leads, $E_F \simeq 5 - 10$ eV and as shown in Fig. 3.1, the substrate and the dot are separated by an insulating layer so that the tunneling between the dot and the leads is weak. Therefore the coupling between the charge and the electric field in Eq. (3.1) is expected to be dominant compared to the direct coupling between the field and a a tunneling electron. This analysis holds also for the coupling between the direct current between the STM tip and the substrate as we expect the tunneling rate to be even weaker. Hence, so far, we have reduced the Hamiltonian to

$$H = H_S + H_B + H_{\text{int}} \tag{3.6}$$

where

$$H_S = \tilde{\varepsilon}_0 d^\dagger d + \omega_c a^\dagger a + \Lambda_d d^\dagger d (a + a^\dagger), \tag{3.7}$$

$$H_B = \sum_{\alpha k} \varepsilon_{\alpha k} c^\dagger_{\alpha k} c_{\alpha k}, \tag{3.8}$$

$$H_{\text{int}} = \sum_{\alpha k} t_{\alpha k} c^\dagger_{\alpha k} d + H.c., \tag{3.9}$$

where $d^\dagger$ is the creation operator for the electron of energy $\tilde{\varepsilon}_0$ on the dot, $a^\dagger$ is the creation operator for the photon field. The two fermionic reservoirs are described by H_B, where $c^\dagger_{\alpha k}$ is the creation operator of an electron in lead α on orbital k of energy $\varepsilon_{\alpha k}$. The tunneling amplitude between the dot and the orbital k of lead α is given by $t_{\alpha k}$. Going further we can diagonalize the Hamiltonian H_S by shifting the equilibrium position of the cavity mode using the Lang–Firsov unitary transformation $U = \exp[\lambda d^\dagger d (a - a^\dagger)]$, where $\lambda \omega_c = \Lambda_d$. Doing so the dot creation operator d is transformed into

$$D^\dagger = d^\dagger e^{\lambda (a^\dagger - a)}, \tag{3.10}$$

while the photonic mode's creation operator a is transformed into

$$\tilde{a}^\dagger = a^\dagger - \lambda d^\dagger d. \tag{3.11}$$

In a way, from Eq. (3.10) we see that upon the creation of a charge in the dot, a coherent state of the photon field is created in the cavity. As a result in the transformed Hamiltonian the dot energy level is shifted by $\lambda^2\omega_c$ and the tunneling term also involves transitions between states with a different number of photons while H_B is left unchanged.

$$\tilde{H}_S = \varepsilon_0 d^\dagger d + \omega_c a^\dagger a \tag{3.12}$$

$$\tilde{H}_I = \sum_{\alpha k} t_{\alpha k} c^\dagger_{\alpha k} D + H.c. \tag{3.13}$$

where $\varepsilon_0 = \tilde{\varepsilon}_0 - \lambda^2\omega_c$. In this representation we can work with the eigenstates of $\tilde{H}_S$ and deduce from $\tilde{H}_I$ the transition rates between them to extract the current or other information from the system. So far we have considered the cavity to be isolated. However, it is known that if the reduced volume of plasmonic cavities allows for stronger couplings compared to bigger cavities, it is nonetheless at the cost of a bad quality factor. Indeed, cavity factors Q of the order of 10 have been reported in plasmonic cavities [29,58,90]. It is expected that an STM cavity exhibits a large damping rate κ. To account for this in our model, we include in the description the presence of the electromagnetic environment, that we model by a collection of harmonic oscillators. The cavity field is coupled linearly to the bosonic environment. Hence, we add to the Hamiltonian H_B a collection of bosonic modes

$$H_B = \sum_{\alpha k} \varepsilon_{\alpha k} c^\dagger_{\alpha k} c_{\alpha k} + \sum_q \omega_q b^\dagger_q b_q, \tag{3.14}$$

where $b^\dagger_q$ is the creation operator of an external photon with pulsation ω_q. The interaction Hamiltonian is then

$$\tilde{H}_I = \sum_{\alpha k} t_{\alpha k} c^\dagger_{\alpha k} D + \sum_q l_q b^\dagger_q a + H.c. \tag{3.15}$$

where l_q is the transition rate between the mode q from the bath an the mode of the cavity. Including the external bath before or after the Lang–Firsov transformation does not affect the physics we want to describe as the shift of the cavity mode will only introduce a new term in the dot energy that is not relevant as we will consider the reservoirs to be at thermal equilibrium.

3.2 Master equation

In order to reduce hybridisation between the substrate and the molecule in STM experiments, an insulating layer is placed above the substrate. As a result the tunneling between the leads and the quantum dot in the junction is weak and the tunneling Hamiltonian can be considered as

a perturbation of the system and bath Hamiltonians. In other words the energies in the system are ordered as $\Gamma \ll k_B T \ll \omega_c$ where $\Gamma = 2\pi \sum_{\alpha k} |t_{\alpha k}|^2 \delta(\omega - \varepsilon_{\alpha k})$ is the electron tunneling rate. This is called the sequential tunneling regime, in which the typical time for an electron tunneling event is the largest time scale at which the system evolves and should dominate the long time evolution. This implies that between two tunneling events the coherence of the electrons is lost. Therefore, the reservoirs evolving at a faster pace can always be considered at equilibrium. This regime fits well the density matrix approach [88, 91].

Depending on the quality factor Q of the cavity, $\kappa = \omega_c/Q$, the damping rate of the cavity, will be smaller or larger than $k_B T$ but always bigger than the tunneling rate in the cases we will consider. Indeed, if we consider that the system is at room temperature, then $k_B T \sim 10^{-2} eV$. For a quality factor $10 < Q < 1000$ the damping rate verifies $0.1 > \kappa/\omega_c > 10^{-3}$, so that in the worst case $\Gamma \ll k_B T \lesssim \kappa \ll \omega_c$ and in the best case $\Gamma \ll \kappa \ll k_B T \ll \omega_c$. We will derive our results in this last limit, for which we can find reliable approximations [92].

The time evolution of the density matrix ρ is given by the Liouville–von Neumann equation

$$\dot{\rho} = -i[H, \rho]. \tag{3.16}$$

By defining $H_0 = \tilde{H}_S + H_B$ and the unitary transformation $U(t, t_0) = e^{-iH_0(t-t_0)}$ we can write Eq. (3.16) in the interaction picture in which the time evolution of the density matrix is set by the interaction Hamiltonian H_I. This treatment allows us to solve the system for any value of the coupling λ as long as $\tilde{H}_I$ can be considered as a perturbation of H_0. It follows that in the interaction picture any operator A evolves with H_0 and becomes

$$A_I(t) = U^\dagger(t, t_0) A U(t, t_0) = e^{iH_0(t-t_0)} A e^{-iH_0(t-t_0)}. \tag{3.17}$$

Using the relation given in Eq. (3.17) on Eq. (3.16) we find the Liouville–von Neumann equation in the interaction picture

$$\dot{\rho}_I(t) = -i[H_{\text{int}I}(t), \rho_I(t)], \tag{3.18}$$

with the initial condition

$$\rho_I(t_0) = \rho(t_0), \tag{3.19}$$

where we chose t_0 as the time at which the interactions between the environments and the system are turned on. This means that at time t_0 the density matrix is in a product state

$$\rho(t_0) = \rho_S(t_0) \otimes \rho_B(t_0). \tag{3.20}$$

Integrating Eq. (3.18) we find that at first order in H_{int} the density matrix is

$$\rho_I(t) = \rho_I(0) - i \int_{t_0}^{t} [H_{\text{int}I}(t'), \rho_I(t')] dt'. \tag{3.21}$$

Re–introducing this last expression in Eq. (3.18) we find the time evolution of ρ_I at second order in the interaction

$$\dot{\rho}_I(t) = -i[H_{\text{int}I}(t), \rho_I(t_0)] - \int_{t_0}^{t} [H_{\text{int}I}(t), [H_{\text{int}I}(t'), \rho_I(t')]]dt'. \quad (3.22)$$

We define $\rho_S = \text{Tr}_B(\rho)$ the reduced density matrix of the system. From the trace invariance properties it follows that

$$\rho_{SI} = \text{Tr}_B(\rho_I), \quad (3.23)$$

and therefore the time evolution of ρ_{SI} is given by

$$\dot{\rho}_{SI}(t) = \text{Tr}_B \left(-i[H_{\text{int}I}(t), \rho_I(t_0)] - \int_{t_0}^{t} [H_{\text{int}I}(t), [H_{\text{int}I}(t'), \rho_I(t')]]dt' \right). \quad (3.24)$$

As the interaction Hamiltonian is a product of bath and system operators and we chose t_0 so that the bath and the system are each in thermal equilibrium, the first term in the right-hand side of Eq. (3.24) vanishes since it is proportional to the bath creation and annihilation operators' averages. Since we consider a weak coupling between the bath and the system and since the bath is supposed to be very large compared to the system, we make the Born approximation [92]. This means that we consider that at all time the density matrix is in a product state between the bath and the system and that we neglect the time dependence of the reduced density matrix of the environment ρ_B. In other words, we neglect the effect of the system on the environment at all times.

$$\rho \simeq \rho_S(t) \otimes \rho_B. \quad (3.25)$$

This approximation simplifies Eq. (3.24) as it allows to trace out the bath's density matrix and write an equation for ρ_S only. The double commutator in Eq. (3.24) involves terms mixing the two electronic reservoirs and the photonic environment. However as nor H_B nor H_{int} mixes directly any of them, they act as three separate environments each in their individual equilibrium state. This means that using an eigenbasis such as the charge states and photon number states, we can show that only the term that does not mix operators from two different environments in the double commutator in Eq. (3.24) will survive. Therefore, it only remains terms proportional to

$$\mathcal{C}_\alpha^+(t, t') = \text{Tr}_B \left(\sum_k |t_{\alpha k}|^2 c_{\alpha k}^\dagger(t) c_{\alpha k}(t') \rho_B \right) \quad (3.26)$$

$$\mathcal{C}_\alpha^-(t, t') = \text{Tr}_B \left(\sum_k |t_{\alpha k}|^2 c_{\alpha k}(t) c_{\alpha k}^\dagger(t') \rho_B \right) \quad (3.27)$$

$$\mathcal{K}^+(t, t') = \text{Tr}_B \left(\sum_q |l_q|^2 b_q^\dagger(t) b_q(t') \rho_B \right) \quad (3.28)$$

$$\mathcal{K}^-(t, t') = \text{Tr}_B \left(\sum_q |l_q|^2 b_q(t) b_q^\dagger(t') \rho_B \right), \quad (3.29)$$

which are the bath self-correlation functions. As ρ_B does not depend on time, it commutes with H_B and using once again the trace-invariant properties, we have for any self-correlator $\mathcal{S}$ of the environment

$$\mathcal{S}(t,t') = \mathcal{S}(t-t',0) = \mathcal{S}(t-t'). \tag{3.30}$$

As the bath is in thermal equilibrium, we can compute the self-correlators

$$\mathcal{C}_\alpha^+(t-t') = \sum_k |t_{\alpha k}|^2 e^{i\varepsilon_{\alpha k}(t-t')} f_\alpha^+(\varepsilon_{\alpha k}) \tag{3.31}$$

$$\mathcal{C}_\alpha^-(t-t') = \sum_k |t_{\alpha k}|^2 e^{-i\varepsilon_{\alpha k}(t-t')} f_\alpha^-(\varepsilon_{\alpha k}) \tag{3.32}$$

$$\mathcal{K}^+(t-t') = \sum_q |l_q|^2 e^{i\omega_q(t-t')} n_B(\omega_q) \tag{3.33}$$

$$\mathcal{K}^-(t-t') = \sum_q |l_q|^2 e^{-i\omega_q(t-t')} [1+n_B(\omega_q)]. \tag{3.34}$$

We define the tunneling rates $\Gamma_\alpha(\omega) = 2\pi \sum_{\alpha k} |t_{\alpha k}|^2 \delta(\omega - \varepsilon_{\alpha k})$ and assume the wide-band approximation and $f_\alpha^+(\omega) = 1 - f_\alpha^-(\omega) = f(\omega - \mu_\alpha)$ where f is the Fermi distribution and μ_α the chemical potential of the lead α. This means that close to the Fermi energy, the rates Γ_α should not depend much on ω.

$$\mathcal{C}_\alpha^+(t-t') = \Gamma_\alpha \int_{-\infty}^{+\infty} e^{i\omega(t-t')} f_\alpha^+(\omega) d\omega/2\pi \tag{3.35}$$

$$\mathcal{C}_\alpha^-(t-t') = \Gamma_\alpha \int_{-\infty}^{+\infty} e^{-i\omega(t-t')} f_\alpha^-(\omega) d\omega/2\pi \tag{3.36}$$

$$\tag{3.37}$$

Introducing this expression of the correlation functions into Eq. (3.24), we find

$$\begin{aligned}\dot{\rho}_{SI}(t) = -\int_{t_0}^{t} \Bigg\{ & \sum_\alpha \mathcal{C}_\alpha^+(\tau)[D_I(t), D_I^\dagger(t')\rho_{SI}(t')] \\ & + \sum_\alpha \mathcal{C}_\alpha^-(-\tau)[\rho_{SI}(t')D_I^\dagger(t'), D_I(t)] \\ & + \mathcal{K}^+(\tau)[a_I(t), a_I^\dagger(t')\rho_{SI}(t')] \\ & + \mathcal{K}^-(-\tau)[\rho_{SI}(t')a_I^\dagger(t'), a_I(t)] + H.c. \Bigg\} dt',\end{aligned} \tag{3.38}$$

where $\tau = t - t'$. In Eq. (3.38) the reduced density matrix at time t depends on its past, therefore it seems that ρ_S has a non-Markovian evolution. A non-Markovian evolution refers to a process of evolution for which the future states can not be predicted solely from the present state but also depends on the past states of the system. However, as we consider the environment to be in thermal equilibrium its correlation time is given by the temperature. Thus, the correlation time of the environment is very small compared to the typical timescale of the interaction

given by Γ and κ over which the reduced density matrix evolves . In this situation we can consider that the density matrix does not evolve in the integral since changes of ρ at times larger than the correlation time are not relevant. It is the so-called Markov approximation [92]. We also change our variable of integration into τ and set t_0 at $-\infty$.

$$\begin{aligned}\dot{\rho}_{SI}(t) = -\int_0^{+\infty}\Big\{ &\sum_\alpha \mathcal{C}_\alpha^+(\tau)[D_I(t), D_I^\dagger(t')\rho_{SI}(t)] \\ &+ \sum_\alpha \mathcal{C}_\alpha^-(-\tau)[\rho_{SI}(t)D_I^\dagger(t'), D_I(t)] \\ &+ \mathcal{K}^+(\tau)[a_I(t), a_I^\dagger(t')\rho_{SI}(t)] \\ &+ \mathcal{K}^-(-\tau)[\rho_{SI}(t)a_I^\dagger(t'), a_I(t)] + H.c.\Big\}d\tau,\end{aligned} \tag{3.39}$$

We now can go back into the Schrödinger picture using the fact that

$$\dot{\rho}_S(t) = -i[H_0, \rho_S(t)] + e^{-iH_0t}\dot{\rho}_{SI}(t)e^{iH_0t}. \tag{3.40}$$

Using Eq. (3.40) onto some products of operators $A_I(t)B_I(t')$ and $A_I(t')B_I(t)$ in the interaction picture, we find

$$e^{-iH_0t}A_I(t)B_I(t')e^{iH_0t} = AB_I(-\tau) \tag{3.41}$$

$$e^{-iH_0t}A_I(t')B_I(t)e^{iH_0t} = A_I(-\tau)B. \tag{3.42}$$

This means that in the Schrödinger representation Eq. (3.39) becomes

$$\begin{aligned}\dot{\rho}_S(t) = &-i[H_0, \rho_S(t)] - \int_0^{+\infty}\Big\{\sum_\alpha \mathcal{C}_\alpha^+(\tau)[D, D_I^\dagger(-\tau)\rho_S(t)] \\ &+ \sum_\alpha \mathcal{C}_\alpha^-(-\tau)[\rho_S(t)D_I^\dagger(-\tau), D] \\ &+ \mathcal{K}^+(\tau)[a, a_I^\dagger(-\tau)\rho_S(t)] \\ &+ \mathcal{K}^-(-\tau)[\rho_S(t)a_I^\dagger(-\tau), a] + H.c.\Big\}d\tau.\end{aligned} \tag{3.43}$$

We can derive the time evolution of the cavity's operators in the interaction picture from

$$\dot{a}^\dagger = i[H_0, a^\dagger] = -i\omega_c a, \tag{3.44}$$

Therefore

$$a_I(t) = ae^{-i\omega_c t}. \tag{3.45}$$

Performing the integration on the terms proportional to the bosonic correlation functions $\mathcal{K}^\pm$ we see that this part takes a Lindblad form

$$e^{-iH_0t}A_I(t)B_I(t')e^{iH_0t} = AB_I(-\tau) \tag{3.46}$$

$$e^{-iH_0t}A_I(t')B_I(t)e^{iH_0t} = A_I(-\tau)B. \tag{3.47}$$

This means that in the Schrödinger representation Eq. (3.39) becomes

$$\begin{aligned}\dot{\rho}_S(t) =& -i[H_0, \rho_S(t)] + [\mathcal{D}_-\rho_S(t) - \rho_S(t)\mathcal{D}_+, D^\dagger] + H.c. \\ &+ \frac{\kappa}{2}(2a\rho_S(t)a^\dagger - a^\dagger a\rho_S(t) - \rho_S(t)a^\dagger a) - \kappa n_B[a^\dagger, [a, \rho_S(t)]],\end{aligned} \tag{3.48}$$

where $\kappa = 2\pi \sum_q |lq|^2 \delta(\omega_c - \omega_q)$ and n_B is taken at the cavity frequency ω_c and

$$\mathcal{D}_\pm = \int_0^{+\infty} \sum_\alpha \mathcal{C}_\alpha^\pm(\pm\tau) D_I(-\tau) d\tau. \tag{3.49}$$

From Eq. (3.48) we define the Liouvillian superoperator $\check{\mathcal{L}}$ such that

$$\dot{\rho}_S(t) = \check{\mathcal{L}}\rho_S(t) = -i[H_0, \rho_S(t)] + (\check{\mathcal{L}}_e + \check{\mathcal{L}}_c)\rho_S(t), \tag{3.50}$$

where we defined

$$\begin{aligned}\check{\mathcal{L}}_e\rho_S(t) &= [\mathcal{D}_-\rho_S(t) - \rho_S(t)\mathcal{D}_+, D^\dagger] + H.c. \\ \check{\mathcal{L}}_c\rho_S(t) &= \frac{\kappa}{2}(2a\rho_S(t)a^\dagger - a^\dagger a\rho_S(t) - \rho_S(t)a^\dagger a) - \kappa n_B[a^\dagger, [a, \rho_S(t)]].\end{aligned} \tag{3.51}$$

Remark. *In the definition of the damping rate κ we dropped the imaginary part proportional to $iP\frac{1}{\omega_0 - \omega_c}$ as it only introduces a renormalisation of the energies.*

3.3 Rate equations approach

In general we cannot find an analytical solution to Eq. (3.50). However, one can derive the rate equations using a secular approximation on the master equation. The rate equations give an approximation of the time evolution of the populations by separating the evolution of the populations, the diagonal part of ρ_S, from the coherences, the off-diagonal part. Let us first project Eq. (3.50) onto the eigenstates of H_0. The unitary evolution of ρ_S only involves off diagonal terms and the damping of the cavity governed by $\check{\mathcal{L}}_c$ does not mix the populations and the coherences. Hence, we focus on the electronic part $\check{\mathcal{L}}_e\rho_S$ of Eq. (3.50). We start from the electronic part of Eq. (3.39) and project it onto an eigenbasis of H_0. We only show the calculations for the second term in the first commutator. The others can be deduced following exactly the same steps. We call A the first term in the electronic part of Eq. (3.39)

$$\begin{aligned}A &= \int_0^{+\infty} \sum_{\alpha,abcd} \mathcal{C}_\alpha^+(\tau) D_{ab}^\dagger \rho_{SIbc} D_{cd} e^{i(E_a - E_b + E_c - E_d)t} e^{i(E_b - E_a)\tau} d\tau |a\rangle\langle d| \\ &= \int_0^{+\infty} \sum_{\alpha,abcd} \mathcal{C}_\alpha^+(\tau) D_{ab}^\dagger \rho_{SIbc} D_{cd} e^{i(E_a - E_d)t} e^{i(E_b - E_a)\tau} d\tau |a\rangle\langle d|.\end{aligned} \tag{3.52}$$

The two different expressions of A in Eq. (3.52) are found using the fact that due to the Markov approximation, ρ_{SI} must commute with $e^{\pm iH_0 t}$.

Doing the secular approximation means we neglect the fast oscillating terms in Eq. (3.52) that average to 0 when looking at the long time evolution of ρ_S. Hence for the two expressions of A in Eq. (3.52) we find

$$\begin{aligned} E_a - E_b + E_c - E_d &= 0 \\ E_a - E_d &= 0. \end{aligned} \tag{3.53}$$

We, therefore, find that $E_c = E_b$ and A is approximated by

$$A \simeq \int_0^{+\infty} \sum_{\alpha,abcd} \mathcal{C}_\alpha^+(\tau) D_{ab}^\dagger \rho_{SIbc} D_{cd} e^{i(E_c - E_b)\tau} d\tau \delta_{E_a,E_d} \delta_{E_b,E_c} |a\rangle\langle d|. \tag{3.54}$$

If ε_0 is not a multiple of the cavity frequency ω_c the only way for two states $|a\rangle$ and $|b\rangle$ to have $E_a = E_b$ is that $|a\rangle = |b\rangle$. Then we find

$$A \simeq \int_0^{+\infty} \sum_{\alpha,a,b} \mathcal{C}_\alpha^+(\tau) D_{ab}^\dagger \rho_{SIbb} D_{ba} e^{i(E_b - E_a)\tau} d\tau \tag{3.55}$$

We can perform the integral over τ in Eq. (3.52) using Eq. (3.31) and find

$$A = \sum_{ab} \Gamma_{ab} \rho_{SIbb}, \tag{3.56}$$

where Γ_{ab} is the transition rate given by the Fermi's golden rule between two eigenstates of H_0. Applying this result on each term of Eq. (3.39) we show that the populations approximately evolves following the rate equations

$$\begin{aligned} \dot{P}(q,n) = &\sum_{q',n'} \Big\{ \Gamma_{q'n'}^{qn} P(q',n') - \Gamma_{qn}^{q'n'} P(q,n) \Big\} \\ &+ \kappa(1+n_B) \Big\{ (n+1)P(q,n+1) - nP(q,n) \Big\} \\ &+ \kappa n_B \Big\{ nP(q,n-1) - (1+n)P(q,n) \Big\}, \end{aligned} \tag{3.57}$$

where $P(q,n)$ is the population of the state $|q,n\rangle$ with q its charge and n its photon number and $\Gamma_{qn}^{q'n'}$ is the transition rate from the state $|q,n\rangle$ to the state $|q',n'\rangle$. When $\kappa = 0$ this is exactly the rate equations used to study the Franck-Condon blockade regime in [86, 88] in molecular electronics. The transition rates $\Gamma_{qn}^{q'n'}$ can be found from the Fermi's golden rule

$$\begin{aligned} \Gamma_{0n}^{1n'} &= \sum_\alpha \Gamma_\alpha |F_{n,n'}|^2 f_\alpha^+([n'-n]\omega_c) \\ \Gamma_{1n}^{0n'} &= \sum_\alpha \Gamma_\alpha |F_{n,n'}|^2 f_\alpha^-([n-n']\omega_c) \end{aligned} \tag{3.58}$$

where $F_{n,n'} = \langle n | e^{\lambda(a-a^\dagger)} | n' \rangle$ is the Franck-Condon matrix element [88]

$$F_{n,n'} = (\mathrm{sgn}(n'-n))^{n-n'} e^{-\lambda^2/2} \lambda^{M-m} \sqrt{\frac{m!}{M!}} L_m^{M-m}(\lambda^2), \tag{3.59}$$

with $m = \min(n,n')$ and $M = \max(n,n')$ and L_α^β are the generalised Laguerre polynomials. The physical process described by the rates in

Eq. (3.58) is the tunneling of an electron between one electrode and the quantum dot with emission or absorption of $n' - n$ photons in the cavity. Taking a closer look at the rates $\Gamma_{qn}^{q'n'}$ the Franck-Condon matrix elements act as intensity factor for the rate while the Fermi distributions $f_\alpha^\pm$ give the energy condition for the rate to be different than zero. We see in Eq. (3.58) that an electronic rate corresponding to the charge of the dot is turned on when $eV_\alpha > (n' - n)\omega_c$, while a rate to discharge the dot is turned on when $eV_\alpha < (n' - n)\omega_c$.

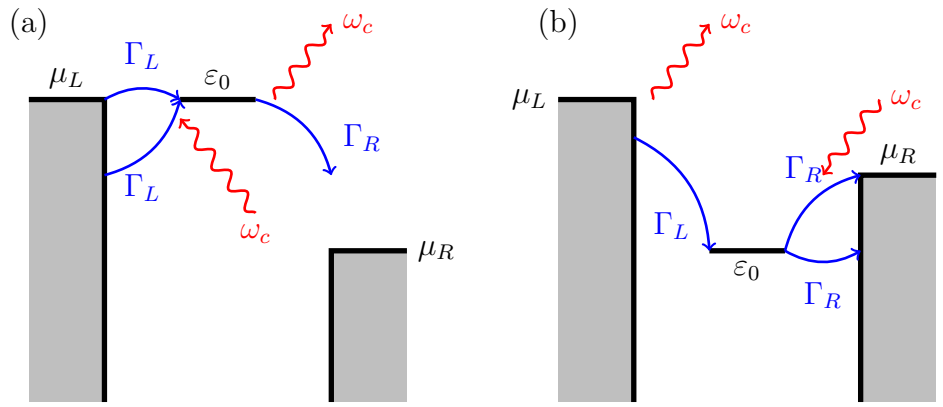

Figure 3.2: Example of configurations of the leads for excitation or dissipation of the cavity mode by the electronic transport from electron tunneling out of or in the dot. Γ_α is the tunneling rate between the dot and the lead α, ω_c the cavity frequency, ε_0 the dot energy and eV_α is the voltage drop between the lead α and the dot energy level.

Fig. 3.2 shows a schematic representation of the processes occurring in the setup where ε_0 shows the dot energy level and $\mu_{L/R}$ shows the position of the left and right potentials. The red arrows show the absorption and emission of photons required for the tunneling event to take place so that the energy balance is fulfilled. Although this representation depicts well the relative positions of the energies in the system, it does not show the actual energy conditions that matter for understanding the rate equations. Indeed, we have seen that thanks to the electron-photon coupling there are actually several channels through which electrons can tunnel. Here, we call a channel the transition from a state $|q, n\rangle$ to a state $|q', n'\rangle$. For each channel there is an energy condition $\varepsilon_0 + k\omega_c$ to be fulfilled for an electron to be able to go through, where $k = n' - n$ is a relative integer.

Fig. 3.3 shows a schematic representation of the energy thresholds corresponding to all the tunneling channels. The relative positions of the electronic leads' potentials with respect to the dot energy level $eV_{L/R}$ are represented by the gray areas while in the middle is given the ladder of energy conditions corresponding to the different types of electronic channels. The channel labeled 0 corresponds to the elastic transport for which no energy is exchanged with the cavity mode. Then the other channels are labeled by $k\omega_c$ with $k \in \mathbb{Z}^*$. k is the number photons created in the cavity during a charging event of the dot, while if the

event corresponds to the electron leaving the dot, it is $-k$ which is the number of photons emitted in the cavity. It means that one energy level $k\omega_c$ corresponds to an infinite number of processes in which $n' - n = k$ where n is the number of photons in the cavity before the tunneling event and n' is the number of photons in the cavity after the tunneling event. The blue arrows show the direction of the electron during the tunneling event with respect to each electronic leads, the middle area corresponding to the quantum dot location. If an arrow has two heads, it means that the electron can go in or out of the dot, if both arrows point toward a lead, this means that the dot can only be discharged and therefore can't be populated, on the contrary if the two arrows point toward the dot it means that the dot can only be charged. In those two cases there is no current through the corresponding channels.

As a summary, if $eV_\alpha > k\omega_c$, all the tunneling event resulting in the emission of k photons while the dot is being charged in the cavity are allowed while if $eV_\alpha < -k\omega_c$ all the tunneling events resulting in the emission of k photons while the dot is being discharged are allowed.

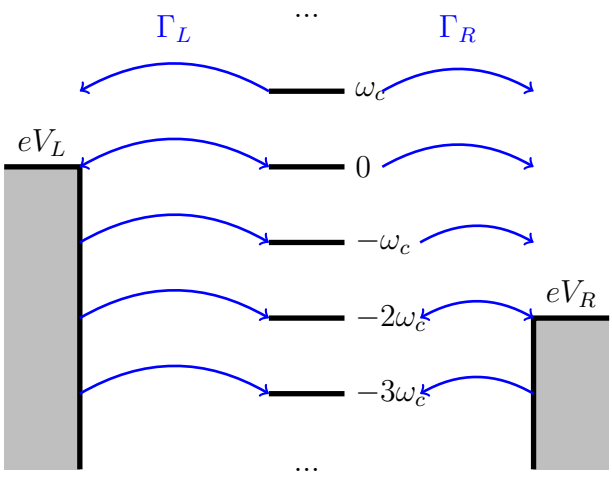

Figure 3.3: Schematic representation of the electronic channels located by the energy condition for the electron to pass through a channel. eV_α gives the relative position of the lead α chemical potential with respect to the dot energy level ε_0 while a tunneling event resulting in the creation of k photons in the cavity is depicted by an energy $k\omega_c$. The blue arrows show the direction of the electron during a tunneling event where the middle area corresponds to the quantum dot. Therefore an arrow going from lead α to the energy level $k\omega_c$ means that an electron can charge the dot creating k photons in the cavity during the tunneling event. Γ_α is the tunneling rate associated to lead α.

Looking at Fig. 3.3 or Eq. (3.58) we see that if both the voltage drops are in $]-\omega_c;\omega_c[$ (disregarding thermal effects), then only elastic tunneling is possible, therefore, the number of photon in the cavity is not affected by the electronic current and the cavity should remain in its initial state. Now if one of the leads has its voltage drop decreased then only the tunneling events resulting in the decrease of the number of photons in

the cavity are allowed and the electronic current can only relax the cavity mode. Therefore, if we start from a cavity at thermal equilibrium with $k_B T \ll \omega_c$, since photons can't be emitted in the junction and the cavity is initially in its ground state, only the charge transfer occurs. However, if one of the voltage drops is raised above the first inelastic threshold at ω_c, the electronic leads can exchange energy with the cavity during a tunneling event and a new channel opens each time the voltage drop verifies $|n' - n| = \lfloor |eV/\omega_c| n \rfloor$.

Remark. *The probability of the processes described in Fig. 3.2 depends on the probability of the stationary state. It is to be expected that the probability of a state with a high number of photons is very small and therefore a process requiring an absorption of photons very unlikely, even if the rate is big, for a cavity that is not driven by a source of light or a very large voltage drop compared to the cavity frequency.*

3.4 Populations

The first step to find any physical quantity is to find the populations or more generally to solve the master equation and find ρ. As usually in experiment only the long time behaviour of a system is measured, we look for the stationary solution of Eq. (3.50) or Eq. (3.57). In the case of the master equation Eq. (3.50), as we mentioned, we can't find an analytical solution. However, this equation can be solved numerically, see appendix A. For this purpose, we developed a code able from a system Hamiltonian of the form (3.8) and an interaction Hamiltonian of the form (3.15) to find the superoperator $\check{\mathcal{L}}$ or the corresponding rate equations and compute the stationary solution of Eq. (3.50) or Eq. (3.57).

However, some interesting approximations can be made in order to find an analytical solution of the rate equations. As we mentioned, the plasmonic cavity formed by the STM has been reported to have a very large damping rate [28]. In this case we have $\kappa \gg \Gamma$, which means that the rates governing the evolution of the populations in the rate equations are dominated by the rates proportional to κ which only acts on the photonic populations $P_p(n)$. Under those conditions, we can assume that the photonic population P_p remain close to their equilibrium distribution. In molecular electronics this is known as equilibrated phonons.

As a first approximation we consider the charge states and the photonic states to be close to independent. This means that the joint probability of the photons and the electrons $P(q, n)$ is approximated by $P(q, n) = P_c(q)P_p(n)$. As a result this allows us to write rate equations for the photons or for the charge summing Eq. (3.57) over q or n

respectively.

$$\dot{P}_c(q) = \sum_{q'} \Big\{ \Gamma^q_{q'} P_c(q') - \Gamma^{q'}_q P_c(q) \Big\} \tag{3.60}$$

$$\begin{aligned} \dot{P}_p(n) = & \sum_{n'} \Big\{ \bar{\Gamma}^n_{n'} P_p(n') - \bar{\Gamma}^{n'}_n P_p(n) \Big\} \\ & + \kappa(1+n_B)\Big\{ (n+1)P_p(n+1) - nP_p(n) \Big\} \\ & + \kappa n_B \Big\{ nP_p(n-1) - (1+n)P_p(n) \Big\}, \end{aligned} \tag{3.61}$$

where

$$\Gamma^{q'}_q = \sum_{n,n'} \Gamma^{n'q'}_{nq} P_p(n) \tag{3.62}$$

and

$$\bar{\Gamma}^{n'}_n = \sum_{q \neq q'} \Gamma^{q'n'}_{qn} P_c(q). \tag{3.63}$$

The solution of Eq. (3.60) is

$$P_c(q) = \Gamma^q_{q'} / \sum_\alpha \Gamma_\alpha. \tag{3.64}$$

Hence, the population of the dot is directly proportional to the rate for an electron tunneling into the dot. From Eq. (3.62) we assume that the photons are equilibrated $P_p(n) = P^{eq}_p(n) = e^{-n\omega_c/k_BT}(1 - e^{-\omega_c/k_BT})$. Since $k_BT \ll \omega_c$ we can take the limit $P^{eq}_p(0) = 1$ and then the populations are

$$\begin{cases} P_c(1) = \dfrac{\sum_{\alpha n} \Gamma_\alpha \frac{\lambda^{2n}}{n!} f^+(n\omega_c - eV_\alpha)}{\sum_{\alpha n} \Gamma_\alpha \frac{\lambda^{2n}}{n!} \left[f^+(n\omega_c - eV_\alpha) + f^-(-n\omega_c - eV_\alpha) \right]} \\ P_c(0) = \dfrac{\sum_{\alpha n} \Gamma_\alpha \frac{\lambda^{2n}}{n!} f^-(-n\omega_c - eV_\alpha)}{\sum_{\alpha n} \Gamma_\alpha \frac{\lambda^{2n}}{n!} \left[f^+(n\omega_c - eV_\alpha) + f^-(-n\omega_c - eV_\alpha) \right]}, \end{cases} \tag{3.65}$$

where $eV_\alpha = \mu_\alpha - \varepsilon_0$.

3.5 Electronic current

The electronic current is computed from the evolution of the number of charges in one electronic reservoirs $N_\alpha = \sum_k c^\dagger_{\alpha k} c_{\alpha k}$

$$I_\alpha = -e\dot{N}_\alpha = ie \sum_k \Big\{ t_{\alpha k} c^\dagger_{\alpha k} D - t_{\alpha k} c_{\alpha k} D^\dagger \Big\}. \tag{3.66}$$

The average current from lead α is then computed thanks to the density matrix

$$\langle I_\alpha \rangle = -e \mathrm{Tr}(I_\alpha \dot{\rho}). \tag{3.67}$$

When we derived Eq. (3.50) we stopped at order 2 in the rates $t_{\alpha k}$ and l_q. In order to have a current at the same order in $t_{\alpha k}$ we therefore use an expansion at first order in the tunneling Hamiltonian for the density

matrix, since the current operator is also an operator of order one in the tunneling rates. We hence use Eq. (3.21) into Eq. (3.67) in the interaction picture to find an adequate expression of the average current

$$\langle I_\alpha \rangle = ie\mathrm{Tr}(\mathrm{I}_{\alpha\mathrm{I}}(\mathrm{t})\rho_{\mathrm{I}}(\mathrm{t}_0)) - e\int_{t_0}^{t} \mathrm{Tr}(I_{\alpha I}(t)[H_{\mathrm{int}I}(t'), \rho_I(t')])dt'. \quad (3.68)$$

As the first term is proportional to the average current at time t_0 this term is 0. The second term can be treated the same way we derived the time evolution of the reduced density matrix. Using the Born-Markov approximation and the invariance of the trace under permutation we find

$$\langle I_\alpha \rangle = 2e\sum_\alpha \mathrm{Re}\int_0^{+\infty} \Big\{\mathcal{C}_\alpha^+(\tau)S^I_{DD^\dagger}(t,t') - \mathcal{C}_\alpha^-(\tau)S^I_{D^\dagger D}(t,t')\Big\}d\tau, \quad (3.69)$$

where $S^I_{AB}(t,t') = \langle A_I(t)B_I(t')\rangle$ is the correlation function between A at time t and B at time t' in the interaction picture. To compute the average current corresponding to the rate equations, we have to also perform the same secular approximation we used on the density matrix on the average current in Eq. (3.69). We show the calculation for the first correlation $S_{DD^\dagger}(\tau)$.

$$S_{DD^\dagger}(t,t') = \sum_{abc} D_{ab}D^\dagger_{bc}\rho_{Sca}e^{i(E_a-E_c)t}e^{i(E_c-E_b)\tau}. \quad (3.70)$$

We neglect in Eq. (3.70) the fast oscillating terms for which $E_a \neq E_c$ which means that we only take into account terms for which $|a\rangle = |c\rangle$

$$S_{DD^\dagger}(t,t') \simeq \sum_{ab} D_{ab}D^\dagger_{ba}\rho_{Saa}e^{i(E_c-E_b)\tau}. \quad (3.71)$$

Using Eq. (3.71) in Eq. (3.69) and integrating over τ, we find

$$\langle I_\alpha \rangle \simeq -e\sum_{nn'} \Big\{\Gamma^{0n'}_{1n:\alpha}P(1,n) - \Gamma^{1n'}_{0n:\alpha}P(0,n)\Big\}. \quad (3.72)$$

Injecting Eq. (3.65) into Eq. (3.72) we find the average current when the charge states and the photonic states can be considered independent in the case of symmetric voltage drops $V_L = -V_R = V$

$$\langle I_\alpha \rangle \simeq I_0\sum_n \mathcal{P}(n)[f(n\omega_c - eV) - f(n\omega_c + eV)], \quad (3.73)$$

Where $\mathcal{P}(n) = \lambda^{2n}e^{-\lambda^2}/n!$ is the Poisson distribution of parameter λ^2 and $I_0 = e\Gamma_L\Gamma_R/(\Gamma_L+\Gamma_R)$. Although this expression only applies in the case of equilibrated photons, we see that the current evolves in steps each time a voltage drop attains a multiple of the photon energy, similarly to the Franck-Condon physics [82, 86, 88]. The height of the step is given by the Poisson distribution, which means that the current is suppressed at low bias voltage. This shows how the energy of the leads is dissipated inside the cavity mode.

3.6 Results on the rate equations

3.6.1 Effect of the voltage

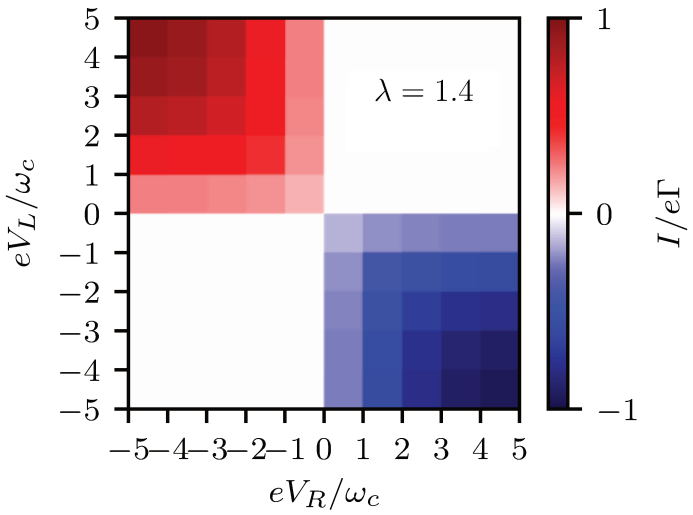

Figure 3.4: Electronic current as a function of the voltage drops eV_L and eV_R for $\lambda = 1.4$. The model parameters are $\kappa = 10k_BT = 0.1\omega_c$ and $\Gamma_L = \Gamma_R = 10^{-3}\omega_c$. Reproduced from Ref. [93].

Fig. 3.4 reports the electronic current I as a function of the relative voltage drops eV_L and eV_R in a regime of parameters that should correspond to an actual experimental setup. See appendix A for the numerical implementation. Here, we clearly see the similarities with the Franck–Condon blockade. The $\{eV_L, eV_R\}$ plan is separated in squared region in which the current is approximately constant. The length of those square region is given by the energy of one photon ω_c. Eq. (3.73) should give a good approximation of a cut along the line $eV_L = -eV_R$ on Fig. 3.4 where we can see the low bias current suppression. This kind of 2_D map is particularly interesting as it allows us to cover all kind of setups for the voltage drops. Therefore a cut along the diagonal between the upper left corner and the lower right corner of Fig. 3.4 shows the evolution of the current for a symmetrically biased junction to which equation Eq. (3.73) corresponds. A vertical cut on Fig. 3.4 corresponds to a junction in which the right voltage drop is constant and only the left one is varying. This would be typically the case for an STM experiment. Fig. 3.5 shows a closer look at the current for a symmetrically biased junction for six different values of the coupling strength λ.

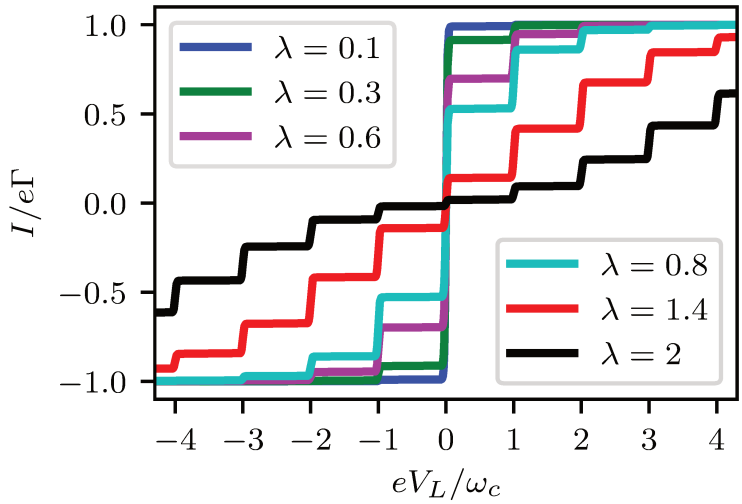

Figure 3.5: Electronic current as a function of the voltage drops eV_L for different values of the coupling strength λ. The model parameters are $\kappa = 10k_BT = 0.1\omega_c$ and $\Gamma_L = \Gamma_R = 10^{-3}\omega_c$.

As expected the suppression of the current increases with the coupling strength and we clearly see the steps of the current at each inelastic threshold, where photons are emitted or absorbed in the cavity. Fig. 3.6 shows the height of the consecutive steps of the current for a set of different values of the coupling strength for a large damping rate of the cavity. As $\kappa \gg k_BT \gg \Gamma$ it is to be expected that the photon population is always very small and thus that $P_p(0) \gg P_p(n)$ for any integer $n > 0$. Moreover we argued earlier that the rate governing the photonic population $P_p(n)$ are dominated by the terms in κ thus the probabilities of a charge state and a photonic state should be close to independent as photon should remain equilibrated. As we predicted that the electronic current for the equilibrated photons should be described by the Poissonian partition function, Fig. 3.6 shows that for $\kappa = 0.1\omega_c$ the approximation of equilibrated photons is valid in this case as the electronic current as a function of the voltage does not deviate much from the Poisson partition function. In fact we see that the stronger the coupling strength the less accurate this approximation is, however in an experimental setup we don't expect coupling strength higher than 10% of the photon energy. Therefore Eq. (3.73) gives a good estimate of the current in the case $\kappa \gg \Gamma$ and the current is proportional to the Poisson partition function.

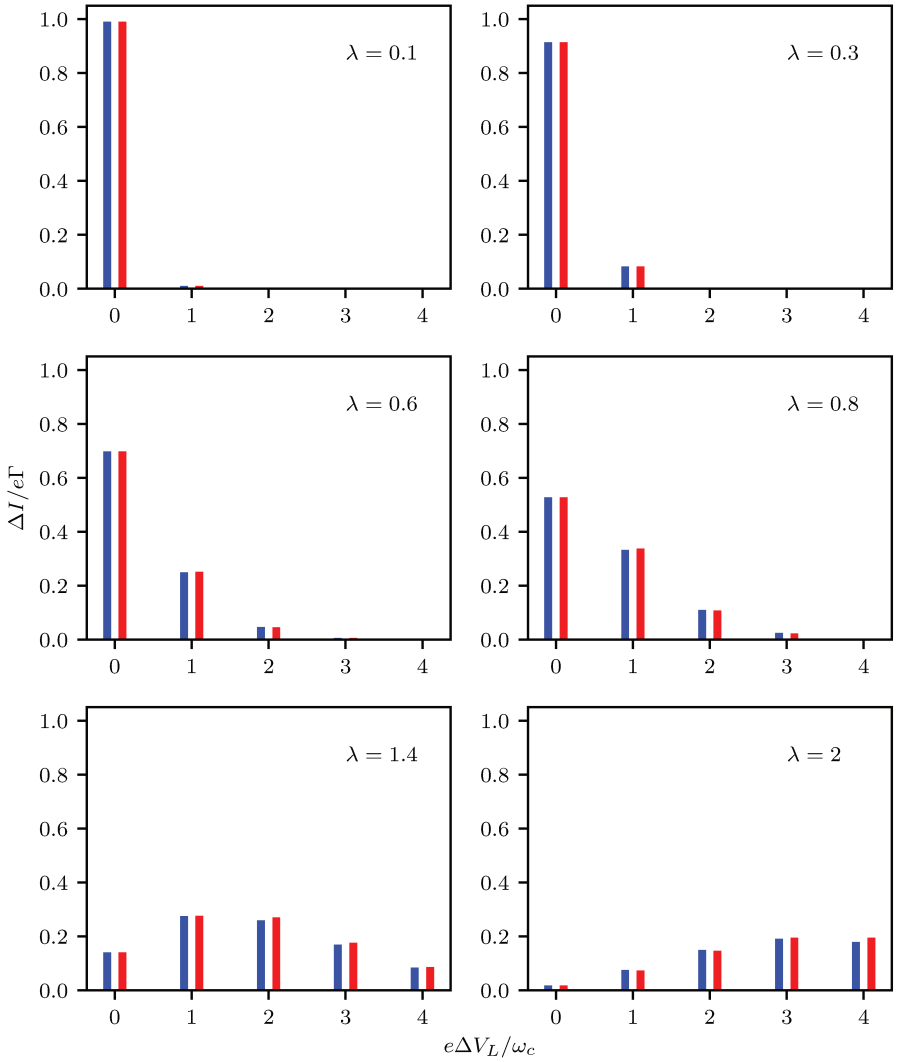

Figure 3.6: Steps heights of the electronic current (in blue) compared to the Poisson distribution (in red) for a symmetric junction ($V_L = -V_R$) with parameters $\kappa = 10k_BT = 0.1\omega_c$ and $\Gamma_L = \Gamma_R$.

Eq. (3.73) also predicts an exponential decrease of the first step's height with the square of the coupling strength λ which is shown in Fig. 3.7.

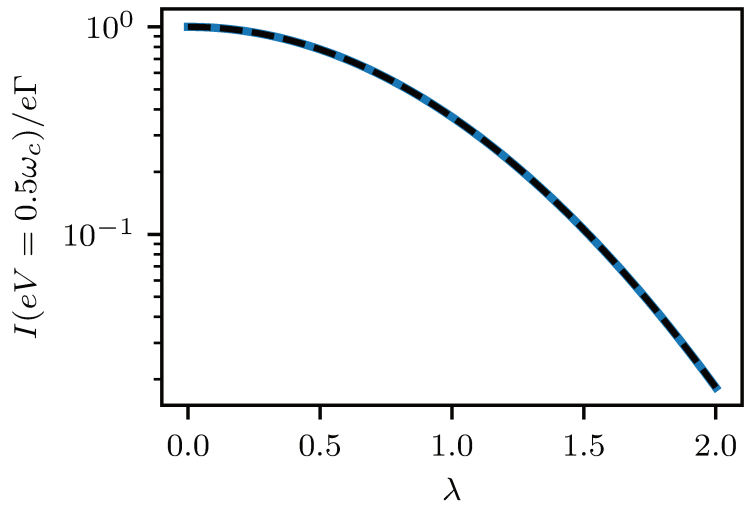

Figure 3.7: Plain blue curve: value of the current I at $eV_L = 0.5\omega_c$ as a function of the coupling strength λ in the case of a fully symmetric junction ($V_L = -V_R = V$, $\Gamma_L = \Gamma_R = 0.001\omega_c$ and $\kappa = 10k_BT = 0.1\omega_c$). In dashed black is represented the expected dependence $\ln(I/\Gamma) \simeq -\lambda^2$ provided by Eq. (3.73).

3.6.2 Effect of the damping

Earlier we saw that a damping rate κ of the cavity of orders of magnitude bigger than the tunneling rates allows us to decouple the electronic state from the photonic state of the cavity. However, we also expect it to have an effect on the current steps' height and width as it is the dominant dissipation mechanism when κ is even larger than k_BT, which is reported to be the case in plasmonic cavities. Fig. 3.8 shows the evolution of the current as a function of the damping rate of the cavity κ at $eV = 2.5\omega_c$ for both a symmetrically (panel (a)) and non-symmetrically (panel (b)) biased junction for three different values of the coupling strength λ. We see in both panel (a) and (b) that as soon as the damping rate of the cavity becomes of the same order as the tunneling rate Γ, the current does not depend much on κ and reaches the strong cavity damping limit. We see for $\lambda = 0.8$ that both for panel (a) and (b) the current increases with κ. This comes from the fact that an increasing damping rate of the cavity implies that the probability of having 0 photons inside the cavity increases accordingly.

Fig. 3.9 shows the evolution of $P_p(0)$ as a function of the coupling strength in panel (a) at $eV_L = -eV_R = 1.5\omega_c$ and as a function of the $eV = eV_L = -eV_R$ in panel (b) for $\lambda = 1.4$ for three different values of κ in both panels. Panel (a) shows that $P_p(0)$ has a minimum close to $\lambda = 1$. This minimum is due to $\Gamma_{q0}^{q'1}$ reaching a maximum. However as the damping rate increases, the population is less sensible to Γ and therefore to the modification of the coupling strength since at large damping rate the effect of κ dominates over the effects of Γ. Panel (b) shows that this

effect is seen along all the voltage drop axis.

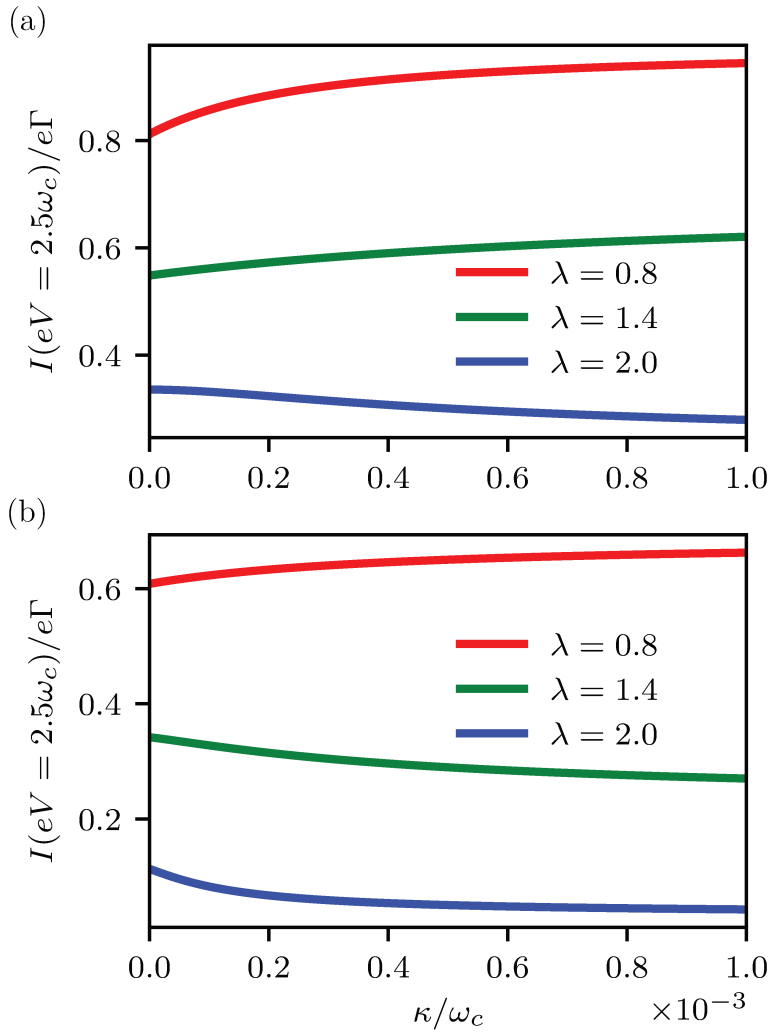

Figure 3.8: Current as a function of the damping rate of the cavity κ at $eV = 2x.5\omega_c$ for (a) a symmetrically biased junction ($V_L = -V_R = V$) and (b) an asymmetrically biased junction ($V_L = V$ and $V_R = -0.5\omega_c$) for three different values of the coupling strength λ. In both cases $\Gamma_L = \Gamma_R = 10^{-3}\omega_c$ and $k_BT = 10^{-2}\omega_c$.

In Fig. 3.8 for $\lambda = 1.4$ the behaviour changes depending on the fact that the junction is symmetrically biased or not. From Eq. (3.58) we know that for a coupling strength $\lambda < 1$ the dominant rates are the ones that conserve the number of photons in the cavity $\Gamma_{qn}^{q'n}$ and in particular $\Gamma_{q0}^{q'0}$ is the biggest one. Since in Eq. (3.72) the electronic current is given by the product between the rates and the populations, we understand from the fact that $\Gamma_{q0}^{q'0}$ is the biggest rate that the contributions associated with $P_p(0)$ has the most impact on the current. Therefore increasing $P_p(0)$ results in the increase of the current we see in Fig. 3.8. On the contrary when $\lambda = 2$ the dominant rates are no longer the rates that conserve the number of photons in the cavity as the rates increase with

the number of photons exchanged up to $\Delta n = 4$, where Δn is the number of photons exchanged, and then decrease with Δn from this value. Therefore when κ increases, it reduces the probability of the states with $n > 0$ and thus the current only goes through channels with a smaller rate Γ resulting in the decrease of the current.

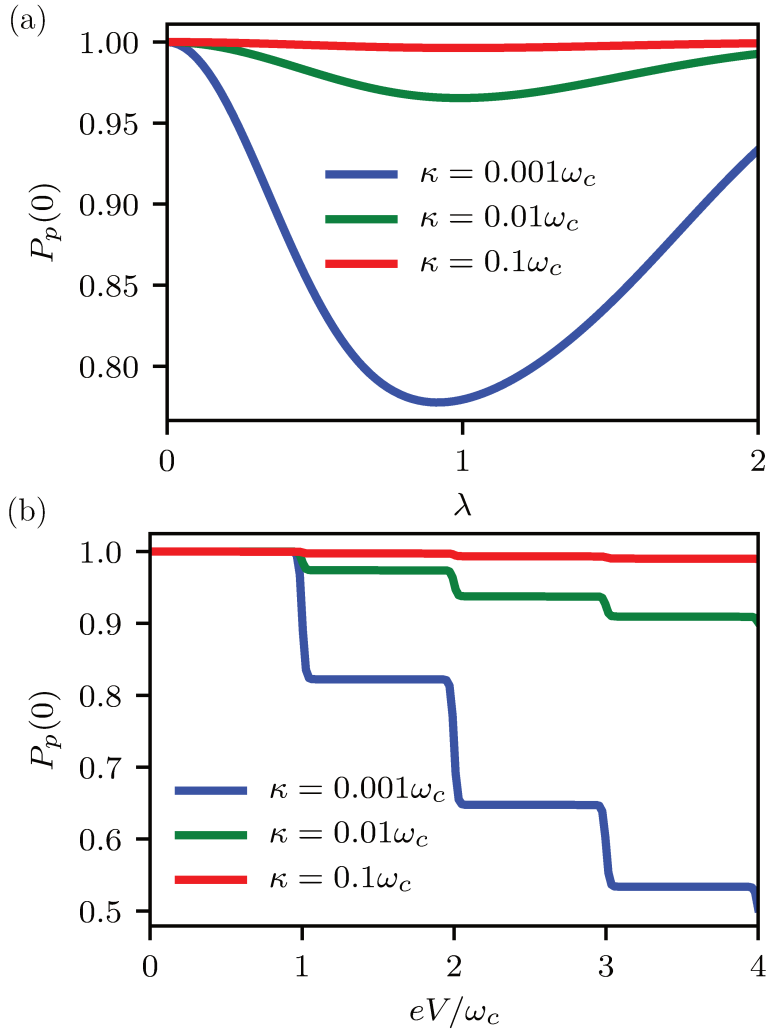

Figure 3.9: Probability of having no photon in the cavity $P_p(0)$ as a function of (a) the coupling strength λ at bias voltage $eV = 1.5\omega_c$ and (b) the bias voltage with coupling strength $\lambda = 1.4$. Both for of a fully symmetric junction ($V_L = -V_R = V$, $\Gamma_L = \Gamma_R = 0.001\omega_c$ and $k_BT = 0.01\omega_c$) and three different values of the damping rate of the cavity κ.

The case $\lambda = 1.4$ seems a bit peculiar since it behaves differently when the junction is symmetrically biased compared to when it is not. We know from Eq. (3.58) that for $\lambda = 1.4$ the biggest contribution in the electronic current comes from the 0 occupancy state of the dot and the cavity $|0, 0\rangle$. The second biggest contribution comes from the state $|1, 0\rangle$ with a negative contribution. In the case of the symmetrically biased junction, we can apply the same reasoning as for $\lambda < 1$ since

as $P_p(0)$ increases the electronic current also increases due to Γ_{00}^{12} being the biggest rate. Therefore when κ increases, $P_p(0)$ also increases and since in Eq. (3.73) the contribution from Γ_{00}^{12} is proportional to $P_p(0)$, the current increases.

However, for the asymmetrically biased junction, the channels at negative energy thresholds can only charge the dot for the two electrodes. Therefore, it introduces an asymmetry between the probability of occupancy of the dot since it is more likely that the dot is charged. Fig. 3.10 shows a schematic representation of this asymmetry. While all the negative energies contribute to the charged state of the dot only the energies above eV_L contributes to the empty state of the dot. The energies between eV_L and eV_R have contributions to both states therefore summing over all the energy we see that there are $\lfloor |e(V_L - V_R)/\omega_c| \rfloor$ more energy thresholds contributing to the charged state of the dot. Hence when κ increases and therefore $P_p(0)$ it is in fact mostly $P(1,0)$ which increases. As mentioned $|1,0\rangle$ has a negative contribution to the current which explains that in this case the current decreases.

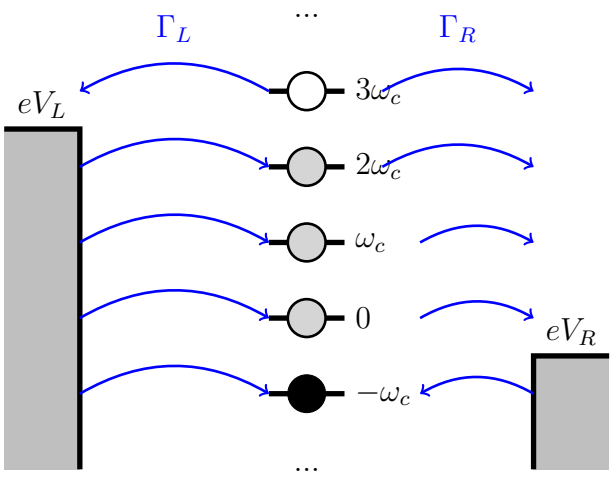

Figure 3.10: Schematic representation of the energy levels of the system relative to the dot energy ε_0. eV_α gives the relative position of the lead α chemical potential with respect to the dot energy level ε_0. The blue arrows show the direction of the electron during a tunneling event where the middle area correspond to the quantum dot. An arrow going from lead α to the energy level $k\omega_c$ means the creation of the state $|1,k\rangle$ while an arrow turning the other way means its destruction. Γ_α is the tunneling rate associated to lead α. The dot on the energy levels represent the contribution of the state to the average number of electron on the dot. Black for 1, white for 0 and gray for $\Gamma_L/(\Gamma_L + \Gamma_R)$.

We now understand how the damping rate of the cavity affects the height of the current's steps. However, if we look at the width of the steps in Eq. (3.73), we see that the width is given by the temperature from the Fermi distribution. The width of the Fermi function is found

by finding the maximum of the absolute value of its derivative

$$f'(x) = -\frac{e^{x/k_BT}}{k_BT(1+e^{x/k_BT})^2}. \tag{3.74}$$

$|f'(0)| = 1/4k_BT$ is the maximum of $|f'|$. Then solving $|f'(x)| = |f'(0)|/2$ we find that the distance between the two roots of this equation is $k_BT\ln\left(\frac{3+2\sqrt{2}}{3-2\sqrt{2}}\right)$. Therefore, the width predicted by the rate equations depends on k_BT only and not on κ. This is confirmed in Fig. 3.11 showing the full width at half maximum (FWHM) of a conductance peak at $eV_L = 1.5\omega_c$ as a function of κ in panel (a) and k_BT in panel (b). We see in panel (a) that whatever the temperature the curves remain flat and the FWHM doesn't depend on the damping rate κ, while the panel (b) shows the same linear dependence of the FWHM with the temperature whatever the damping rate of the cavity κ.

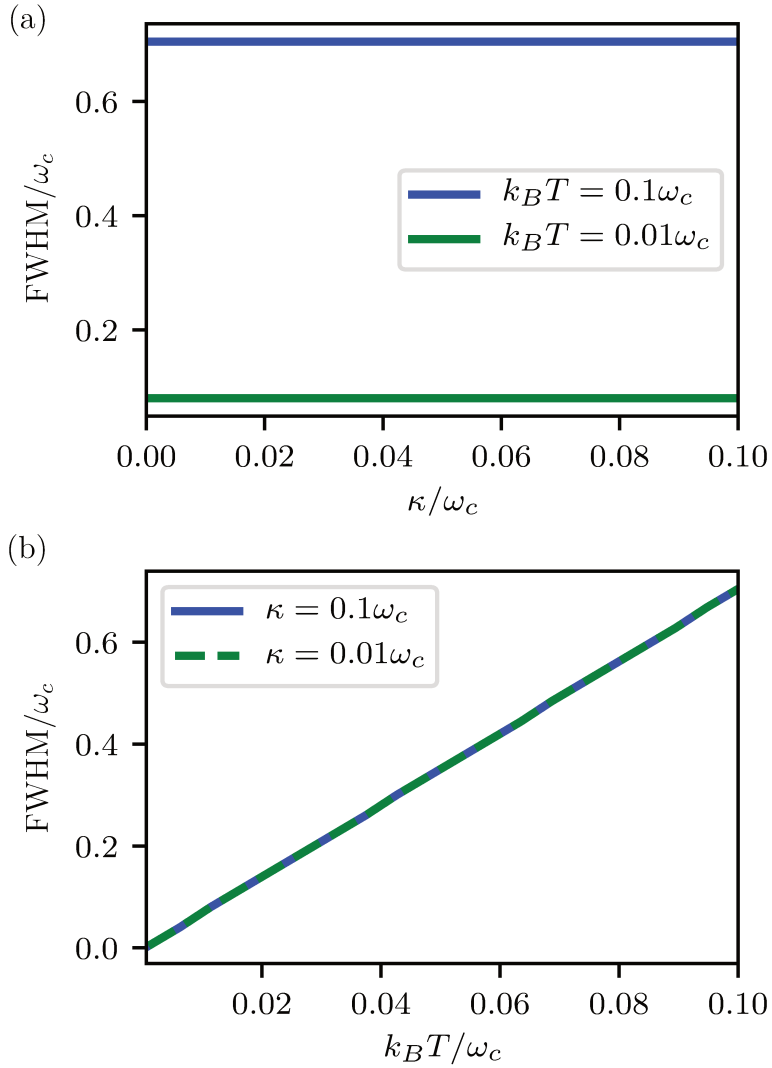

Figure 3.11: Full width at half maximum of the conductance's peak at $eV_L = \omega_c$ for a symmetrically biased junction as a function of (a) κ for two different values of the temperature k_BT and (b) k_BT for two different values of the damping rate of the cavity κ. For both panels, $\Gamma_L = \Gamma_R = 10^{-3}\omega_c$.

3.7 Full computation of the density matrix

When the damping rate of the cavity exceeds the temperature, we expect the population and the current to evolve on a scale given by κ since it is the dominant channel for dissipation. However, when we computed the current at second order in $H_{\rm int}$ in the interaction picture, we neglected terms accounting for the relaxation coming from κ. In order to recover the effect of κ on the width of each current's step we start from Eq. (3.69) and re–sum all the terms by using the full time evolution of the system instead of the system only, thus replacing e^{iH_0t} by e^{iHt},

$$\langle I_\alpha\rangle = 2e\sum_\alpha \mathrm{Re}\int_0^{+\infty}\Big\{\mathcal{C}_\alpha^+(\tau)S_{DD^\dagger}(t,t') - \mathcal{C}_\alpha^-(\tau)S_{D^\dagger D}(t,t')\Big\}d\tau, \quad (3.75)$$

where $S_{AB}(t,t') = \langle A(t)_H B_H(t')\rangle = \langle A(0)_H B_H(\tau)\rangle$. To compute the correlation functions of the dot, we can use the quantum regression theorem [94,95]. We call $\chi = B_H(\tau)\rho$. Then $\dot\chi = -i[H,\chi]$ and since D and $D^\dagger$ only act on the system, we conclude that $\chi_S(t) = \mathrm{Tr}_S(\chi(t)) = B_H(t)\rho_S$ time evolution is given by Eq. (3.48). In other words $\chi(t) = e^{\check{\mathcal{L}}t}\chi(0)$ and $S_{AB}(t,t') = S_{AB}(\tau) = \mathrm{Tr}(Ae^{\check{\mathcal{L}}t}B)$. Let us define $i_\pm^\alpha$ such that

$$i_\pm^\alpha = \int_0^{+\infty}\mathcal{C}_\pm^\alpha(\tau)e^{\check{\mathcal{L}}\tau}d\tau. \quad (3.76)$$

Using the Fourier transform of $\mathcal{C}_\pm^\alpha$, we can write $i_\pm^\alpha$ in the frequency domain instead of time domain as following

$$i_\pm^\alpha = \int_{-\infty}^{+\infty}\int_0^{+\infty}\Gamma_\alpha f_\alpha^\pm(\omega)e^{(\pm i\omega+\check{\mathcal{L}})\tau}d\tau\frac{d\omega}{2\pi}, \quad (3.77)$$

where we used the wide band approximation on Γ_α. At this point, we can perform the time integral and find an approximate expression of $i_\pm^\alpha$,

$$i_\pm^\alpha \simeq \mp\frac{\Gamma_\alpha}{2\pi}\int_{-\infty}^{+\infty}\frac{f_\alpha^\pm(\omega)}{(i\omega\mp\eta)Id\pm\check{\mathcal{L}}}d\omega, \quad (3.78)$$

where $\eta\to 0$ and Id is the identity super-operator. The full expression for the current then reads

$$\langle I_\alpha\rangle_{st} = -\frac{2e}{\pi}\Gamma_\alpha Re\Bigg\{\int_{-\infty}^{+\infty}f_\alpha^+(\omega)\,{}^t\underline{w}\check{D}\frac{1}{(i\omega-\eta)Id+\check{\mathcal{L}}}\check{D}^\dagger\underline{\rho}_s^{st} + f_\alpha^-(\omega)\,{}^t\underline{w}\check{D}^\dagger\frac{1}{(i\omega+\eta)Id-\check{\mathcal{L}}}\check{D}\underline{\rho}_s^{st}d\omega\Bigg\}. \quad (3.79)$$

This expression of the current was used in this work to compute numerically the current, see appendix A.

Remark. *In fact, in general the Born–Markov approximation is not enough to conserve the positivity of the density matrix, in our previous calculation of the current and of the rate equations, it was the secular approximation that was ensuring the positivity of the density matrix. In*

the case of Eq. (3.79), we can have an idea of the error we make on the current by considering the non-interacting case $\lambda = \kappa = 0$, case between the cavity mode and the electrons. In this case we can reduce the Hilbert space to the charge states of the molecule only and write the Liouvillian $\check{\mathcal{L}}$ as a 4×4 matrix

$$\check{\mathcal{L}} = \begin{pmatrix} -\Gamma_+ & 0 & 0 & \Gamma_- \\ 0 & -\Gamma/2 - i\varepsilon_0 & 0 & 0 \\ 0 & 0 & -\Gamma/2 + i\varepsilon_0 & 0 \\ \Gamma_+ & 0 & 0 & -\Gamma_- \end{pmatrix}, \tag{3.80}$$

where $\Gamma_\pm \sum_\alpha \Gamma_\alpha f_\alpha^\pm(\varepsilon_0)$ and $\Gamma = \sum_\alpha \Gamma_\alpha$. We can find the eigenvalues of this matrix and, therefore, directly compute the current in this case.

$$\langle I_\alpha \rangle = -\frac{e}{\pi\hbar} \int_{-\infty}^{+\infty} \sum_\beta \frac{\Gamma_\alpha \Gamma_\beta [f_\beta(\varepsilon_0) - f_\alpha(\omega)]}{[\Gamma^2/4 + (\omega - \varepsilon_0)^2]} d\omega, \tag{3.81}$$

We see that in Eq. (3.81) the term $\alpha \neq \beta$ has a Landauer-like form, however the term $\alpha = \beta$ correspond to an artifact coming from the Born–Markov approximation that is not vanishing at 0 bias voltage nor when there is only one electronic lead coupled to the transport. This error is of order $\Gamma/k_B T \ll 1$. We also see that for non-trivial cases where the junction is not fully symmetric, this expression is not current-conserving, i.e. $\langle I_L \rangle \neq \langle I_R \rangle$.

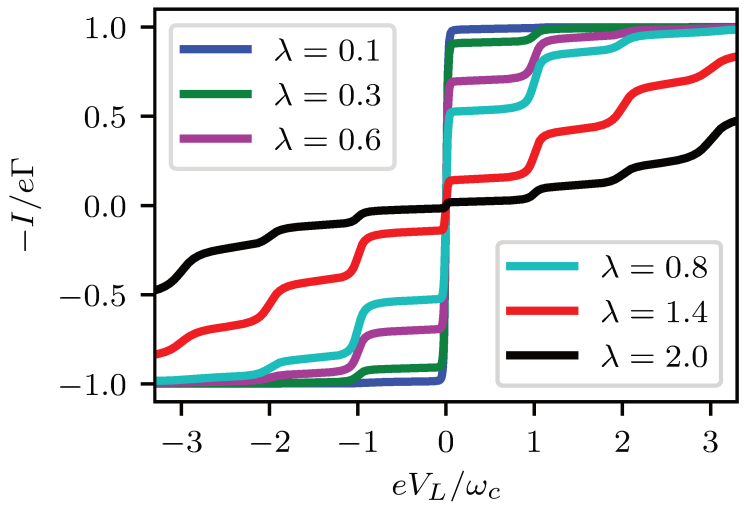

Figure 3.12: Electronic current I as a function of the left voltage drop eV_L for a symmetrically biased junction for six different values of the coupling strength λ. For all the curves $k_B T = 10^{-2}\omega_c$, $\kappa = 10^{-1}\omega_c$ and $\Gamma_L = \Gamma_R = 10^{-3}\omega_c$. Reproduced from Ref. [93].

Fig. 3.12 shows the electronic current as a function of the left voltage drop for a symmetrically biased junction ($V_L = -V_R$) at large damping rate ($\kappa = 0.1\omega_c$). We see exactly the same features as when we used the

rate equations in Fig. 3.5. The current exhibit steps each time we add to the voltage the energy of one photon, which correspond to energy being exchange between the electron and the cavity in an inelastic tunneling process. The heights of the plateaus shown in the two plots are the same which means that the rate equations predicts well the populations far from an inelastic threshold. However, we see in Fig. 3.12 that the current steps are broadened as expected.

Previous work by Braig and Flensberg [89] already shown a way to incorporate the broadening of the vibration mode into the electronic current in the Franck–Condon physics. Compared to this method, our method is able to take into account the effect of the damping of the cavity on the current without making any assumption on the photon distribution.

We know in the case of the rate equations that the width of the steps is controlled by temperature and grows as $k_B T \ln\left(\frac{3+2\sqrt{2}}{3-2\sqrt{2}}\right)$ from Eq. (3.73). Only the first step at $eV_L = 0$ is not impacted by the damping of the cavity which is explained by the fact that this step correspond to elastic tunneling of electrons where there isn't any exchange of photons. Therefore, since photons are not involved the width is only controlled by the thermal fluctuations in the electronic leads. Fig. 3.13 shows FWHM of the conductance's peak at $eV_L = \omega_c$. In panel (a) is presented the dependence of the FWHM on the damping rate of the cavity κ for two different values of the temperature and panel (b) presents the dependence of the FWHM on the temperature for two different values of the damping rate of the cavity.

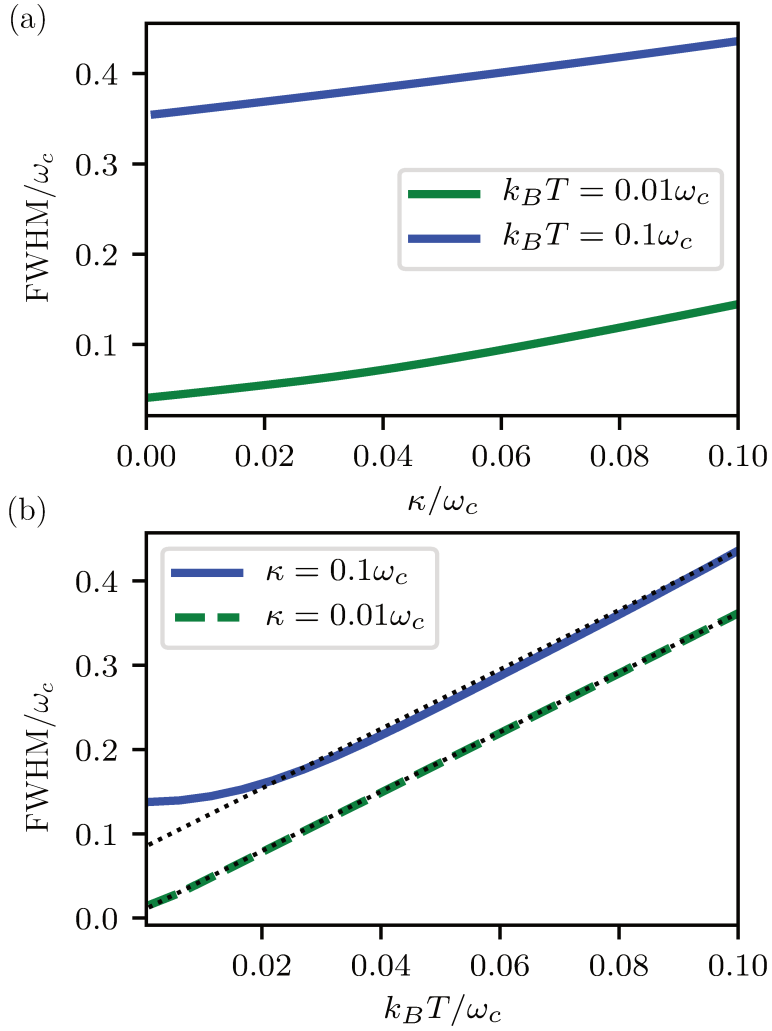

Figure 3.13: Full width at half maximum of the conductance's peak at $eV_L = \omega_c$ for a symmetrically biased junction as a function of (a) κ for two different values of the temperature k_BT and (b) k_BT for two different values of the damping rate of the cavity κ. In dashed black are the width of the Fermi distribution corresponding to each cases. For both panels, $\Gamma_L = \Gamma_R = 10^{-3}\omega_c$.

As we just discussed the expression in Eq. (3.79) allows us to take into account the broadening of the electronic current by the damping rate κ of the cavity. We see in panel (a) that at high temperature, in blue, the width grows linearly with κ, with FWHM $\simeq \kappa + k_BT\ln\left(\frac{3+2\sqrt{2}}{3-2\sqrt{2}}\right)$. This means that although the width is mostly given by the temperature when $k_BT > \kappa$ there is always a contribution proportional to κ with a ratio of ~ 1. In this regime it seems that the contribution from the temperature and from the damping rate of the cavity adds up linearly. However when the temperature is smaller, in green in Fig. 3.13, the width mixes the effect of the temperature non linearly as the slope changes when κ becomes bigger than k_BT where it is expected that the width is mostly given by κ. In panel (b), we show the dependence of the width with the

temperature k_BT for a damping rate $\kappa > k_BT$ in blue and a damping rate $\kappa < k_BT$ in green. We see that when temperature is very large compared to κ the width is only given by the width of the Fermi distribution and therefore by the temperature (shown by the lower black dotted line) and only depends on T (green curve), whereas when $\kappa > k_BT$ for very small temperature the width is only given by κ and therefore we see a plateau at low temperature for the blue curve. However when k_BT reaches 0.1κ, the FWHM grows with k_BT linearly with a slope given by the Fermi distribution as shown by the upper black dotted line.

3.8 Strong drive

3.8.1 Derivation

So far, we have studied the electronic current in a molecular tunnel junction coupled to an electromagnetic cavity in its ground state. However, it is interesting to look at the action of the cavity mode on the current. One way to do that is to drive the cavity out of its ground state. In this section we will consider that the number of photons in the cavity is kept constant thanks to the damping of the cavity. The driven system Hamiltonian is

$$H_S = \varepsilon_0 d^\dagger d + \omega_c a^\dagger a + \Lambda d^\dagger d(a + a^\dagger) + \alpha\omega_c \cos(\omega_L t)(a + a^\dagger). \tag{3.82}$$

The interaction Hamiltonian only contains the interaction between the electronic leads and the dot

$$H_{int} = \sum_{\alpha k} t_{\alpha k} c^\dagger_{\alpha k} d + H.c. \tag{3.83}$$

and the environment is only composed of the electronic leads

$$H_B = \sum_{\alpha k} \varepsilon_{\alpha k} c^\dagger_{\alpha k} c_{\alpha k}, \tag{3.84}$$

where the total Hamiltonian is $H = H_S + H_B + H_{int}$. We want to derive the master equation for this problem but first we would like to remove the time dependence from H_0. First of all we can remove the terms coupling the dot and the cavity mode $\Lambda d^\dagger d(a + a^\dagger)$ using the unitary transformation

$$U_0 = e^{\lambda d^\dagger d(a - a^\dagger)}. \tag{3.85}$$

This transforms the system Hamiltonian into

$$H'_S = [\varepsilon'_0 - 2\Lambda\alpha \cos(\omega_L t)] d^\dagger d + \omega_c a^\dagger a + \alpha\omega_c \cos(\omega_L t)(a + a^\dagger), \tag{3.86}$$

where $\varepsilon'_0 = \varepsilon_0 + \lambda^2\omega_c$. The interaction Hamiltonian is transformed into

$$H'_{int} = \sum_{\alpha k} t_{\alpha k} e^{\lambda(a - a^\dagger)} c^\dagger_{\alpha k} d + H.c. \tag{3.87}$$

In order to remove the time-dependence in the driving term $\alpha\omega_c \cos(\omega_L t)(a+a^\dagger)$, we use the unitary time-dependent transformation

$$U_1(t) = e^{i\omega_L a^\dagger a t} \tag{3.88}$$

and neglecting all terms rotating at a frequency bigger than $\omega_c - \omega_L$, we find

$$H_S'' = [\varepsilon_0' - 2\Lambda\alpha\cos(\omega_L t)]d^\dagger d + (\omega_c - \omega_L)a^\dagger a + \frac{\alpha}{2}\omega_c(a + a^\dagger) \tag{3.89}$$

for the system Hamiltonian and

$$H_{int}'' = \sum_{\alpha k} t_{\alpha k} e^{\lambda(ae^{-i\omega_L t} - a^\dagger e^{i\omega_L t})} c_{\alpha k}^\dagger d + H.c. \tag{3.90}$$

for the interaction Hamiltonian. Now we want to remove the time-dependence of the dot energy level. Here we have a dot energy which is oscillating between two leads, which is equivalent to having the leads' potential oscillating. This problem has been studied in electronic transport by C. Bruder and H. Schoeller [96]. We define the transformation

$$U_2(t) = e^{i\epsilon(t)d^\dagger d}, \tag{3.91}$$

where $\epsilon(t) = \int_0^t 2\alpha\Lambda\cos(\omega_L t')dt' = 2\alpha\Lambda\sin(\omega_L t)/\omega_L$. Using Eq. (3.91) on H_S'' removes the time variation in the dot's energy

$$H_S''' = \varepsilon_0' d^\dagger d + (\omega_c - \omega_L)a^\dagger a + \frac{\alpha}{2}\omega_c(a + a^\dagger) \tag{3.92}$$

and moves it in the tunneling rates in H_{int}''

$$H_{int}''' = \sum_{\alpha k} t_{\alpha k} e^{\lambda(ae^{-i\omega_L t} - a^\dagger e^{i\omega_L t}) + i\epsilon(t)} c_{\alpha k}^\dagger d + H.c. \tag{3.93}$$

Finally we can diagonalise H_S''' by shifting the cavity mode by $-\alpha$ using the unitary transformation

$$U_3 = e^{\frac{\alpha\omega_c}{2(\omega_c - \omega_L)}(a - a^\dagger)}. \tag{3.94}$$

In the end the system Hamiltonian is

$$H_S = \varepsilon_0 d^\dagger d + (\omega_c - \omega_L)a^\dagger a \tag{3.95}$$

and the interaction Hamiltonian is

$$H_{int} = \sum_{\alpha k} t_{\alpha k} e^{\lambda(ae^{-i\omega_L t} - a^\dagger e^{i\omega_L t}) + i\epsilon(t)} c_{\alpha k}^\dagger d + H.c. \tag{3.96}$$

where we dropped all the superscripts and redefined ϵ as

$$\epsilon(t) = \alpha\Lambda\frac{3\omega_L - 2\omega_c}{(\omega_c - \omega_L)\omega_L}\sin(\omega_L t). \tag{3.97}$$

Eq. (3.96) can be simplified further in the small coupling λ and large drive α so that $\lambda\alpha \gg \lambda$. Then the tunneling rates could be approximated by

$t_{\alpha k}(t) = t_{\alpha k}e^{-i\epsilon(t)}$. More generally, we consider that α is very large so that we can average a and $a^\dagger$ by $\sqrt{N}$. Then the Hamiltonian becomes the Hamiltonian of a single dot coupled to electronic leads

$$H_S = \varepsilon_0 d^\dagger d \tag{3.98}$$

with time-dependent tunneling rates

$$H_{int} = \sum_{\alpha k} t_{\alpha k} e^{-i\epsilon(t)} c^\dagger_{\alpha k} d + H.c. \tag{3.99}$$

where we redefined $\epsilon(t) = (2\lambda\sqrt{N} - 2\alpha\Lambda\frac{2\omega_L-\omega_c}{(\omega_c-\omega_L)\omega_L})\sin(\omega_L t)$. We define $\Delta = (2\lambda\sqrt{N} - 2\alpha\Lambda\frac{2\omega_L-\omega_c}{(\omega_c-\omega_L)\omega_L})$. We still work in the sequential tunneling regime $k_BT \gg \Gamma$, however since the driving introduces a fast time evolution for in the density matrix, we won't use the Markov approximation. As a result we find time dependent rates in the master equation. We can start from the time-evolution of the density matrix in the interaction picture in Eq. (3.18) since H_S is time independent. Then expending Eq. (3.18) at second order in H_{int}, and tracing over the leads' degrees of freedom following the derivation in [96], we find

$$\begin{aligned}\dot{\rho}_{SI}(t) = -\int_{t_0}^{t} \sum_{\alpha k} \Big\{ &[D_I(t), D_I^\dagger(t')\rho_{SI}(t')]\langle c^\dagger_{\alpha k} c\ (t)_{\alpha k}(t')\rangle \\ &+[D_I^\dagger(t), D_I(t')\rho_{SI}(t')]\langle c_{\alpha k} c^\dagger(t)_{\alpha k}(t')\rangle \Big\} dt' + H.c.\end{aligned} \tag{3.100}$$

where we defined $D = de^{-i\epsilon(t)}$. Using the Born approximation, we consider that the electronic leads are kept at thermal equilibrium since the perturbation provoked by the dot should be negligible. This approximation allows us to express the average values of the electronic leads in term of the Fermi distribution following Eq. (3.31) to Eq. (3.34). Then in the Schrödinger picture we find that the reduced density matrix ρ_S evolves following

$$\begin{aligned}\dot{\rho}_S(t) = -i[H_0, \rho_S(t)] - \int_{t_0}^{t} \sum_{\alpha k} |t_{\alpha k}|^2 e^{-iH_S(t-t_0)} \times \\ \Big([D_I(t), D_I^\dagger(t')\rho_{SI}(t')] e^{i\varepsilon_{\alpha k}(t-t')} f_\alpha^+(\varepsilon_{\alpha k}) \\ +[D_I^\dagger(t), D_I(t')\rho_{SI}(t')] e^{-i\varepsilon_{\alpha k}(t-t')} f_\alpha^-(\varepsilon_{\alpha k}) \Big) e^{iH_S(t-t_0)} dt' + H.c.\end{aligned} \tag{3.101}$$

In order to find the rate equations we project Eq. (3.101) on the dot's states $|q\rangle$ where $q \in \{0, 1\}$

$$\dot{P}_q(t) = \langle q|\dot{\rho}_S(t)|q\rangle. \tag{3.102}$$

Since $D|q\rangle = \delta_{q,1}e^{-i\epsilon(t)}$ and $D^\dagger|q\rangle = \delta_{q,0}e^{i\epsilon(t)}$, this last equation reduces to a simple expression

$$\begin{aligned}\dot{P}_q(t) = 2Re \int_{-\infty}^{t} \sum_{\alpha k} |t_{\alpha k}|^2 \Big(&\delta_{q,0} f_\alpha^-(\varepsilon_{\alpha k}) P_1(t') - \delta_{q,1} f_\alpha^-(\varepsilon_{\alpha k}) P_1(t') \\ &-\delta_{q,0} f_\alpha^+(\varepsilon_{\alpha k}) P_0(t') + \delta_{q,1} f_\alpha^+(\varepsilon_{\alpha k}) P_0(t') \Big) e^{i(\varepsilon_{\alpha k}-\varepsilon_0)(t-t') - i(\varepsilon(t)-\varepsilon(t'))} dt',\end{aligned}$$

where we took the limit $t_0 \to -\infty$. We finally have an expression of the populations as a function of time. Since the drive is periodic, it seems natural to study the Fourier transformation of the population

$$\dot{P}_q(t) = \frac{1}{\pi} Re \int_{-\infty}^{t} \int_{-\infty}^{+\infty} \sum_{\alpha} \Gamma_\alpha \left\{ (\delta_{q,0} - \delta_{q,1}) P_1(t') + (\delta_{q,1} - \delta_{q,0}) f_\alpha^+(\omega') \right\} \times e^{i(\omega' - \varepsilon_0)(t-t') - i(\varepsilon(t) - \varepsilon(t'))} d\omega' dt', \tag{3.103}$$

where we defined $\Gamma_\alpha = 2\pi \sum_k |t_{\alpha k}|^2 \delta(\omega - \varepsilon_{\alpha k})$, applied the wide-band approximation and used the fact that $P_0(t) + P_1(t) = 1$. Since P_q must be periodic due to the driving, we expand P_q into a Fourier series

$$P_q(t) = \sum_k P_q(k) e^{-ik\omega t}. \tag{3.104}$$

Integrating Eq. (3.103) over time and using $e^{-i\frac{\alpha}{\omega} sin(\omega t)} = \sum_k e^{-ik\omega t} J_k\left(\frac{\alpha}{\omega}\right)$, we find that the Fourier components of P_q follow the equation

$$\begin{aligned} -i\omega \sum_m m P_q(m) e^{-i\omega m t} = & \sum_m \Gamma (\delta_{q,0} - \delta_{q,1}) P_1(m) e^{-i\omega m t} \\ & + 2Re \left\{ \sum_{\alpha m} \Gamma_\alpha (2q-1) F_{0m}^{\Delta}(E_0^\alpha) e^{-im\omega t} \right\}, \end{aligned} \tag{3.105}$$

where we defined $F_{nm}^{\Delta}(E) = (-1)^{m-n} \sum_k J_{k+n}\left(\frac{\Delta}{\omega}\right) J_{k+m}\left(\frac{\Delta}{\omega}\right) Y(E + k\omega)$, J_n being the Bessel's functions and $Y(\omega) = \frac{1}{2}\left(f(\omega) - i\mathcal{H}[f](\omega)\right)$, where f is the Fermi distribution, $\mathcal{H}[f]$ is its Hilbert transform and $E_0^\alpha = \varepsilon_0 - \mu_\alpha$. The normalisation of the probabilities imposes that $\sum_i P_i(n) = \delta_{n,0}$. Identifying each Fourier components on each sides of Eq. (3.105), we show that

$$P_1(m) = \frac{\sum_\alpha \Gamma_\alpha \left[F_{0m}^{\Delta}(E_0^\alpha) + F_{0-m}^{\Delta *}(E_0^\alpha) \right]}{\Gamma - im\omega}, \tag{3.106}$$

for any $m \in \mathbb{N}$, and

$$P_1(m) = -P_0(m) \tag{3.107}$$

for $m > 0$ and

$$P_0(0) = 1 - P_1(0). \tag{3.108}$$

Since the real part of Y is the Fermi distribution over 2, the populations for $m = 0$ are

$$P_1(0) = \frac{1}{\Gamma} \sum_{\alpha k} \Gamma_\alpha J_k^2(\Delta/\omega) f(E_0^\alpha + k\omega). \tag{3.109}$$

So, from the Fermi distribution, the populations show steps widened by the temperature at each multiple of the photon energy, the height of the steps being given by the square of the Bessel function $J_k(\Delta/\omega)$. This is very similar to the undriven case we discussed in the previous sections except for the height that was given by the Poisson distribution [88]. The electronic current can be derived from Eq. (3.67) which in this case is equivalent to

$$\langle I_\alpha \rangle (t) = e \sum_{qq'} \int_{-\infty}^{t} \Gamma_{qq'}(t, t') [N_\alpha(q') - N_\alpha(q)] P_q(t') dt', \tag{3.110}$$

where N_α is the number of electron in the lead α and

$$\Gamma_{qq'}(t,t') = 2Re\left\{\langle q|\, H_{int}(t)\,|q'\rangle\,\langle q'|\, H_{int}(t')\,|q\rangle\, e^{i(E_q-E_{q'})(t-t')}\right\}. \quad (3.111)$$

We can write the populations P_q using their Fourier series in Eq. (3.110)

$$\langle I_\alpha\rangle(t) = e\sum_m \Gamma_\alpha P_1(m)e^{-in\omega t} - e\sum_m \Gamma_\alpha(F^{\Delta}_{0m}(E^\alpha_0) + F^{\Delta *}_{0-m}(E^\alpha_0))e^{-im\omega t}. \quad (3.112)$$

We are interested in the DC component of the current $n = 0$. Using the analytical expression of the populations from Eq. (3.8.1) in Eq. (3.112) we find

$$\langle I_\alpha\rangle = \frac{e\Gamma_L\Gamma_R}{\Gamma}\sum_k J_k^2(\Delta/\omega)\left[f(E_0^R + k\omega) - f(E_0^L + k\omega)\right]. \quad (3.113)$$

As we already mentioned for the populations, we see that the current is quantized with steps at each multiple of the drive frequency and their height is given by the square of the Bessel's functions. This formula is equivalent to the Landauer–Bütikker formula where the transmission coefficients are given by $J_k^2(\Delta/\omega)$.

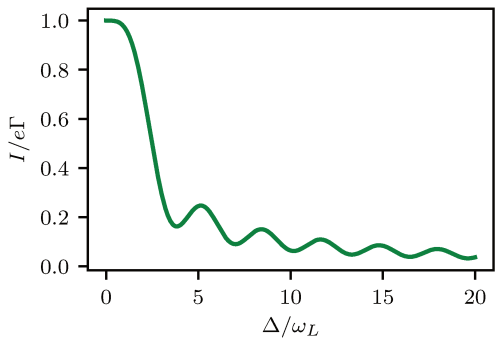

Figure 3.14: DC current as a function of the drive intensity Δ at $k_BT = 10^{-2}$ and $eV_L = -eV_R = 5\omega_L$ in a weakly coupled junction $\Gamma_L = \Gamma_R = 10^{-3}\omega_L$.

3.8.2 Results

As a result of the transmission coefficients, the DC current oscillates with Δ as shown in Fig. 3.14. This is also shown on a larger scale in Fig. 3.15. In panel (b) where we see the DC current as a function of the bias voltage and Δ in a symmetrically biased junction $eV_L = -eV_R = eV/2$ while panel (a) shows the dependence with the bias voltage and the dot energy level ε_0. We see in panel (a) that the DC current is suppressed in diamond shaped regions along the line $eV = 0$ where due to the value of Δ the first Bessel function are being suppressed. Panel (b) shows that the smallest Δ is, the less suppressed is the current around $eV = 0$ and it also shows that with Δ increasing, the current is reduced on a larger scale. In fact the DC current behave in a way very similar to the non-driven current.

Indeed in both cases the current exhibits steps and is suppressed at low voltage as the coupling strength increases. Here Δ is playing the role of the coupling strength.

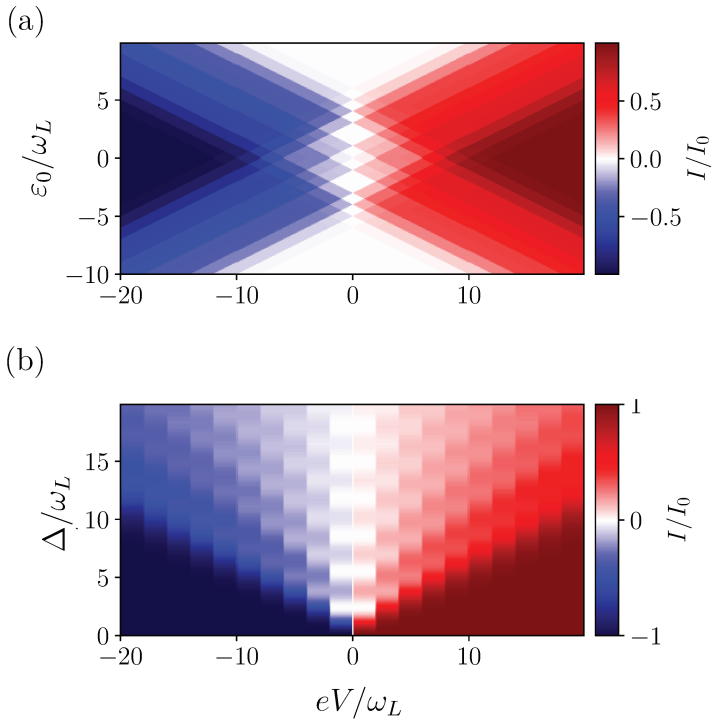

Figure 3.15: DC current as a function of (a) the bias voltage in a symmetrically biased junction ($eV_L = -eV_R = eV/2$) and the dot energy ε_0 at $k_BT = 10^{-2}\omega_L$ for a weakly coupled junction $\Gamma_L = \Gamma_R = 10^3\omega_L$ at $\Delta = 5\omega_L$. (b) is the DC current in the same junction as a function of Δ and the bias voltage with $\varepsilon_0 = 0$.

Fig. 3.16 shows some currents as a function of the bias voltage in the symmetrically biased junction for different values of Δ all taken at the same coupling strength λ. The blue curve shows the un-driven case studied in the previous sections of this chapter for which the steps are Poissonians. We see that as the average number of photons, and therefore the intensity of the drive increases, the current suppression is getting more important at low bias voltage. Therefore, we have shown that a strong drive of the cavity induces a current blockade in the junction.

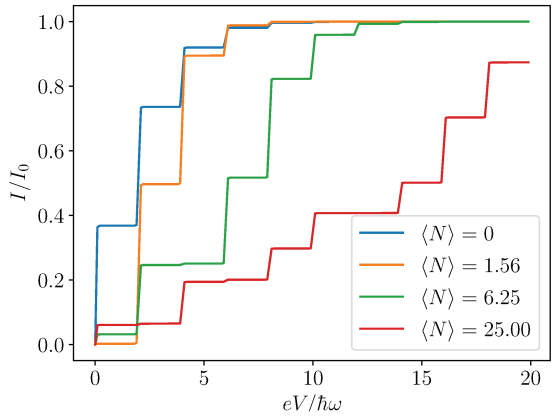

Figure 3.16: DC current as a function of the bias voltage in a symmetrically biased junction ($eV_L = -eV_R = eV/2$) weakly coupled $\Gamma_L = \Gamma_R = 10^{-3}\omega_L$, for different values of the average number of photons $\langle N\rangle = \Delta/2\lambda$ with $\lambda = 1$ and $k_BT = 10^{-2}\omega_L$.

Remark. *We have mentioned the similarities with the Franck-Condon physics as the current shows steps at the same thresholds and the current is suppressed at low voltage drops, pointing one difference in that the tunneling rates are not Poissonian but given by the Bessel's function. Another difference is that the tunneling channels in an energy diagram where organised in an infinite ladder from $-\infty$ to $+\infty$ whereas in this case only positive values are allowed.*

Chapter 4

Current-driven light emission from a single-level dot

As we emphasized in the introduction chapter 1 one major goal for mesoscopic QED as well as STM light emission experiments is to design single photon sources. Therefore, we want to know how the electronic current drives the cavity and what kind of photon distribution it generates. Also, the light emission spectrum gives an additional spectroscopic tool to explore the states of the cavity and of the electronic system. In this section we call $\lambda \leq 0.1$ the weak coupling regime and $\lambda \geq 1$ the strong coupling regime although experimentally $\lambda \sim 0.1$ is already the strong coupling regime.

4.1 Light-emission spectrum

As we mentioned while studying the current through the junction Fig. 3.5, the current characteristics shows steps corresponding to inelastic tunneling events during which light is emitted. A step occurs when the voltage drop is a multiple of the photon energy in the cavity $eV = n\omega_c$ where n is a relative integer. In fact each step corresponds to the opening of a channel for electronic transport, where a channel is in fact a process in which one electron is exchanged between the dot and one lead. In order to prove that this corresponds to light emission, one can look at the light emission spectrum of the cavity. The light emitted from the junction is proportional to the average number of photons in the cavity $\sim \kappa\omega_c\langle a^\dagger a\rangle$. Fig. 4.1 shows the average number of photons in the cavity as a function of the left and right voltage drops, eV_L and eV_R, for three different coupling strengths. We recognise in Fig. 4.1 the same step-like behaviour as the current characteristics. Each time the voltage drop hit a multiple of the energy of a photon in the cavity, the average number of photons increases abruptly. Note that at $eV_\alpha = 0$ no step is seen in the average number of photons, contrary to the current. The tunneling events occurring at $eV_\alpha = 0$ corresponds to elastic processes for which the electron conserves its energy. Therefore, no light can be emitted during these tunneling events.

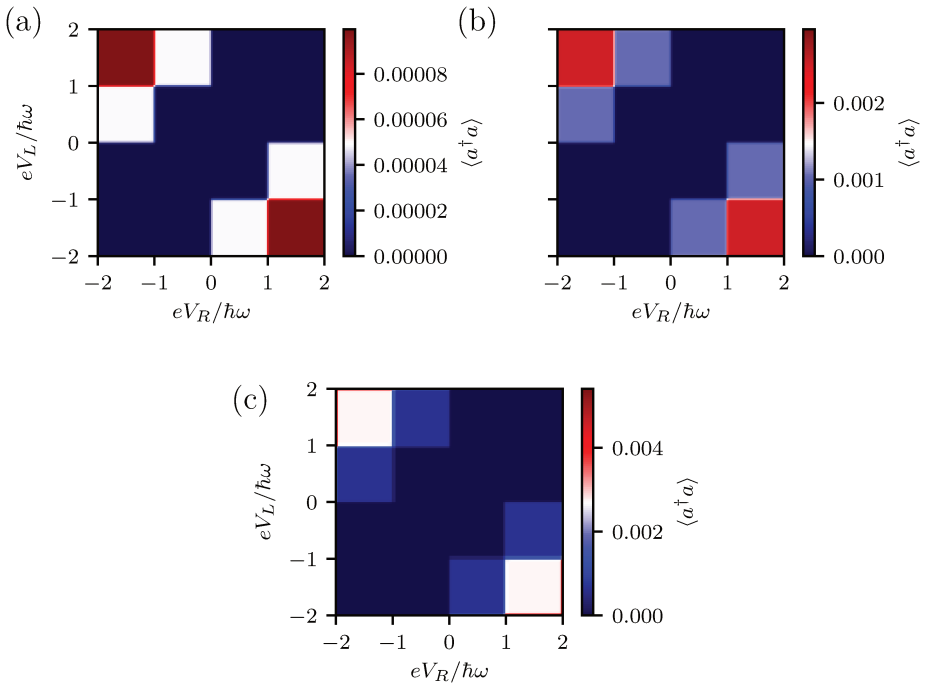

Figure 4.1: Average number of photons in the cavity N as a function of the left and right voltage drops $eV_{L/R}$ for weak coupling (a) $\lambda = 0.1$, average coupling (b) $\lambda = 0.6$ and strong coupling (c) $\lambda = 1.4$ in a strongly damped cavity $\kappa = 0.1\omega_c$ and weakly coupled tunnel junction $\Gamma_L = \Gamma_R = 10^{-3}\omega_c$ at room temperature $k_BT = 10^{-2}\omega_c$.

We have seen in chapter 3 that the rate equations Eq. (3.57), Eq. (3.60) and Eq. (3.61) are sufficient to understand the energy exchange process between the dot, the leads and the cavity. It gives a good description of the plateau in the populations. Also, the average number of photons is simply given by the photonic populations in our shifted basis, since the operator $a^\dagger a$ is diagonal in this basis. Therefore,

$$\langle a^\dagger a\rangle = \mathrm{Tr}(a^\dagger a\rho) = \sum_n nP_p(n). \tag{4.1}$$

The populations of the cavity are given, when the charge and the photons can be assumed to be independent, meaning $P(n,q) = P(n)P(q)$, from Eq. (3.61). Assuming low temperature so that $n_B \simeq 0$, Eq. (3.61) simplifies into

$$\dot{P}_p(n) = \sum_{n'} \left\{\bar{\Gamma}^n_{n'}P_p(n') - \bar{\Gamma}^{n'}_n P_p(n)\right\} + \kappa\left\{(n+1)P_p(n+1) - nP_p(n)\right\}, \tag{4.2}$$

where we remind that $\bar{\Gamma}^{n'}_n = \sum_{q\neq q'}\Gamma^{q'n'}_{qn}P_c(q)$. Thought the idea that the charge and the photonic populations are uncorrelated might seems surprising at first glance, it is in fact very natural in the case of a symmetric junction ($\Gamma_L = \Gamma_R$ and $eV_L = -eV_R = eV$). In this case the probability of any charge state is always $1/2$, whatever the value of the voltage V. Therefore, the photon emission is necessarily independent of

the charge population. In general the photon emission is a consequence of the charge's fluctuations. But not directly of the charge states of the molecule. A photon can be emitted during a tunneling event regardless of the event being the charge or the discharge of the molecule and thus regardless of the state of the molecule. However since in a lot of cases the fluctuations of the charge is correlated to the charge state the photonic state and the charge states are not independent. This is typically the case when a state of the molecule is preferred due to the fermionic environment.

Assuming the charge and the number of photons are independent, for instance in a symmetric junction, Eq. (4.2) shows that the number of photons in the cavity is regulated by two different processes. The obvious one is the relaxation of the cavity into its external environment that is described by the terms proportional to κ and the population of photons in the cavity. As we mentioned this term in plasmonic cavities is expected to be largely dominant given that $\kappa \gg \Gamma$ and ensures that the cavity is always close to its ground state. The other process acting on the photonic population is the charging and discharging of the dot given by the terms proportional to Γ. This corresponds to the inelastic tunneling of the electron. Thanks to the electron-photon coupling, electrons, while tunneling, can dissipate some energy in the cavity emitting some photons, or on the contrary, absorb some energy by absorbing some photons from the cavity.

The rates for those processes are given by $\bar{\Gamma}_n^{n'}$, which are proportional to the charge on the dot P_c. The tunneling rates, $\Gamma_{qn}^{q'n'}$, are given in Eq. (3.58). In the rates $\bar{\Gamma}$ the fact that the quantum dot is being charged or discharged is taken into account in the Fermi distributions $f^{\pm}$ and the charge probability P_c. Apart from that the photonic part, in those terms, does not depend on the charge state of the molecule. This means that as long as the energy difference appearing in the argument of the function $f^{\pm}$ is negative for the charge of the dot (f^{+}) or positive for the discharge of the dot (f^{-}), the corresponding rate is turned on and the process of emitting a photon in the cavity, or absorbing a photon from the cavity respectively, is allowed. It is only the voltage drops that regulates which process is allowed due to the state of the electronic leads, since the voltage drops also regulate the dot electronic population P_c.

Strictly speaking, each steps in the current I and photon average population $\langle a^{\dagger}a \rangle$ corresponds to the opening of new transport channels with a given energy $|eV_{\alpha}| = n\omega_c$ being exchanged. However, as this always corresponds to a transition between a state with 0 photon and a state with n photons, this can also be viewed as the spectroscopy of the cavity.

Fig. 4.1 also shows that the electronic current acting like the source of the photons in the cavity allows for the control of the intensity of the light inside the cavity. As in experiment we have typically $\kappa \gg \Gamma$ in plasmonic cavities, the typical time between two tunneling events (given by $1/\Gamma$) is much longer than the damping time (given by $1/\kappa$). In other words, a photon emitted during the tunneling of an electron

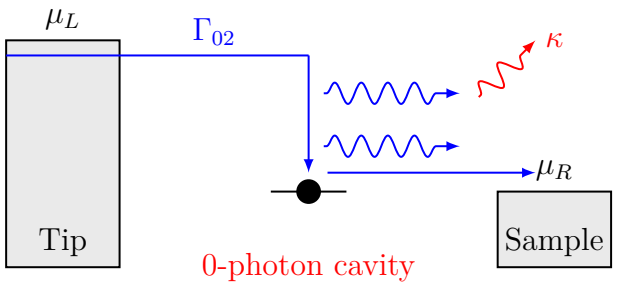

Figure 4.2: Representation of an inelastic tunneling event during which 2 photons are emitted in the empty cavity.

should dissipate before another tunneling event occurs, and therefore before another photon is emitted in the cavity. This limit corresponds to taking $P_p(0) \simeq 1$ and $P_p(0) \gg P_p(n)$ for any integer n other then 0.

Let us apply this limit to Eq. (3.57):

$$\begin{aligned}\dot{P}(q,n) =&\Gamma^{q,n}_{q',0}P(q',0) - \delta_{n,0}\sum_{n'}\Gamma^{q',n'}_{q,n}P(q,n)\\ &+\kappa(1+n_B)\Big\{(n+1)P(q,n+1) - nP(q,n)\Big\}\\ &+\kappa n_B\Big\{nP(q,n-1) - (1+n)P(q,n)\Big\}.\end{aligned} \tag{4.3}$$

For simplicity we take the symmetrically biased junction for which $\Gamma_L = \Gamma_R$ and $eV_L = -eV_R$. In this case, the electronic rates $\Gamma^{q',n'}_{q,n}$ and $\Gamma^{q',n}_{q,n'}$ are equal. This allows to find the rate equations for the photons only by summing Eq. (4.3) over the charge q, without assuming the charge and the photons to be independent.

$$\begin{aligned}\dot{P}_p(n) =&\Gamma_{0n}P_p(0) - \delta_{n,0}\sum_{n'}\Gamma_{nn'}P_p(n)\\ &+\kappa(1+n_B)\Big\{(n+1)P_p(n+1) - nP_p(n)\Big\}\\ &+\kappa n_B\Big\{nP_p(n-1) - (1+n)P_p(n)\Big\},\end{aligned} \tag{4.4}$$

where

$$\Gamma_{nn'} = \Gamma^{1n'}_{0n} = \Gamma^{0n'}_{1n}. \tag{4.5}$$

Typically in optics experiments $k_BT \ll \omega_c$, thus $n_B \simeq 0$. This simplifies the rate equations further Eq. (4.3) since now the only way to populate the cavity is through the tunneling of an electron from the ground state of the cavity Fig. 4.2,

$$\begin{aligned}\dot{P}_p(n) =&\Gamma_{0n}P_p(0) - \delta_{n,0}\sum_{n'}\Gamma_{nn'}P_p(n)\\ &+\kappa\Big\{(n+1)P_p(n+1) - nP_p(n)\Big\}.\end{aligned} \tag{4.6}$$

From Eq. (4.6), we deduce that in the stationary regime

$$\kappa P_p(1) = \sum_n \Gamma_{0n}P_p(0). \tag{4.7}$$

This corresponds to the equilibrium between the rate at which the cavity goes into its ground state from an excitation (proportional to κ) and the rate at which the electronic current excites other modes of the cavity from the ground state (proportional to Γ). Since the relaxation of the cavity is almost instantaneous, the probability of having one photon in the cavity is proportional to the ratio between the emission rate and the damping rate $P_p(1) = \sum_n \Gamma_{0n} P_p(0)/\kappa \simeq \sum_n \Gamma_{0n}/\kappa$. This is actually a pretty good estimate of the average number of photons in the cavity.

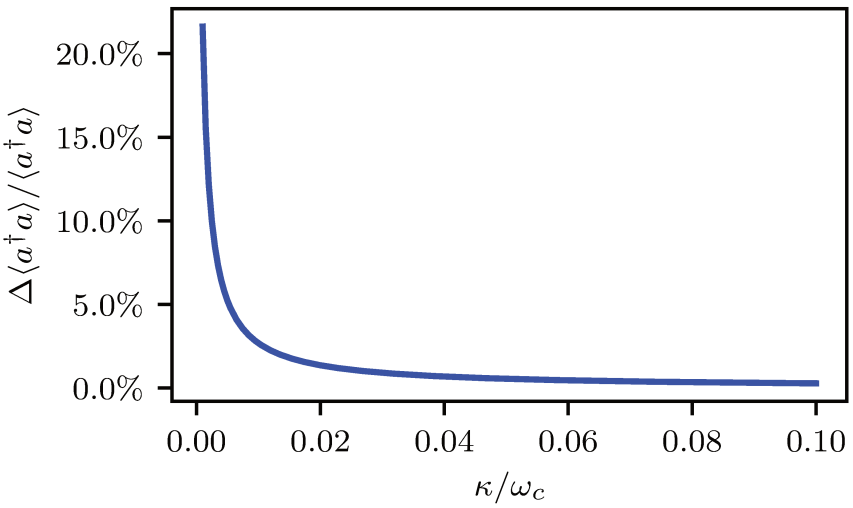

Figure 4.3: Normalized difference between the analytical prediction of Eq. (4.10) and the numerical result using Eq. (3.50) $\Delta\langle a^\dagger a\rangle/\langle a^\dagger a\rangle$ as a function of cavity damping rate κ for a coupling strength $\lambda = 1.4$ and a weakly coupled symmetric junction, $\Gamma_L = \Gamma_R = 10^{-3}\omega_c$ and $eV_L = -eV_R = 5.5\omega_c$.

Using the recurrence principle we show that for $n > 0$

$$P_p(n) = P_p(0) \sum_{k \geq n} \Gamma_{0k}/\kappa n. \tag{4.8}$$

Using the normalisation of the probability P_p we find

$$P_p(0) = \left(1 + \sum_{n \geq 1} \frac{\Gamma_{0n}}{\kappa} \sum_{k \leq n} \frac{1}{k}\right)^{-1}. \tag{4.9}$$

From the expression we found of the populations, we can compute $\langle a^\dagger a\rangle$

$$\langle a^\dagger a\rangle = \sum_n n P_p(n) = \frac{\sum_{n\geq 1} n\Gamma_{0n}}{\kappa + \sum_{n\geq 1} \Gamma_{0n}}. \tag{4.10}$$

Where we recall that $\Gamma_{0n} = e^{-\lambda^2}\lambda^{2n} f(n - eV)/n!$. Let us define $S_n(x) = \sum_{k=0}^{n} x^k/k!$, the partial sum up to n of the exponential power series. Then, assuming a very low temperature, so that the Fermi distribution

can be approximated by a θ function, Eq. (4.10) can be written as

$$\langle a^\dagger a\rangle = \frac{\Gamma e^{-\lambda^2}\lambda^2 S_{N_V-1}(\lambda^2)}{\kappa + \Gamma e^{-\lambda^2}[S_{N_V}(\lambda^2)-1]}, \tag{4.11}$$

where $N_V = \lfloor eV/\omega_c \rfloor$ is the greatest integer smaller than eV/ω_c. In the limit of infinite bias voltage, we therefore find that $\langle a^\dagger a\rangle$ scales as

$$\lim_{N_V\to+\infty}\langle a^\dagger a\rangle = \frac{\lambda^2\Gamma}{\kappa+\Gamma(1-e^{-\lambda^2})}. \tag{4.12}$$

This expression can be simplified further using the fact that $\kappa \gg \Gamma$ to find that

$$\lim_{N_V\to+\infty}\langle a^\dagger a\rangle = \lambda^2\Gamma/\kappa. \tag{4.13}$$

We therefore predict that the light intensity in the cavity scales as $\lambda^2\Gamma/\kappa$ at large bias voltage. However large bias voltage is not the limit that is usually explored. In STML experiments for instance, the bias voltage does not in general go far beyond $2eV$ [68].

Using again the fact that $\kappa \gg \Gamma$ in Eq. (4.11), we can expand the denominator in the right-hand side around $\Gamma/\kappa = 0$

$$\langle a^\dagger a\rangle \simeq \frac{\Gamma}{\kappa}e^{-\lambda^2}\lambda^2 S_{N_V-1}(\lambda^2)\left[1-\frac{\Gamma}{\kappa}e^{-\lambda^2}\{S_{N_V}(\lambda^2)-1\}\right] + o\left(\left[\frac{\Gamma}{\kappa}\right]^2\right). \tag{4.14}$$

At first order in Γ/κ, Eq. (4.14) gives that

$$\langle a^\dagger a\rangle \simeq \frac{\Gamma}{\kappa}e^{-\lambda^2}\lambda^2 S_{N_V-1}(\lambda^2). \tag{4.15}$$

From Eq. (4.14) it appears that the voltage drop gives the number of terms from the power series of $e^{-\lambda^2}$ we need to find the light intensity. Another way to see that the bias voltage controls the accuracy of the approximation we make using Eq. (4.13) instead of Eq. (4.15) for the light intensity. Indeed the error we make using the large bias voltage limit is of the order of $\Gamma e^{-\lambda^2}\lambda^{2(N_V+1)}/\kappa$ and therefore gives a very good approximation in the weak coupling regime. Thus in the weak coupling regime Eq. (4.13) gives a very good approximation of $\langle a^\dagger a\rangle$ at any voltage drop.

Fig. 4.3 shows the comparison between formula Eq. (4.10) and the numerical computation of $\langle a^\dagger a\rangle$ using Eq. (3.50) as a function of the damping rate of the cavity κ in a symmetrically biased junction at voltage drop $eV = 5.5\omega_c$. The difference between the numerical and analytical solution seems to scale as $1/\kappa$.

As expected we see that when κ gets closer to Γ the analytical solution fails to recover the full numerical result since the cavity does not have the time to fully dissipate between two tunneling events and therefore dissipation is compensated by the inelastic tunneling of the electrons. However for $\kappa = 0.1\omega_c$ the comparison between the numerical and analytical results is very good, $< 0.3\%$, and it appears that we can neglect electron-tunneling processes between the excited states of the cavity.

The coupling strength also impacts the photon emission since the electronic rates not only depend on Γ, but also on λ as reported on Fig. 4.4. Indeed, We see that even though $\Gamma \ll \kappa$ it is possible that some rates Γ_{0n} or even more generally Γ_{nm} become bigger than the cavity damping rates with the increase of λ. For instance it is the case for Γ_{02} when $\lambda > 1.8$. However, this is not enough to significantly impact the populations. Fig. 4.5 shows the difference between the predicted average number of photon in the cavity from Eq. (4.10) and the numerical calculation. even though some fluctuations are reported, the difference between the two is in the range of less than a percent. Therefore, it seems that the ground state of the cavity remains largely dominant.

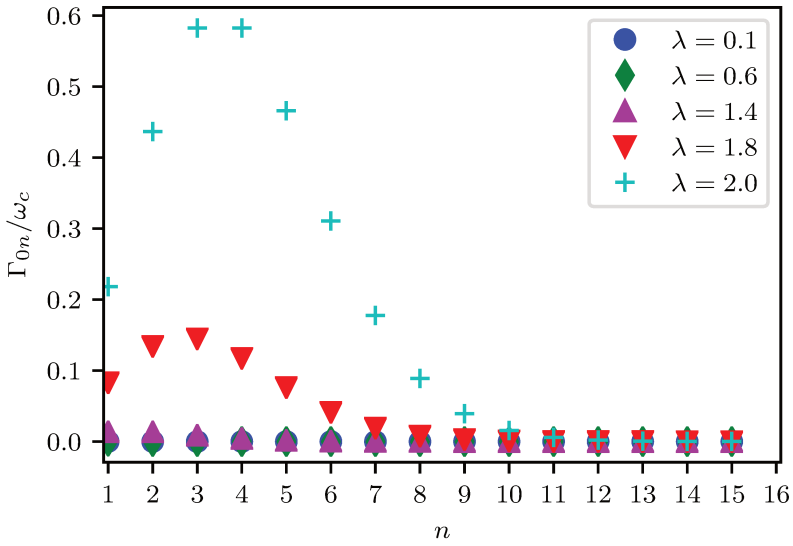

Figure 4.4: Inelastic tunneling rates from the ground state of the cavity Γ_{0n} as a function of the number of photons n in for different values of the coupling strength ranging from small $\lambda = 0.1$ to large $\lambda = 2$ coupling Eq. (4.5).

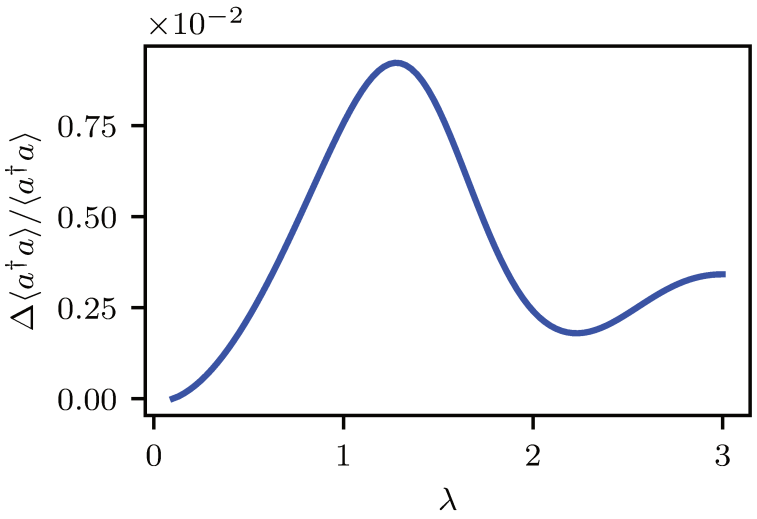

Figure 4.5: Normalized difference between the analytical prediction of Eq. (4.10) and the numerical result using Eq. (3.50) $\Delta\langle a^\dagger a\rangle/\langle a^\dagger a\rangle$ as a function of the coupling strength λ for a strongly damped cavity, $\kappa = 0.1\omega_c$ and a weakly coupled symmetric junction, $\Gamma_L = \Gamma_R = 10^{-3}\omega_c$ and $eV_L = -eV_R = 5.5\omega_c$.

So far we have treated the photo-emission using the rate equation, however, the same way we argued for the electronic current that the width of the steps should be given by κ rather than the temperature when $\kappa \gg k_B T$, the same should go for the steps of the number of photons in the cavity or the emitted light out of the cavity. We won't show any calculation of the sort here as it appeared that for the understanding of the populations we didn't need to capture the width of the steps. However, we could take into account this broadening by κ deriving the photo-current $\langle \sum_q f_q b_q^\dagger a - H.c.\rangle$ emitted from the cavity using the same approach we used for the electronic current in chapter 3.

4.2 Photon statistics

We have shown so far that due to the coupling between the fluctuating charge and the electromagnetic field of the cavity, the inelastic tunneling of the electrons in the junction results in the emission of light with a small intensity. We now study the photon statistics, in order to characterize the emitted light.

Experimentally, photon statistics is studied by counting the number of photons emitted from the system. The probability of photon absorption is proportional to the following matrix element

$$T_{if} = |\langle f|E^{(+)}(r,t)|i\rangle|^2, \tag{4.16}$$

where $|i\rangle$ and $|f\rangle$ are the initial and the final state, respectively, and $E^{(+)}(r,t)$ is the positive frequency part of the electric field [97,98]. Hence,

the total probability for the detector to absorb a photon is the sum over all the final states of T_{if} averaged over the initial states. This is the measured average field intensity

$$I(r,t) = \sum_{if} P(i)T_{if} = \mathrm{Tr}[E^{(-)}(r,t)E^{(+)}(r,t)\rho]. \tag{4.17}$$

The degree of coherence $G^{(1)}(x,x')$ was first introduced in optics to characterize interference of two superposed light fields in interference experiments. It is defined as the correlation function of the electric field at two different times and spaces

$$G^{(1)}(x,x') = \mathrm{Tr}[E^{(-)}(x)E^{(+)}(x')\rho], \tag{4.18}$$

where $x = (r,t)$. Two fields showing interference fringes are called coherent. If instead the interference contrast vanishes, then the two fields do not produce interference fringes and are called incoherent. In this last case one can show that the intensity collected at r from two light sources at r_1 and r_2 and at distance from r s_1 and s_2, respectively is:

$$I(x) = G^{(1)}(x_1,x_1) + G^{(1)}(x_2,x_2) + 2\mathrm{Re}[G^{(1)}(x_1,x_2)], \tag{4.19}$$

where $x_i = (r_i, t - s_i/c)$. Nowadays, in STML experiments, for instance, physicists measure the joint probability of detecting a photon at time t and a second one at time $t+\tau$. Fig. 4.6 shows an actual experimental setup extracted from [72]. The sample emits light that is collected through two single-photon avalanche diodes delayed in time. It was shown by Glauber [97] that this corresponds to the calculation of the second order degree of coherence or second order correlation function of the light

$$G^{(2)}(\tau) = \langle : I(t)I(t+\tau) : \rangle, \tag{4.20}$$

where :: indicates the normal ordering (all creation operators are placed on the left-hand side of the expression). Instead of using $G^{(2)}$ we will study the normalized second-order correlation function

$$g^{(2)}(t) = \frac{G^{(2)}(t)}{|G^{(1)}(0)|^2}. \tag{4.21}$$

In second-quantization formalism this reads:

$$g^{(2)}(\tau) = \frac{\langle a^\dagger(t)a^\dagger(t+\tau)a(t+\tau)a(t)\rangle}{\langle a^\dagger a\rangle^2}. \tag{4.22}$$

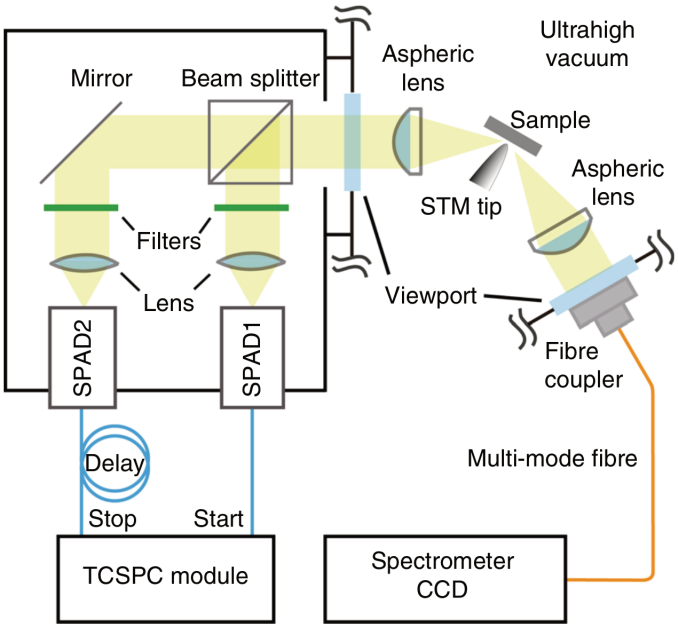

Figure 4.6: Experimental setup for measuring the photon statistics in an STML experiment. Reproduced from Ref. [72].

Of course for $\tau \gg \tau_c$ where τ_c is the correlation time of the field, the electric field will lose its correlation and therefore $g^{(2)}(+\infty) = 1$. $g^{(2)}(\tau) < g^{(2)}(0)$ characterise photon bunching. It means that it is more likely to detect a photon soon after the first detection. On the contrary when $g^{(2)}(\tau) > g^{(2)}(0)$ it is less likely to measure a second photon after some time, this behaviour is called anti-bunching. Actually $g^{(2)}(0) < 1$ is enough to characterize anti-bunching since $g^{(2)}(+\infty) = 1$, although it is in fact characteristic of sub-Poissonian statistics [99]. It can be shown that classical light can only exhibit bunching behaviour therefore anti-bunching is currently used to show that the radiation is in a non-classical state.

4.2.1 Bare cavity

As an introduction to the degree of coherence, we show its calculation for a cavity mode damped by an external bath. The Hamiltonian of a bare cavity coupled with a bath is

$$H_c = \omega_c a^\dagger a + \sum_j \omega_j b_j^\dagger b_j + \sum_j \{\kappa_j b_j a^\dagger + \kappa_j^* b_j^\dagger a\}, \tag{4.23}$$

where $a^\dagger$ is the creation operator of the cavity mode and $b_j^\dagger$ of the mode j in the bath. From H_c the time evolution of the operators a and b_j is deduced

$$\dot{a} = -i\omega_c a - i\sum_j \kappa_j b_j \tag{4.24}$$

$$\dot{b}_j = -i\omega_j b_j - i\kappa_j^* a. \tag{4.25}$$

Eq. (4.25) is integrated to find

$$b_j(t) = e^{-i\omega_j t} b_j(0) - i\kappa_j^* \int_0^t a(t') e^{i\omega_j (t'-t)} dt'. \tag{4.26}$$

Using Eq. (4.26) in Eq. (4.24) shows

$$\dot{a} = -i\omega_c a - \sum_j |\kappa_j|^2 \int_0^t a(t') e^{i\omega_j (t'-t)} dt' - i \sum_j \kappa_j e^{-i\omega_j t} b_j(0). \tag{4.27}$$

We define

$$a(s) = \int_0^{+\infty} e^{-st} a(t) dt, \tag{4.28}$$

the Laplace transform of a. The time evolution of $a(s)$ is given by

$$\dot{a}(s) = \int_0^{+\infty} \dot{a}(t) e^{-st} dt = \lim_{x\to\infty} [a(t)e^{-st}]_0^x + s \int_0^{+\infty} a(t) e^{-st} dt = sa(s) - a(0). \tag{4.29}$$

Therefore using Eq. (4.29) in Eq. (4.27) we show that

$$\begin{aligned} sa(s) - a(0) = &- i\omega_c a(s) - i \sum_j \frac{\kappa_j}{i\omega_j + s} b_j(0) \\ &- \sum_j |\kappa_j|^2 \int_0^{+\infty} \int_0^t a(t') e^{-(s+i\omega_j)t} e^{i\omega_j t'} dt' dt. \end{aligned} \tag{4.30}$$

By switching the order of the integrals in the last term in Eq. (4.30) whe show that

$$\int_0^{+\infty} \int_0^t a(t') e^{-(s+i\omega_j)t} e^{i\omega_j t'} dt' dt = -\frac{a(s)}{s + i\omega_j}. \tag{4.31}$$

This manipulation allows us to simplify a lot Eq. (4.30) and we find

$$a(s) = \frac{a(0) - i \sum_j \frac{\kappa_j}{i\omega_j + s} b_j(0)}{s + i\omega_c - \sum_j \frac{|\kappa_j|^2}{s + i\omega_j}}. \tag{4.32}$$

Using Wigner–Weisskopf approximation [100] on Eq. (4.32) it simplifies into

$$a(s) = \frac{a(0) - i \sum_j \frac{\kappa_j}{i\omega_j + s} b_j(0)}{s + i\omega_c + \kappa/2}. \tag{4.33}$$

We use the inverse Laplace transform on Eq. (4.33) to find $a(t)$

$$a(t) = e^{-(\kappa/2 + i\omega_c)t} a(0) - \sum_j \frac{e^{-i\omega_j t} - e^{-(i\omega_c + \kappa/2)t}}{\omega_c - \omega_j - i\kappa/2} \kappa_j b_j(0). \tag{4.34}$$

As the aim is to compute $G^{(2)}$, we first compute $a^\dagger(t)a(t)$. This can be done directly from Eq. (4.24) and Eq. (4.25)

$$\frac{d}{dt} a^\dagger a = -\kappa a^\dagger a + i \sum_j [\kappa_j^* b_j^\dagger(0) e^{i\omega_j t} a - \kappa_j a^\dagger b_j(0) e^{-i\omega_j t}]. \tag{4.35}$$

Using Eq. (4.34) in Eq. (4.35) and averaging over the bath degrees of freedom assuming the bath to be in thermal equilibrium, we find $\langle a^\dagger a\rangle_B$

$$\frac{d}{dt}\langle a^\dagger a\rangle_B = -\kappa\langle a^\dagger a\rangle_B + \sum_j 2|\kappa_j|^2 n_j Re\frac{1-e^{(\kappa/2+i(\omega_j-\omega_c))t}}{\kappa/2-i(\omega_j-\omega_c)}, \tag{4.36}$$

where $n_j = \langle b_j^\dagger(0)b_j(0)\rangle$ follows the Bose distribution and $\dot{\langle\rangle}_B$ is the average over the bath. We can approximate the summation over j with an integral over the frequency ω as the fraction is strongly peaked around $\omega_j = \omega_c$ and $|\kappa_j|^2 n_j$ should vary very slowly with j. Doing so, we show that

$$\frac{d}{dt}\langle a^\dagger a\rangle_R = -\kappa\langle a^\dagger a\rangle_R + \kappa n. \tag{4.37}$$

The solution of this equation is

$$\langle a^\dagger(t)a(t)\rangle_R = e^{-\kappa t}a^\dagger(0)a(0) + n[1-e^{-\kappa t}] \tag{4.38}$$

From the definition of $G^{(2)}$ in Eq. (4.20) and Eq. (4.38)

$$G^{(2)}(t) = \langle a^\dagger(0)^2 a(0)^2\rangle e^{-\kappa t} + n\langle a^\dagger(0)a(0)\rangle[1-e^{-\kappa t}]. \tag{4.39}$$

Using Wick's theorem we know that $\langle a^{\dagger 2}a^2\rangle = 2\langle a^\dagger a\rangle^2$. Hence,

$$g^{(2)}(t) = 1 + e^{-\kappa t}). \tag{4.40}$$

Therefore, the degree of coherence of the bare cavity starts from 2 at time $t = 0$ and decreases towards 1 and $t \to \infty$, with an exponential decay of $-\kappa$. This means that the photons in the cavity are always bunched and have a super Poissonian statistic.

4.2.2 Single–level dot junction

The degree of coherence is defined in Eq. (4.22) as the normalised second order correlation function of the electric field. In the density matrix formalism Eq. (4.22) is

$$g^{(2)}(t) = \mathrm{Tr}[a^\dagger a^\dagger(t)a(t)a\rho_{st}]/\langle a^\dagger a\rangle^2. \tag{4.41}$$

Eq. (4.41) can be used to find numerically the degree of coherence. Indeed, using the properties of the trace Eq. (4.41) is equivalent to

$$g^{(2)}(t) = \mathrm{Tr}[a^\dagger a e^{-iHt}a\rho_{st}a^\dagger e^{iHt}]/\langle a^\dagger a\rangle^2. \tag{4.42}$$

From Eq. (4.42) we define the operator $A(t) = e^{-iHt}a\rho_{st}a^\dagger e^{iHt}$. We can compute the time derivative of A and show that A satisfies the same Liouville-von Neumann equation of ρ

$$\dot{A}(t) = -i[H, A(t)]. \tag{4.43}$$

Therefore since a and $a^\dagger$ are system operators only, we can trace out the environment degrees of freedom the same way we did for the density matrix. This means that we can define a reduced operator A_S that has

the same time evolution as ρ_S. In terms of the Liouvillian super-operator, one can then write:

$$g^{(2)}(t) = \mathrm{Tr}[\check{a}^\dagger \check{a} e^{\check{\mathcal{L}}t} \check{a} \underline{\rho}_{st} \check{a}^\dagger]. \tag{4.44}$$

Since we are able to solve numerically Eq. (3.50), we can use Eq. (4.44) to compute the degree of coherence $g^{(2)}$. See appendix A. Fig. 4.7 shows the degree of coherence as a function of time for a symmetrically biased junction and a strongly damped cavity. We see that for a weak coupling strength the behaviour is a simple exponential decrease similarly to the cavity in thermal equilibrium shown subsection 4.2.1. Thus, there is a smooth crossover between $g^{(2)}(0) = 2$ and $g^{(2)}(\infty) = 1$ on a timescale $1/\kappa$. The fact that in the weak coupling regime the interacting system behaves like the non-interacting cavity at thermal equilibrium is of course not surprising. What is more interesting is that for any coupling strength the second order correlation function conserves its exponential decrease in time. However, the initial value depends on the coupling strength λ. Apart for small oscillations in time, the correlation scales to zero on the time scale $1/\kappa$.

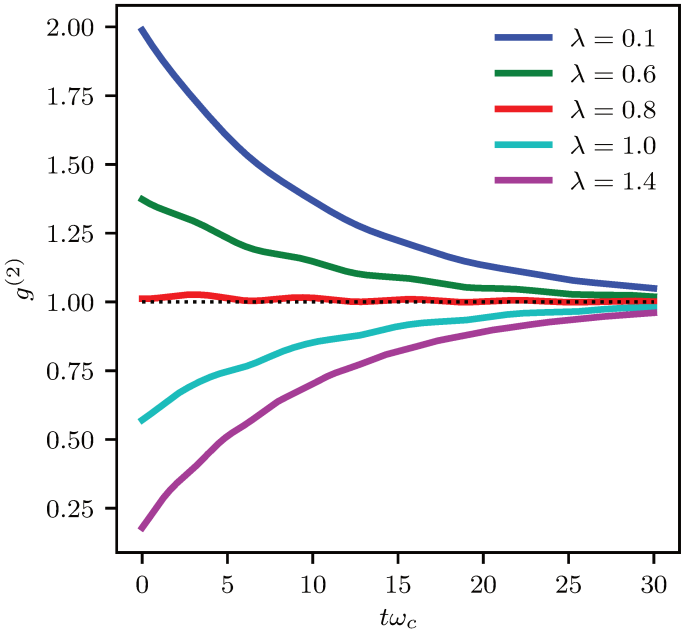

Figure 4.7: Second order photon correlation function $g^{(2)}$ as a function of time t for various values of the coupling strength λ for a single-level dot junction in the weak tunneling regime $\Gamma_L = \Gamma_R = 10^{-3}\omega_c$. The junction is symmetrically biased $eV_L = -eV_R = 1.2\omega_c$ and the cavity strongly damped $\kappa = k_B T = 0.1\omega_c$. The dotted black line shows the value 1. Reproduced from Ref. [93].

Moving now to the strong coupling case, we see that Fig. 4.7 shows that photon anti-bunching ($g^{(2)}(0) < 1$) is possible for a single-level molecular junction. This is quite surprising and, to our knowledge,

was not reported before from the theoretical point of view. Also, from Fig. 4.7, we see that in the case of a single-level dot junction, sub-Poissonian distribution and photon anti-bunching appear to be equivalent. Indeed, both these behaviours are given by the condition $g^{(2)}(0) < 1$. Thus, we can focus on the initial value of the degree of coherence $g^{(2)}(0)$ only to differentiate photon-bunching and photon anti-bunching behaviour.

From Eq. (4.41) we can find an analytical formula for the second order correlation function of the electromagnetic field. Indeed, in the basis of the shifted cavity, after the Lang-Firsov transformation, the basis states are $|q, n\rangle$ where q is the charge on the quantum dot and n is the number of photons in the cavity. Projecting Eq. (4.41) on the basis vectors, we find a simple expression for the second order correlation function

$$g^{(2)}(0) = \sum_n n(n-1)P_p(n)/[\sum_n nP_p(n)]^2, \tag{4.45}$$

That only depends on the populations. This stems from the fact that the operators $a^\dagger a$ and $a^\dagger a^\dagger aa$ are diagonal in this basis. This means that as for the average intensity, we only need the populations to obtain the correlation function. Therefore the diagonal part of the reduced density matrix ρ_S is sufficient to compute the second order correlation function. We already solved the rate equations in the regime of strong damping of the cavity and weak tunneling rates $\kappa \gg \Gamma$ in Eq. (4.8) and Eq. (4.9). Introducing Eq. (4.8) in Eq. (4.45), we find that

$$g^{(2)}(0) = \frac{\kappa \sum_n (n-1) \sum_{k \geq n} \Gamma_{0k}}{P_p(0)[\sum_n n\Gamma_{0n}]^2}, \tag{4.46}$$

which can be expressed using the partial sums $S_n(x)$ as

$$g^{(2)}(0) = \frac{\kappa e^{\lambda^2} S_{N_V-2}(\lambda^2)}{P_p(0)\Gamma S_{N_V-1}(\lambda^2)}. \tag{4.47}$$

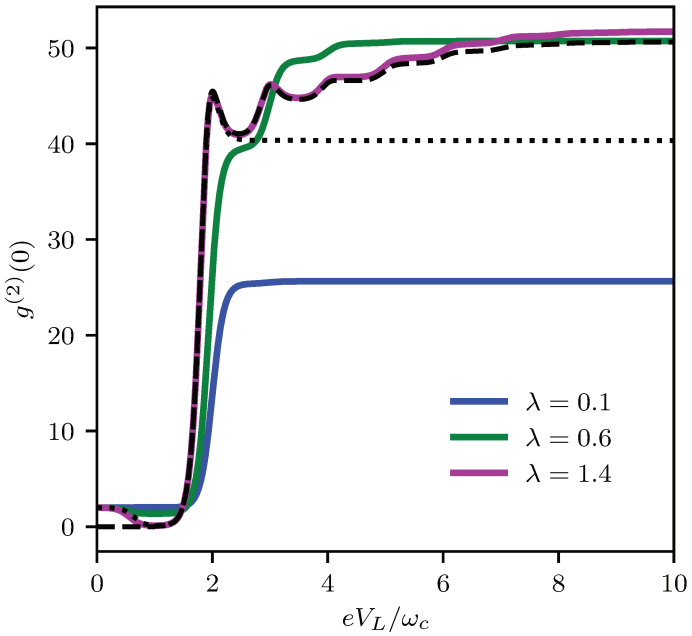

Figure 4.8: Second order photon correlation function at time $t = 0$, $g^{(2)}(0)$, as a function of the voltage drop eV_L in a symmetrically biased junction $eV_L = -eV_R$, for various values of the coupling strength λ for a single-level dot junction in the weak tunneling regime $\Gamma_L = \Gamma_R = 10^{-3}\omega_c$. The cavity is strongly damped $\kappa = k_BT = 0.1\omega_c$. The dashed black line shows the analytical prediction assuming that electronic tunneling always occurs when the cavity is in its ground state from Eq. (4.47). The dotted black line shows the analytical prediction from Eq. (4.52) taking into account electronic transitions from the first excited mode of the cavity. Both of these curves are shown for $\lambda = \sqrt{2}$. Reproduced from [93].

Fig. 4.8 shows the second order correlation function of the light at time $t = 0$ as a function of the voltage drop eV_L for a symmetrically biased junction ($eV_L = -eV_R$). We see that at very low bias voltage ($e|V_L - V_R| \ll k_BT$), before the first inelastic threshold, the current does not influence the cavity as noticed earlier. Hence whatever the coupling strength the cavity remains in thermal equilibrium and $g^{(2)}(0) = 2$. However, around the first inelastic threshold, there is enough energy available to excite a photon and the photon distribution in the cavity deviates from thermal equilibrium. This threshold corresponds to only one photon emitted for each electron–tunneling event. Therefore, it is where photon anti-bunching is the most expected. We see in Fig. 4.8 that indeed, for sufficiently strong coupling, photon anti-bunching is possible for a single-level molecular junction at the first inelastic threshold of the tunneling electrons, but as soon as the second threshold is attained, the cavity enters a regime of "super-bunching" where the degree of coherence suddenly increases up to around 50. The impossibility to see anti-bunching a large voltage for a single electronic level quantum dot and the limit of strong bunching has been reported recently in Ref. [28]. Now comparing the

analytical result we found in Eq. (4.47) to the numerical results, we see that at large bias voltage the analytical prediction only depends on the ratio between κ and Γ

$$g^{(2)}(0) = \frac{\kappa}{2\Gamma}. \tag{4.48}$$

Taking $\kappa = 0.1\omega_c$ and $\Gamma = 10^{-3}\omega_c$ in Eq. (4.48) we find that

$$\lim_{V\to+\infty} g^{(2)}(0) = 50. \tag{4.49}$$

However for a voltage drop $eV_L < 2\omega_c$, since we only took into account transitions starting from the ground state of the cavity, Γ_{0n} in Eq. (4.6), at the first inelastic threshold only Γ_{01} is different from 0. This means that only $P_p(0)$ and $P_p(1)$ are not vanishing and since there is no process allowing to attain more populated states of the cavity, the probability of those states is equal to 0. So there is at most one photon in the cavity at any given time, and therefore the degree of coherence vanishes. Photon-bunching can only occur when more than one photon exist in the cavity. Since at the first inelastic threshold only one photon can be emitted in a tunneling event, successive tunneling events are needed to increase the number of photons in the cavity. Therefore, we need to go to higher order in the population to take into account tunneling rates between populated states of the cavity. Let us relax a bit the condition that the cavity is always in its ground state and admit that $P_p(n)$ for $n \leq 2$ can be non-vanishing. In this case the rate equations Eq. (3.61) become

$$\begin{cases} \dot{P}_2 = \Gamma_{02}P_0 + \Gamma_{12}P_1 - P_2(\Gamma_{21} + \Gamma_{20}) + 2\kappa_\uparrow P_1 - 2\kappa_\downarrow P_2 \\ \dot{P}_0 = \kappa_\downarrow P_1 - P_0(\kappa_\uparrow + \Gamma_{0,1} + \Gamma_{02}) \\ P_0 + P_1 + P_2 = 1, \end{cases} \tag{4.50}$$

Where two new electronic tunneling rates enter the equations: $\Gamma_{01} = \Gamma e^{-\lambda^2}\lambda^2 \sum_\alpha f_\alpha(\omega_c)$ and $\Gamma_{12} = \Gamma e^{-\lambda^2}\lambda^2 \frac{(2-\lambda^2)^2}{2} \sum_\alpha f_\alpha(\omega_c)$.

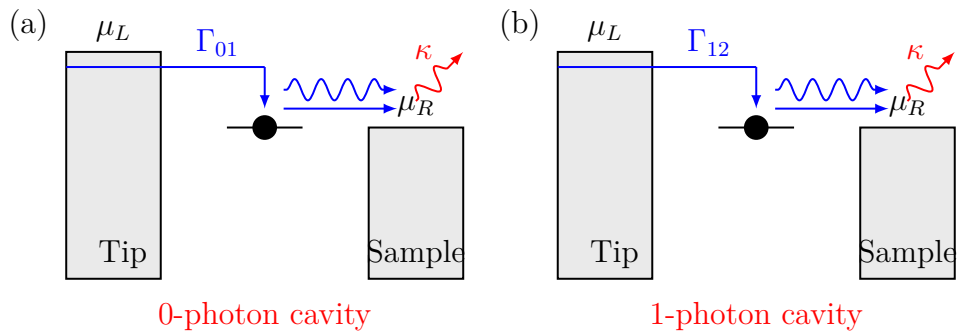

Figure 4.9: Photon emission processes considered. (a) Photon emission from the ground state by an electron tunneling through the junction with rate Γ_{01}. (b) Photon emission from the first excitation of the cavity by an electron tunneling with rate Γ_{12}

Fig. 4.9 shows the two processes involved in the photon emission. In panel (a), we recognize the process that we already took into account in Eq. (4.6). It corresponds to a photon being excited by the fluctuation of the charge of the quantum dot in the cavity in its ground state. The rate Γ_{01} is the product of the tunneling rate Γ, the Fermi distribution and the Franck–Condon overlap between the wave function of the cavity mode at 0 photon and the wave function of the cavity mode displaced by Λ due to the electron on the molecule at 1 photon. As mentioned earlier, the Fermi distribution leads to the condition on the voltage drops that allows for this transition. The Franck–Condon overlap between the two wave functions of the cavity mode involved in Γ_{01} is $e^{-\lambda^2}\lambda^2$.

The second process, panel (b), that we consider is the excitation of an additional photon from the charge's fluctuations on the dot in the cavity populated by one photon. The rate corresponding to this process is Γ_{12} and is proportional to the overlap between the wave function of the cavity mode with 1 photon and the wave function of the cavity mode with 2 photons displaced by λ due to the additional electron on the dot. This overlap is given by $e^{-\lambda^2}\lambda^2(2-\lambda^2)^2/2$. Since the rate equations Eq. (4.50) involve a finite number of unknowns, it is solvable and the populations are found in

$$\begin{cases} P_0 = 2\kappa_\downarrow^2/\Delta \\ \\ P_1 = \dfrac{2\kappa_\downarrow}{\Delta}(\kappa_\uparrow + \Gamma_{01} + \Gamma_{02}) \\ \\ P_2 = (\kappa_\downarrow\Gamma_{02} + (2\kappa_\uparrow + \Gamma_{12})(\kappa_\uparrow + \Gamma_{01} + \Gamma_{02}))/\Delta, \end{cases} \tag{4.51}$$

Here we defined $\Delta = \kappa_\downarrow(\Gamma_{02} + 2\kappa_\downarrow) + (\kappa_\downarrow + \Gamma_{01} + \Gamma_{02})(\Gamma_{12} + 2(\kappa_\uparrow + \kappa_\downarrow))$, $\kappa_\uparrow = \kappa n_B$ and $\kappa_\downarrow = \kappa(n_B + 1)$. Introducing Eq. (4.51) into Eq. (4.44) we find at the first inelastic threshold $eV_L = \omega_C$

$$g^{(2)}(0) = \frac{2P_p(2)}{P_p(1)^2} = \frac{\Gamma_{12}}{\Gamma_{01}} = \frac{(2-\lambda^2)^2}{2}. \tag{4.52}$$

This approximation of the degree of coherence shows that $g^{(2)}$ at the first inelastic threshold mainly depends on the coupling strength λ. From Eq. (4.52) we predict that anti-bunching is possible when $\sqrt{2-\sqrt{(2)}} \leq \lambda \leq \sqrt{2+\sqrt{2}}$ for a symmetrically biased junction, with a minimum of $g^{(2)}(0) = 0$ at $\lambda = \sqrt{2}$. The comparison between the analytical formula Eq. (4.52) and the numerical calculation is shown on Fig. 4.8 in the dotted black curve that represents Eq. (4.52) at $\lambda = \sqrt{2}$. We see that Eq. (4.52) fit very well the purple curve $\lambda = 1.4$ even up until the second inelastic threshold at $eV_L = 2\omega_c$. Of course this is due to the fact that we took into consideration all the rates involving $P_p(2)$, $P_p(1)$ and $P_p(0)$, a better fit at higher voltage drops could be found by considering more populations in the rate equations.

As a conclusion anti-bunching for a single-electronic level is possible depending on the coupling strength since the emission of a second photon

in the cavity is possible even at $eV_L \simeq \omega_c$. The emission of the second photon is allowed thanks to the overlap between the first exited state of the cavity mode and the second excited state of the displaced cavity mode giving the rate Γ_{12}. This rate is controlled by the coupling strength between the charge and the electromagnetic field, therefore it vanishes in the small coupling regime. Γ_{12} hits its minimal value at $\lambda = 0$, $\lambda = \sqrt{2}$ and then vanishes again as the coupling strength increases since the cavity mode and the displaced cavity mode become too far apart for any overlap to exist and the states become independent. This phenomenon is similar to the anti-bunching reported in Josephson junctions [51].

This behaviour is confirmed numerically in Fig. 4.10 where we show the $g^{(2)}(0)$ as a function of the left (eV_L) and right (eV_R) voltage drops and Fig. 4.11 panel (c) showing the absolute minimum of $g^{(2)}$ as a function of the coupling strength.

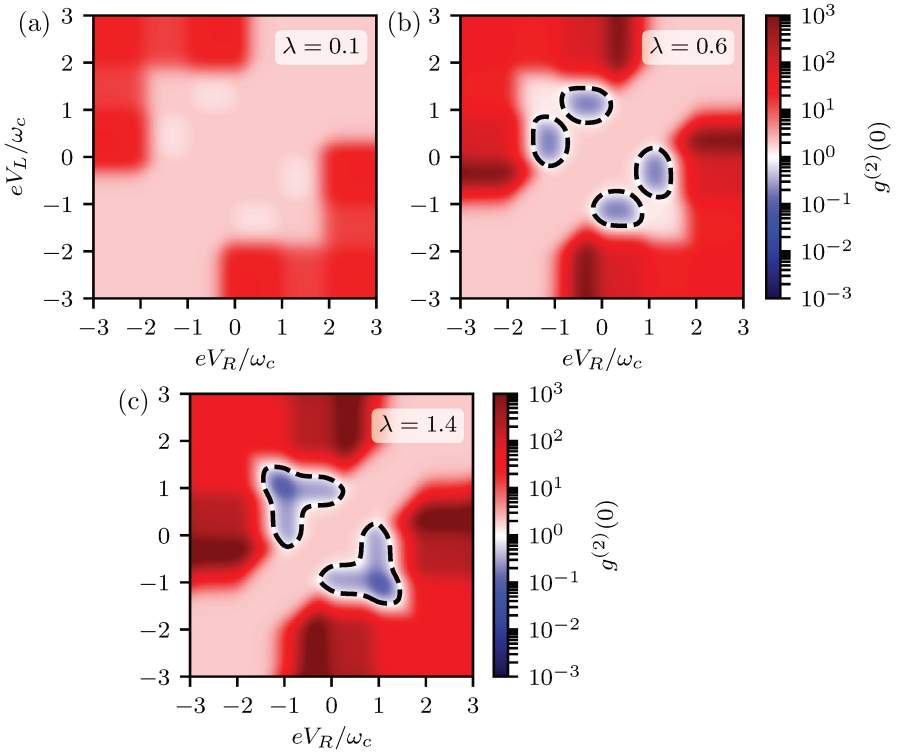

Figure 4.10: Degree of coherence $g^{(2)}(0)$ for different electron–photon coupling strengths (a) $\lambda = 0.1$, (b) $\lambda = 0.6$, and (c) $\lambda = 1.4$, respectively. The black dashed lines mark the contour $g^{(2)}(0) = 1$ delimiting the regions of anti-bunching (blue areas). The model parameters are $\kappa = k_B T = 0.1\omega_c$ and $\Gamma_L = \Gamma_R = 10^{-3}\omega_c$. Reproduced from Ref. [93].

Fig. 4.10 shows a 2D map of the second order degree of coherence $g^{(0)}(0)$ as a function of the left and right voltage drops eV_L and eV_R. We distinguish two regions, the red region in which $g^{(2)}(0) > 1$, meaning that the photons are bunched. The blue region in which $g^{(2)}(0) < 1$, meaning that the photons are antibunched. In panel (a) in Fig. 4.10 the coupling strength is $\lambda = 0.1$ thus only photon bunching appears. The light red region is dominated by the thermal distribution of the photons while the

red regions at the upper left and lower right corners shows the super-bunching due to electron-tunneling assisted multi-photon emission in the junction. As λ increases in panel (b) the strong bunching in the upper left and lower right corners becomes even stronger due to the increase of the photon-assisted electronic tunneling rates given in Eq. (3.58). Also four blue regions in which the photons are anti-bunched appear. Increasing further the coupling strength up to $\lambda = 1.4$ in panel (c), we see that the blue regions expand toward the line $eV_L = -eV_R$ corresponding to the symmetrically biased junction. As the blue regions merged together, $g^{(2)}(0)$ goes to even smaller values for the symmetrically biased junction. Hence, it seems that anti-bunching is attained for a wider range of coupling strength in a non symmetrically biased junction. This has some interest since in most experimental setups the junction should not be symmetrical. However, the strongest suppression of the photon-bunching is obtained in the symmetrically biased junction. This is confirmed in Fig. 4.11 panel (c) which shows the minimal value obtained for $g^{(2)}(0)$ over any value of the left and right voltage drops (blue line) and for a symmetrically biased junction (purple dashed line) as a function of the coupling strength λ.

We explained the anti-bunching using Eq. (4.52) as the suppression of the electron tunneling assisted photon rate Γ_{12}. This rate is actually the sum of four electron tunneling rates: $\Gamma^{12}_{01:L/R}$ and $\Gamma^{02}_{11:L/R}$ each producing a photon in the cavity starting from the cavity already populated by one photon. Fig. 4.12 shows a representation of the electron tunneling processes at the first inelastic thresholds resulting in the emission of a photon (panel (a) and (b)) and the representation of their corresponding energy thresholds (panel (c) and (d)) for a symmetrically biased junction (panel (a) and (c)) and a non-symmetrically biased junction ((b) and (d)). In the case of the symmetrically biased junction, the channels can be considered as pairs since when eV_L passes an energy threshold for the charge of the dot corresponding to the emission of k photons ($eV_L > k\omega_c$), at a given bias voltage ($eV_L = -eV_R = eV/2$ where eV defines the bias voltage) eV_R meets the threshold for the emission of k photons from the discharge of the dot ($eV_R < -k$). Therefore at the first inelastic threshold in a symmetrically biased junction there are two tunneling channels contributing to $g^{(2)}(0)$. Whereas for a non-symmetrically biased junction only one tunneling channel is contributing since only one of the voltage drop passes through an inelastic threshold. An example of that is shown in Fig. 4.12 panel (b) and (d) where the left potential μ_R is tuned to the dot energy ε_0 and therefore the electrons on average only tunnel in the direction of the right lead and photons are only emitted during the charging process when an electron leaves the left lead to go onto the dot. This explains why the anti-bunching in the case of a symmetrically biased junction requires a bigger coupling strength.

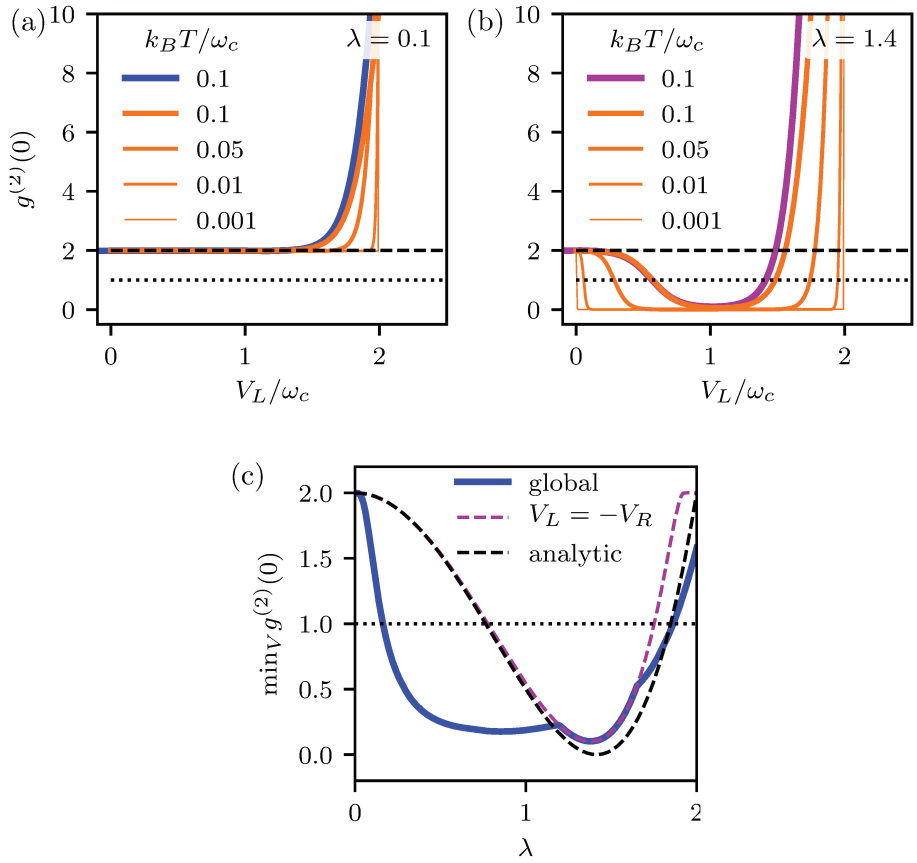

Figure 4.11: (a), (b) Role of temperature T on the degree of coherence $g^{(2)}(0)$ for $V_L = -V_R$ with (a) $\lambda = 0.1$ and (b) $\lambda = 1.4$. Blue and magenta thick lines are obtained from Fig. 4.10, while the orange ones are computed from Eq. (4.52). Dashed (dotted) horizontal line indicates $g^{(2)}(0) = 2$ (1) for thermal (uncorrelated) photon emission. (c) Minimum value of $g^{(2)}(0)$ (thick blue line) on the plane (V_L, V_R), for fixed λ and $k_BT = 0.1\omega_c$. Dashed magenta line shows that minimum constrained to $V_L = -V_R$. Dashed black line gives the $T = 0$ analytical prediction $(\lambda^2 - 2)^2/2$. Other parameters are those of Fig. 4.10. Reproduced from [93].

In conclusion, we expect that the regime of parameters allowing for the photon anti-bunching is in fact broader than what is predicted from Eq. (4.52). This is shown in Fig. 4.11 panel (c). In this plot we represent the minimum value of $g^{(2)}(0)$ (plain blue curve), obtained numerically, as a function of λ for any value of the left and right voltage drops. The minimum of $g^{(2)}(0)$ is compared to the value of $g^{(2)}(0)$ obtained for a symmetrically biased junction (dashed purple curve) and the analytical prediction of Eq. (4.52) (dashed black curve). We see, comparing the analytical prediction to the numerical results for a symmetrically biased junction, that we predict well the position of the minimum of $g^{(2)}(0)$ at $\lambda = \sqrt{2}$. However, for large values of the coupling strength, we underestimate the degree of coherence since we neglect other transitions of the type $\Gamma_{n,n+1}$. As a result we overestimate the upper-limit of anti-bunching since the additional photon emission we neglect results in the increase of

the degree of coherence. Nevertheless looking at the minimization over the full plane (eV_L, eV_R), we see that in general we largely underestimated the range for which anti-bunching is possible. Indeed, the condition of anti-bunching is $0.17 \leq \lambda \leq 1.85$ from the numerical results. Surprisingly the upper-limit we predicted from Eq. (4.52) at $\lambda = \sqrt{2+\sqrt{2}}$ is pretty accurate though the actual maximum value of λ for which anti-bunching is found correspond to an asymmetrically biased junction since the blue curve and the dashed purple curve do not coincide for $1.7 < \lambda < 2$. Fig. 4.11 panels (a) and (b) shows $g^{(2)}(0)$ as a function for various values of the temperature. Temperature has a very straight forward effect on $g^{(2)}(0)$ as it sharpened the thresholds at each integer values of eV_L.

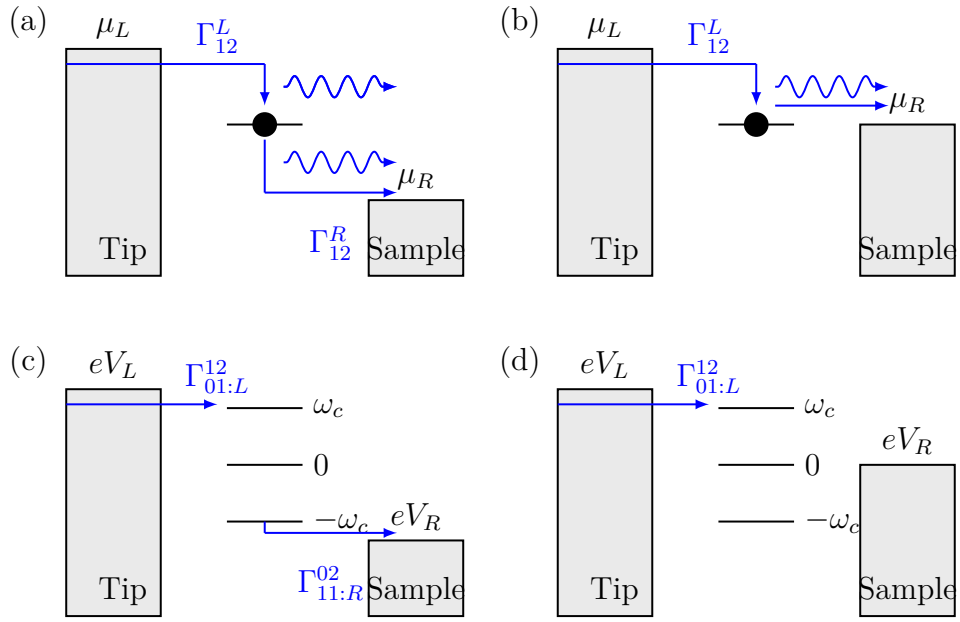

Figure 4.12: Photon emission processes. (a) for a symmetrically biased junction and (b) for an unsymmetrically biases junction. Panel (c) and (d) represent the energy thresholds corresponding to the tunneling channels in panel (a) and (b), respectively.

Chapter 5

Dipolar coupling of a two-level quantum dot

So far we have studied the single–level quantum dot. We found that the charge fluctuations, when coupled to the electromagnetic field of a cavity, allows to observe new phenomena not expected otherwise: Specifically non-classical photon emission. However, the case of the presence of two electronic levels is also of great interest and it has attracted much attention from the STM community as the most regarded explanation of light emission in molecular STM junctions [66, 68, 71]. An important difference with the single level case is the presence of the dipolar interaction [14, 95, 101]. The system has two states with the same total charge on the molecule, corresponding to an electron in either the lower or the higher electronic level.

The dipolar momentum between the two states couples to the electromagnetic field of the cavity. One major effect of this coupling is that it impacts drastically the spectrum of the two–level dot and the cavity when the detuning between the levels is close to resonant with the cavity frequency [102–108]. On top of this effect, electronic current through two–level quantum dot has been shown to impact photon emission in the cavity and conversely [74, 75, 108–112]. It is clear that in this problem the interplay between the energy splitting Δ of the two-level system and the cavity resonating frequency will play an important role. We will assume in the following that the cavity is tuned at this difference of energy $\omega_c = \Delta$.

5.1 Model Hamiltonian

In this chapter we want to explore the light emission from a two-level molecular junction in a cavity. More precisely we want to focus on the dipolar interaction between the electronic transition in the molecule and the cavity electromagnetic field. Doing so, we want to predict from a theoretical point of view what would be the response of the cavity under electronic current excitation neglecting the monopolar interaction of the two electronic levels of the molecule with the cavity field. Therefore, our system is similar to the system we studied in the previous chapters.

A nanocircuit made of two electronic reservoirs at respective voltages V_L and V_R and a quantum dot placed between the two reservoirs. The quantum dot is modeled by two electronic levels, neglecting the spin degree of freedom. The electronic reservoirs of the nanocircuit also act as the boundaries of an electromagnetic cavity of pulsation ω_c. Fig. 5.1 shows a graphic representation of the system.

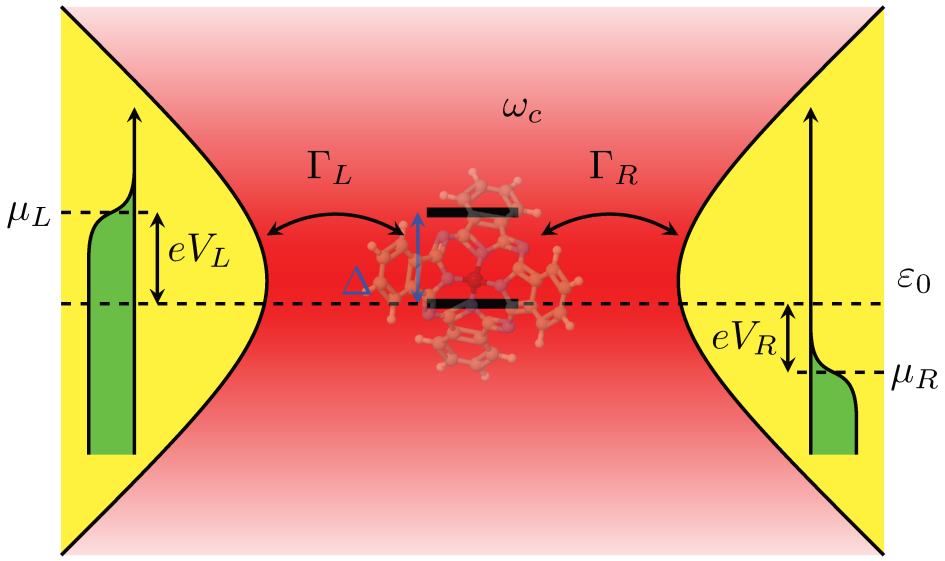

Figure 5.1: Schematic of two metallic electrodes forming a plasmonic nanocavity characterized by a resonating frequency $\omega_c/2\pi$.Two electronic levels ε_0 and $\varepsilon_0 + \Delta$ of a molecule in the nanogap couples to the electromagnetic radiation with coupling constant Λ. Electrons can tunnel to and from the dot with tunneling rates Γ_α. Voltage drops, V_α, with respect to ε_0 are indicated.

In this chapter we study only the effects of the dipolar coupling, neglecting the effects studied in chapter 3 and chapter 4.

$$\Lambda = -e \int V_\perp(r)\phi_g^*(r)\phi_e(r)d^3r, \tag{5.1}$$

where $\Lambda = \lambda\omega_c$ is the dipolar coupling, ϕ_e is the wave function of the lowest unoccupied orbital (LUMO) of the dot and ϕ_g is the highest occupied orbital (HOMO) of the dot. Let's write the Hamiltonian corresponding to the two-level dot junction in a cavity

$$H = H_S + H_B + H_{int}, \tag{5.2}$$

where the system Hamiltonian describes the two-level dot the cavity mode and their interaction

$$H_S = \varepsilon_0 d_g^\dagger d_g + (\varepsilon_0 + \Delta) d_e^\dagger d_e + \omega_c a^\dagger a + \Lambda(a + a^\dagger)(d_g^\dagger d_e + d_g^\dagger d_e), \tag{5.3}$$

$d_i^\dagger$ being the creation operators of the dot's orbitals and $a^\dagger$ the creation operator of the cavity mode at frequency ω_c. The bath Hamiltonian H_B

is exactly the same as for the single–level dot since we consider the same environment

$$H_B = \sum_{\alpha k} \varepsilon_{\alpha k} c^\dagger_{\alpha k} \varepsilon_{\alpha k} + \sum_q \omega_q b^\dagger_q b_q \tag{5.4}$$

and last, the interaction Hamiltonian couples the two electronic levels to the electronic leads and the cavity mode to the bosonic environment

$$H_{int} = \sum_{\alpha k i} t_{\alpha k i} c^\dagger_{\alpha k} d_i + \sum_q l_q b^\dagger_q a + H.c. \tag{5.5}$$

Our system Hamiltonian is very similar to the Rabi Hamiltonian with the difference that the Hilbert space contain also the doubly occupied state and the empty state for the quantum dot [74, 75, 108].

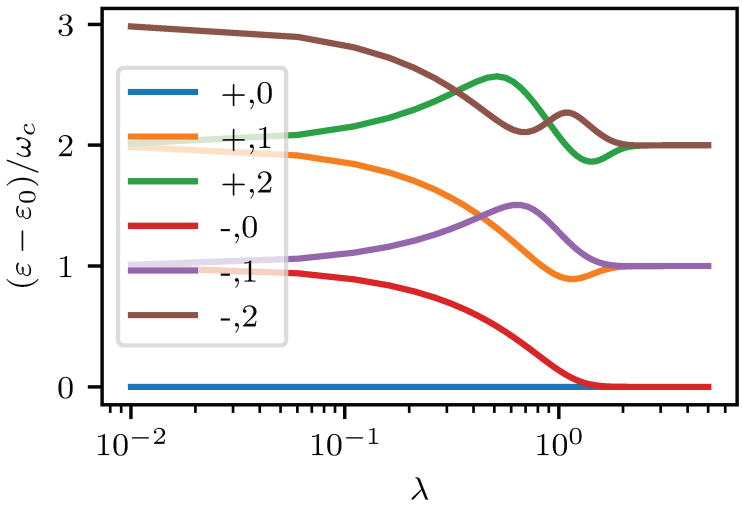

Figure 5.2: Eigenvalues for one–electron states of the molecule depending en the coupling constant λ. The states are denoted $\pm, i$. $+$ stands for an even number of excitation of the system (number of electron in the excited state of the molecule+number of photons), $-$ for an odd number of excitations and i is the ordering of the levels among those of same parity.

We call the number of excitations the number of electrons in the excited state of the dot plus the number of photons in the cavity $N_e = d^\dagger_e d_e + a^\dagger a$. Defining $P_{N_e} = e^{i\pi N_e}$ as the parity operator of the excitation number, we show by calculating the commutator $[H_S, P_{N_e}]$ that the parity of the number of excitation is conserved by H_S when $\Delta = \omega_c$. Therefore, we can use the parity as a quantum number for the eigenstates of H_S. Fig. 5.2 shows the energy spectrum of the system Hamiltonian H_S, the states are labelled by their parity and order in the energy spectrum. We can separate the spectrum into three parts; at low coupling $\lambda \leq 0.45$ we recognise the anti-crossing between the states $n-1,-$ and $n,+$ for $n \in \mathbb{N}^*$. At low values of the coupling constant, we can use a rotating wave approximation to neglect the terms that do not conserve the number

of excitations in H_S [103, 105, 106]

$$H_S^r = \varepsilon_0 d_g^\dagger d_g + (\varepsilon_0 + \Delta) d_e^\dagger d_e + \omega_c a^\dagger a + \Lambda_2 (d_g^\dagger d_e a^\dagger + d_g^\dagger d_e a). \tag{5.6}$$

This form is similar to the Jaynes–Cummings Hamiltonian. Then at moderate coupling-constant values $0.45 \leq \lambda \leq 2$ the energy ordering of states $n,+$ and $n,-$, for $n > 0$, changes and the even states become of higher energy than their corresponding odd states. At $\lambda = 0.45$ the energies predicted using the rotating wave approximation significantly deviate from their real values [103,104]. The Lamb shift, originating from virtual transitions, are of order $\lambda^2\omega_c$. However, they are not taken into account in the rotating wave approximation since this effect is generated by the counter–rotating terms in the coupling. This explain the deviation between the energy predicted using H_S^r compared to H_S [103]. Finally for $\lambda > 1$ the states $n,+$ and $n,-$ are degenerate. We will concentrate on the low coupling regime, since so far, experiments on single molecules do not reach coupling strength above a few percent of the photon energy [29]. As in this regime the rotating wave approximation gives good results, we will work with that. This means that in the following we neglect the terms that do not conserve the number of excitation in H [108]. However starting from the moderate coupling regime the rotating wave approximation fails, therefore, we drop it.

We focus on the resonance between the dipole and the cavity mode $\Delta = \omega_c$. The Hamiltonian H_S^r is exactly solvable [92, 107]. We first use the basis $\{|0,q\rangle, |g,q\rangle, |e,q\rangle, |2,q\rangle\}_q$, where q is the number of photons in the cavity and $\{0, g, e, 2\}$ are the states of the quantum dot (0 and 2 for the unoccupied and doubly occupied dot and g and e for the occupation of the LUMO and HOMO alone respectively) and we find the eigenstates $\{|0,n\rangle, |S,n\rangle, |A,n\rangle, |2,n\rangle\}_n$ with corresponding eigenvalues $\{n\omega_c, n\omega_c + \varepsilon_0 - \Lambda\sqrt{n}, n + \varepsilon_0 + \Lambda\sqrt{n}, (n+1)\omega_c + 2\varepsilon_0\}_n$, where $n \in \mathbb{N}$ is the number of excitations of a state [102, 107, 109]. $|0,n\rangle$ designates the states with n excitations and 0 electrons on the dot while $|2,n\rangle$ designates the state with n excitations and 2 electrons on the dot. We define $|S_n\rangle = \frac{|e,n-1\rangle + |g,n\rangle}{\sqrt{2}}$ and $|A_n\rangle = \frac{|e,n-1\rangle - |g,n\rangle}{\sqrt{2}}$ for $n > 0$. For $n = 0$, we define $|S_0\rangle = |g,0\rangle$ and $|A_0\rangle$ doesn't exist. Therefore the gap we found between two consecutive energies of same parity is the Rabi splitting $2\Lambda\sqrt{n}$ which is the energy separating $|S_n\rangle$ and $|A_n\rangle$.

5.2 Electronic current

Let us first look at the current characteristics and obtain a description for the current assisted light emission [74, 75, 108]. We use the rate equation approach to find the electronic current. As we identified three coupling regimes, we separate this section into three parts, one for each regime, plus an additional section for the non-interacting case.

5.2.1 Non-interacting case ($\lambda = 0$)

In the simplest case, the coupling Λ is set to 0.

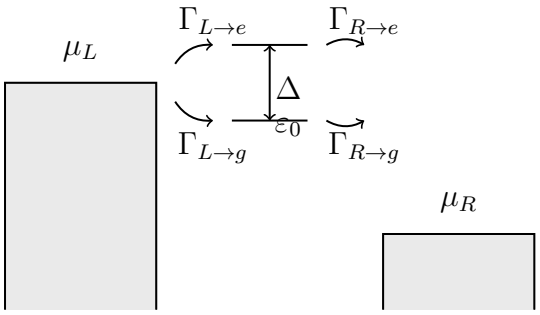

Figure 5.3: Two-level quantum dot tunnel junction

As for the single–level dot, we consider the sequential tunneling regime where $k_BT \gg \Gamma$. We regard the tunneling Hamiltonian H_{int} as a perturbation, and we diagonalize exactly the system Hamiltonian H_S. Then we compute the tunneling rates using Fermi's golden rule. We find a very simple expression of the tunneling rates

$$\begin{cases} \Gamma_{\alpha\to g} = \Gamma_{\alpha g} f_\alpha^+(0) \\ \Gamma_{\alpha\to e} = \Gamma_{\alpha e} f_\alpha^+(\Delta) \\ \Gamma_{\alpha\leftarrow g} = \Gamma_{\alpha g} f_\alpha^-(0) \\ \Gamma_{\alpha\leftarrow e} = \Gamma_{\alpha e} f_\alpha^-(\Delta), \end{cases} \tag{5.7}$$

where $\Gamma_{\alpha\to k}$ designates the rate for an electron to tunnel from lead α to the dot's level k. From the tunneling rates we deduce the rate equations:

$$\begin{cases} \dot{P}(0) = \Gamma_{\leftarrow g} P(g) + \Gamma_{\leftarrow e} P(e) - (\Gamma_{\to g} + \Gamma_{\to e}) P(0) \\ \dot{P}(g) = \Gamma_{\to g} P(0) + \Gamma_{\leftarrow e} P(2) - (\Gamma_{\leftarrow g} + \Gamma_{\to e}) P(g) \\ \dot{P}(e) = \Gamma_{\to e} P(0) + \Gamma_{\leftarrow g} P(2) - (\Gamma_{\leftarrow e} + \Gamma_{\to g}) P(e) \\ \dot{P}(2) = \Gamma_{\to e} P(g) + \Gamma_{\to g} P(e) - (\Gamma_{\leftarrow g} + \Gamma_{\leftarrow e}) P(2), \end{cases} \tag{5.8}$$

where $\Gamma_{\to k} = \sum_\alpha \Gamma_{\alpha\to k}$. Solving Eq. (5.8) we find the populations

$$\begin{cases} P(0) = \dfrac{\Gamma_{\leftarrow e}\Gamma_{\leftarrow g}}{\Gamma_\Sigma} \\ P(g) = \dfrac{\Gamma_{\leftarrow e}\Gamma_{\to g}}{\Gamma_\Sigma} \\ P(e) = \dfrac{\Gamma_{\to e}\Gamma_{\leftarrow g}}{\Gamma_\Sigma} \\ P(2) = \dfrac{\Gamma_{\to e}\Gamma_{\to g}}{\Gamma_\Sigma} \end{cases} \tag{5.9}$$

where $\Gamma_\Sigma = \Gamma_{\to e}\Gamma_{\to g} + \Gamma_{\to e}\Gamma_{\leftarrow g} + \Gamma_{\leftarrow e}\Gamma_{\to g} + \Gamma_{\leftarrow e}\Gamma_{\leftarrow g}$. The expression for

the current is then

$$\begin{aligned} I_L =& e[(\Gamma_{L\leftarrow g} - \Gamma_{L\to e})P(g) - (\Gamma_{L\to e} + \Gamma_{L\to g})P(0) \\ &+ (\Gamma_{L\leftarrow e} - \Gamma_{L\to g})P(e) + (\Gamma_{L\leftarrow e} + \Gamma_{L\leftarrow g})P(2)]. \end{aligned} \tag{5.10}$$

Fig. 5.4 shows the 2D map of the current as a function of the left and right voltage drops eV_L and eV_R. In the three white regions the current is blocked, this corresponds in the upper right corner to the population $P(0) = 1$, the middle block to $P(g) = 1$ and the lower left corner to $P(2) = 1$. The light blue and light red region corresponds to the opening of a tunneling channel for the electrons, on the left through the excited state of the dot and on the right through the ground state. In the deep red and blue regions both channels are open [109].

Hence, we detect in the current the eigenstates of the Hamiltonian. The thresholds of the current corresponds to $eV_\alpha = E_\psi$ where ψ is an eigenstate of H_S.

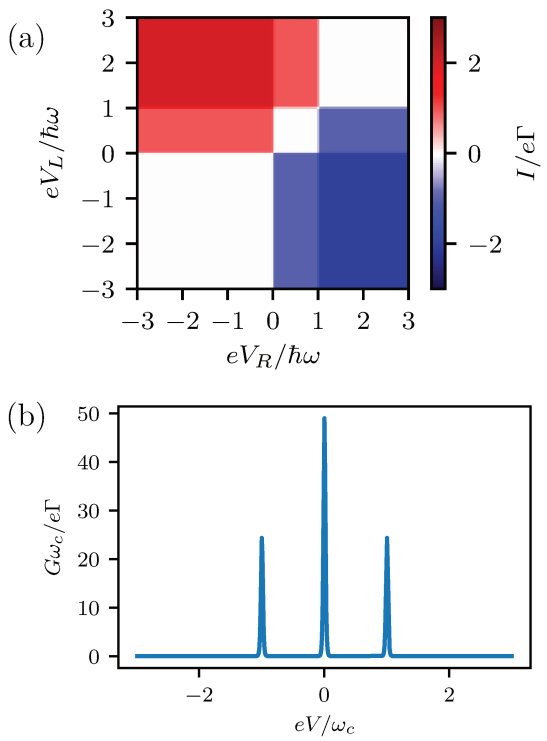

Figure 5.4: (a) Current through the dot as a function of the left and right voltage drops eV_L and eV_R at temperature $k_BT = 10^{-3}\omega_c$. (b) Conductance as a function of $eV_L = eV$ along the line $eV_L = -eV_R$ corresponding to a symmetrically biased junction. In both panels $\lambda = 0$.

We will see in the following how this simple picture is modified by the interaction with the photon cavity.

5.2.2 "Weak" coupling $\lambda < 0.45$

In section 5.1, we showed the eigenstates and eigenenergies of the Hamiltonian H_S. From these eigenstates, we can use the Fermi's golden rule with the interaction Hamiltonian H_{int} as a perturbation of H_S to find the rates for an electron tunneling from the leads to the dot [75, 86, 88, 111]

$$\begin{cases} \Gamma^{n}_{\alpha\rightarrow} = \Gamma_{\alpha g} f^{+}_{\alpha}(-\Lambda\sqrt{n}) \\ \Gamma^{n+}_{\alpha\rightarrow} = \Gamma_{\alpha e} f^{+}_{\alpha}(\omega_c - \Lambda\sqrt{n}) \\ \overline{\Gamma}^{n}_{\alpha\rightarrow} = \Gamma_{\alpha g} f^{+}_{\alpha}(\Lambda\sqrt{n}) \\ \overline{\Gamma}^{n+}_{\alpha\rightarrow} = \Gamma_{\alpha e} f^{+}_{\alpha}(\omega_c + \Lambda\sqrt{n}) \end{cases} \tag{5.11}$$

and the rates for an electron tunneling from the dot to the leads

$$\begin{cases} \overline{\Gamma}^{n+}_{\alpha\leftarrow} = \Gamma_{\alpha e} f^{-}_{\alpha}(\omega_c + \Lambda\sqrt{n}) \\ \overline{\Gamma}^{n}_{\alpha\leftarrow} = \Gamma_{\alpha g} f^{-}_{\alpha}(\Lambda\sqrt{n}) \\ \Gamma^{n+}_{\alpha\leftarrow} = \Gamma_{\alpha e} f^{-}_{\alpha}(\omega_c - \Lambda\sqrt{n}) \\ \Gamma^{n}_{\alpha\leftarrow} = \Gamma_{\alpha g} f^{-}_{\alpha}(-\Lambda\sqrt{n}) \end{cases} \tag{5.12}$$

We can start by comparing the two-electronic level case to the single–electronic level case for the rates. Indeed, in the case of a single–level dot, the tunneling rates couple any states of the cavity to one another, as long as the Franck–Condon overlap is not vanishing Eq. (3.58). However, in the two-level case in the weak coupling regime, the electronic tunneling is dominated by the coupling between states of the same excitation number. In our approximation this translates in having tunneling rates only between states of the same excitation number. This is easily seen from the fact that the tunneling rates between an initial state $|i\rangle$ and a final state $|f\rangle$ is proportional to $|\langle i|H_{int}|f\rangle|^2$, and that the tunneling Hamiltonian H_{int} is purely electronic. Therefore, a tunneling event can at most modify the number of photons by one. Intrinsically we can't have multiple photon emission or absorption for the two-level system for $\lambda < 0.45$.

Another striking difference is seen in the Fermi function's argument. In the case of a single level, the energy condition in the Fermi functions corresponded to the difference of photon number between the two states involved in the transition. Therefore, it was an integer multiple of the photon energy. In the case of the two-level dot, this energy difference depends on the coupling strength and on the square root of the number of photons. Thus, we expect that steps in the electronic current will appear at each $\Lambda\sqrt{n}$ or $\omega_c \pm \Lambda\sqrt{n}$ instead of each $n\omega_c$.

The rate equations read

$$\begin{cases} \dot{P}(|n,0\rangle) = P(|S_n\rangle)\Gamma^n_{\leftarrow} + P(|A_n\rangle)\overline{\Gamma}^n_{\leftarrow} + P(|S_{n+1}\rangle)\Gamma^{(n+1)+}_{\leftarrow} \\ \qquad + P(|A_{n+1}\rangle)\overline{\Gamma}^{(n+1)+}_{\leftarrow} - P(|n,0\rangle)(\Gamma^n_{\rightarrow} + \overline{\Gamma}^n_{\rightarrow} + \Gamma^{(n+1)+}_{\rightarrow} + \overline{\Gamma}^{(n+1)+}_{\rightarrow}) \\ \dot{P}(|S_n\rangle) = P(|n,0\rangle)\Gamma^n_{\rightarrow} + P(|n-1,0\rangle)\Gamma^{n+}_{\rightarrow} + P(|n-1,2\rangle)\overline{\Gamma}^n_{\leftarrow} \\ \qquad + P(|n,2\rangle)\overline{\Gamma}^{n+}_{\leftarrow} - P(|S_n\rangle)(\Gamma^n_{\leftarrow} + \overline{\Gamma}^n_{\rightarrow} + \Gamma^{n+}_{\leftarrow} + \overline{\Gamma}^{n+}_{\rightarrow}) \\ \dot{P}(|A_n\rangle) = P(|n,2\rangle)\Gamma^{n+}_{\leftarrow} + P(|n-1,2\rangle)\Gamma^n_{\leftarrow} + P(|n-1,0\rangle)\overline{\Gamma}^{n+}_{\rightarrow} \\ \qquad + P(|n,0\rangle)\overline{\Gamma}^n_{\rightarrow} - P(|A_n\rangle)(\Gamma^n_{\rightarrow} + \overline{\Gamma}^n_{\leftarrow} + \Gamma^{n+}_{\rightarrow} + \overline{\Gamma}^{n+}_{\leftarrow}) \\ \dot{P}(|n,2\rangle) = P(|A_n\rangle)\Gamma^{n+}_{\rightarrow} + P(|S_n\rangle)\overline{\Gamma}^{n+}_{\rightarrow} + P(|A_{n+1}\rangle)\Gamma^{(n+1)}_{\rightarrow} \\ \qquad + P(|S_{n+1}\rangle)\overline{\Gamma}^{(n+1)}_{\rightarrow} - P(|n,2\rangle)(\Gamma^{n+}_{\leftarrow} + \overline{\Gamma}^{n+}_{\leftarrow} + \Gamma^{(n+1)}_{\leftarrow} + \overline{\Gamma}^{(n+1)}_{\leftarrow}) \end{cases} \tag{5.13}$$

Here we don't take into account the damping of the cavity. From these equations we obtain for the tunneling current in the stationary regime:

$$\begin{aligned} I_{L\rightarrow} = & \sum_n \Big\{ P(|n,0\rangle)(\Gamma^n_{L\rightarrow} + \overline{\Gamma}^n_{L\rightarrow} + \Gamma^{(n+1)+}_{L\rightarrow} + \overline{\Gamma}^{(n+1)+}_{L\rightarrow}) \\ & + P(|S_n\rangle)(\overline{\Gamma}^{n+}_{L\rightarrow} + \overline{\Gamma}^n_{L\rightarrow}) + P(|A_n\rangle)(\Gamma^n_{L\rightarrow} + \Gamma^{n+}_{L\rightarrow}) \Big\} \\ I_{L\leftarrow} = & \sum_n \Big\{ P(|n,2\rangle)(\Gamma^{n+1}_{L\leftarrow} + \overline{\Gamma}^{n+1}_{L\leftarrow} + \Gamma^{n+}_{L\leftarrow} + \overline{\Gamma}^{n+}_{L\leftarrow}) \\ & + P(|A_n\rangle)(\overline{\Gamma}^{n+}_{L\leftarrow} + \overline{\Gamma}^n_{L\leftarrow}) + P(|S_n\rangle)(\Gamma^n_{L\leftarrow} + \Gamma^{n+}_{L\leftarrow}) \Big\}, \end{aligned} \tag{5.14}$$

where the net tunneling current I_L is

$$I_L = I_{L\rightarrow} - I_{L\leftarrow}. \tag{5.15}$$

Fig. 5.5 shows the electronic current as a function of the voltage drops.

As expected we see in the conductance the signature of the Rabi splitting in the splitting of the two peaks at $eV_\alpha = \omega_c$. This means that in an experiment, a two-level dot junction coupled to a cavity mode with only a dipolar coupling should exhibit the Rabi splitting in its conductance for a coupling $\lambda < 0.45$ and we predict light emission from the split states at $eV_\alpha = \omega_c \pm \Lambda$ [109, 112]. We see in the conductance a first pick at $eV_L = 0$ which corresponds to $\mu_L = \varepsilon_0$. This peak corresponds to electronic tunneling through the ground state $|S_0\rangle$. Then there is another pick at $eV_L = \Delta = \omega_c$ ($\mu_L = \varepsilon_0 + \Delta$) corresponding to electrons tunneling through the excited state while the ground state is already populated. In other words, this is a transition from $|S_0\rangle$ to $|0,2\rangle$. Those two kinds of tunneling events do not involve photon emission nor absorption. Close this last pick we discussed there are two side smaller picks, for $eV_L = \omega_c \pm \Lambda$. These picks correspond to transitions from the

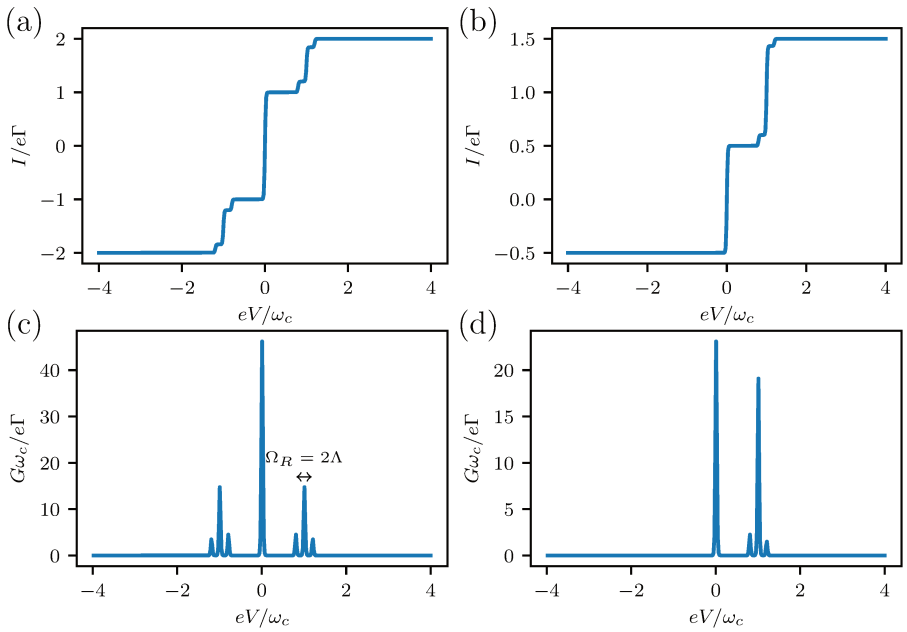

Figure 5.5: (a),(b) electronic current as a function of the voltage drop in a two-electronic level tunnel junction coupled to a cavity with dipolar coupling $\lambda = 0.2$ at $k_B T = 10^{-3}\omega_c$ and $\kappa = 0.1\omega_c$. (a) for a symmetrically biased junction $eV_L = -eV_R = eV$ and (b) for a right lead tuned to the dot's ground state, $eV_L = eV$ and $eV_R = 0$. (c) and (d) shows the corresponding conductance $G = dI/dV_L$.

unoccupied state of the molecule $|0,0\rangle$ to the states $|S_1\rangle$ and $|A_1\rangle$. Only these two transitions involve the emission of one photon in the cavity.

It is worth to note that in Fig. 5.5 panels (b) and (c) would be the closest to an actual experimental setup and in the conductance we see that the two main picks correspond to the energy of the eigenstates of the bare molecule at $eV_L = 0$ and $eV_L = \omega_c$ and do not involve photon emission.

In our approach using the rate equations, we neglect the broadening coming from the damping of the cavity. From the analysis we made on the electronic current in chapter 3 and the impact of the damping of the cavity on the electronic current, we expect that the broadening should be of the order of κ. Chikkaraddy et al. [29] were able to measure a coupling strength $\Lambda \sim 90meV$ in a plasmonic cavity with a resonance at $\omega_c = 2eV$. This means that $\lambda \sim 0.045$. Therefore as long as $\kappa/\omega_c < 0.045$, it should be possible to measure the side peaks in the conductance at $eV_\alpha = \omega_c \pm \Lambda$. Such a value of κ correspond to $Q \sim 22$ for the quality factor which is in the range known for plasmonic cavities (between $Q \sim 10$ and $Q \sim 100$). However, if the cavity has a very bad quality factor and considering the dipolar coupling should not exceed a few percent [29] only two peaks should be distinguished in the conductance corresponding the the states of the bare molecule. As we mentioned these peaks at $eV_\alpha = 0$ and $eV_\alpha = \omega_c$ do not account for photon emission. Hence when $\kappa > \Lambda$, we can't conclude on light emission in the cavity from the current–voltage characteristics. In this case it may be required to directly measure the light intensity in the cavity.

The full structure of the current characteristics is shown in Fig. 5.6. The electronic current is plotted as a function of the left and right bias voltage. We see three white regions where the current is totally blocked, the light blue and light red regions correspond to regions where electronic current goes only through one of the states $|0,g\rangle$ or $|0,2\rangle$ and finally the strong blue and red correspond to when both those states are involved.

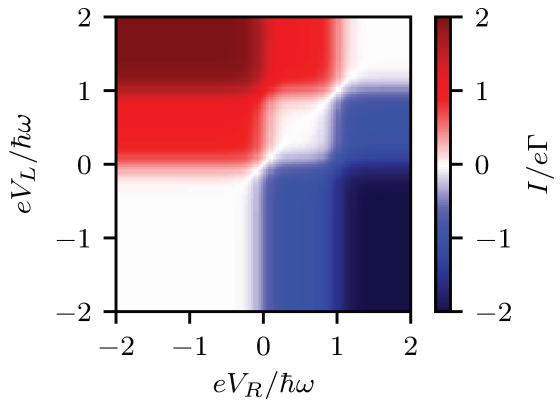

Figure 5.6: Current through the dot as a function of the left and right voltage drops eV_L and eV_R at temperature $k_BT = 10^{-1}\omega_c$ for a coupling strength $\lambda = 0.2$.

5.2.3 "Moderate" coupling $0.45 < \lambda < 1$

In the "moderate" coupling regime an analytical diagonalization of the Hamiltonian is not possible. Hence, we can only rely on the numerical calculation. We developed a python library to diagonalize the Hamiltonian, solve the master equations and compute the physical quantities such as the current and the light emission numerically for various scenarios. We then used this library in the case of a two-level dot junction coupled to a cavity to treat the case of the moderate coupling for the two–level system.

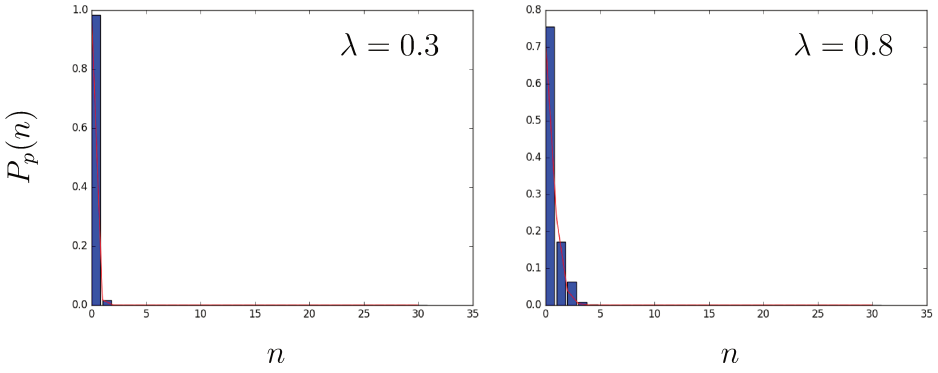

Figure 5.7: Photonic population in the cavity $P_p(n)$ for two different values of the coupling strength λ with n being the number of photons at $eV_\alpha = 0$, $k_B T = 10^{-3}\omega_c$ and $eV = 0$. The red curve shows a Poissonian distribution with expected value λ^2.

Fig. 5.7 shows the population of the cavity for two different values of the coupling strength λ at 0 bias voltage. It appears that, independently of the current, the cavity field is being heated with the increasing coupling strength. This corresponds to the bare cavity vacuum not being anymore an eigenstate of the Hamiltonian. We will develop more on that point in a following section.

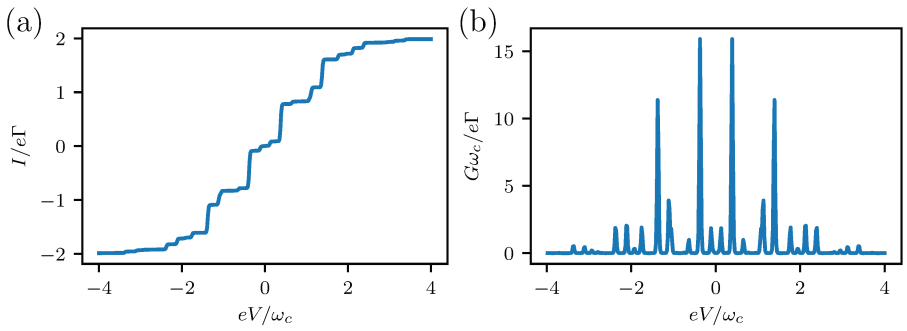

Figure 5.8: (a) electronic current as a function of the voltage drop in a two-electronic level tunnel junction coupled to a cavity with dipolar coupling $\lambda = 0.8$ at $k_BT = 10^{-3}\omega_c$ and $\kappa = 0.1\omega_c$. (a) for a symmetrically biased junction $eV_L = -eV_R = eV$. (b) shows the corresponding conductance $G = dI/dV_L$.

Fig. 5.8 shows the current and conductance in a symmetrically biased junction for a coupling strength $\lambda = 0.8\omega_c$. We see several peaks in the conductance and it becomes hard to predict the corresponding transitions [109]. However, it is noticeable that the peak initially at $eV_\alpha = 0$ is being split, which corresponds to a shift of the dot energy level ε_0 by the quantity $\lambda^2\omega_c$ as we predicted looking at Fig. 5.7.

5.2.4 Ultra strong coupling $\lambda > 1$

In the ultra strong coupling regime the coupling strength λ becomes larger than the photon energy and therefore larger than the gap between the two energy levels of the molecule. In this regime considering $\Lambda \gg \Delta$ we can try neglecting the dot energy levels and approximate the system Hamiltonian by

$$H_S = \omega_c a^\dagger a + \Lambda(a^\dagger + a)(d_e^\dagger d_g + d_g^\dagger d_e), \tag{5.16}$$

meaning that the molecule is only seen as a perturbation of the cavity field. This system Hamiltonian is equivalent to a charge interacting with the cavity mode since we can diagonalize the electronic part $d_e^\dagger d_g + d_g^\dagger d_e$ independently. We define

$$d_\pm^\dagger = \frac{d_e^\dagger \pm d_g^\dagger}{\sqrt{2}}. \tag{5.17}$$

Using Eq. (5.17) into Eq. (5.16), we find

$$H_S = \omega_c a^\dagger a + \Lambda(a^\dagger + a)(d_+^\dagger d_+ - d_-^\dagger d_-). \tag{5.18}$$

In this representation the Hamiltonian shows the interaction between two charges and the electric field of the cavity. Therefore, we expect a behaviour similar to two single–level dots coupled through their charge

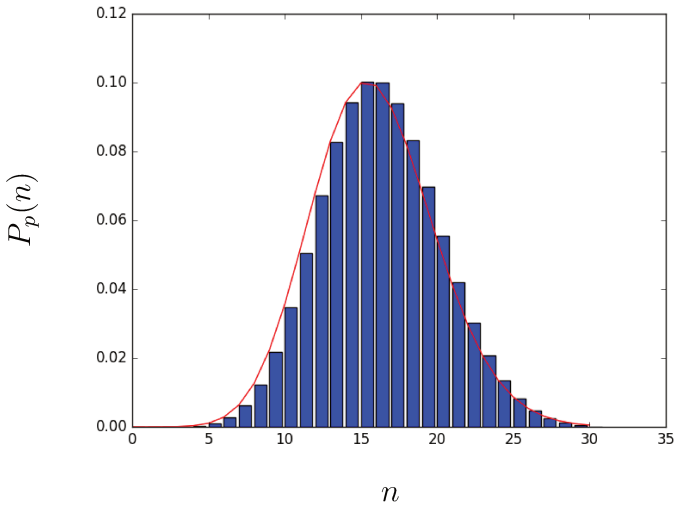

Figure 5.9: Photonic population in the cavity $P_p(n)$ with n being the number of photons at $eV_\alpha = 0$ at $k_BT = 10^{-3}\omega_c$ and $\lambda = 4$. The red curve shows a Poissonian distribution with expected value λ^2.

fluctuation to the cavity mode. Using the unitary transformation $U = e^{\lambda(a-a^\dagger)(d_+^\dagger d_+ - d_-^\dagger d_-)}$ we diagonalize H_S

$$\tilde{H}_S = U^\dagger H_S U = \omega_c a^\dagger a - \lambda^2\omega_c(d_+^\dagger d_+ - d_-^\dagger d_-)^2. \tag{5.19}$$

In turn this transformation also modifies the tunneling Hamiltonian

$$\begin{aligned}\tilde{H}_{int} = &\sum_{\alpha k} e^{\lambda(a^\dagger - a)(d_+^\dagger d_+ - d_-^\dagger d_-)} c_{\alpha k}^\dagger \left(\left(\frac{t_{\alpha kg} + t_{\alpha ke}}{\sqrt{2}} \right) d_+ + \left(\frac{t_{\alpha ke} - t_{\alpha kg}}{\sqrt{2}} \right) d_- \right) \\ &+ H.c.\end{aligned} \tag{5.20}$$

From Eq. (5.19), we see that the one-electron states have their energies shifted by $\lambda^2\omega_c$. The photon population can be deduced at $eV_\alpha = 0$ from $|\langle 0,0|i\rangle|^2$ where $|i\rangle$ is an eigenstate of H_S. This is equivalent to the expected value for a coherent state of the photon field with $|\alpha|^2 = \lambda^2$. Therefore, we predict that the photon population follows a Poissonian distribution with expected value λ^2. This prediction is confirmed in Fig. 5.9 where we plot the result of the full numerical calculation for the photonic population in the cavity at vanishing voltage drop. From the diagonalization of H_S, we can derive the tunneling rates between the eigenstates of H_S. The rates for an electron to tunnel from a lead to the dot are

$$\begin{cases} \Gamma_{n,n':\alpha}^{0\Pi_+} = \Gamma_+^\alpha |M_{n,n'}|^2 f_\alpha^+([n' - n - \lambda^2]\omega_c) \\ \Gamma_{n,n':\alpha}^{0\Pi_-} = \Gamma_-^\alpha |M_{n,n'}|^2 f_\alpha^+([n' - n - \lambda^2]\omega_c) \\ \Gamma_{n,n':\alpha}^{\Pi_+ 2} = \Gamma_-^\alpha |M_{n,n'}|^2 f_\alpha^+([n' - n - \lambda^2]\omega_c) \\ \Gamma_{n,n':\alpha}^{\Pi_- 2} = \Gamma_+^\alpha |M_{n,n'}|^2 f_\alpha^+([n' - n - \lambda^2]\omega_c). \end{cases} \tag{5.21}$$

While the tunnel rates from the dot to a lead are

$$\begin{cases} \Gamma^{\Pi_+ 0}_{n,n':\alpha} = \Gamma^{\alpha}_{+}|M_{n,n'}|^2 f^{-}_{\alpha}([n-n'-\lambda^2]\omega_c) \\ \Gamma^{\Pi_- 0}_{n,n':\alpha} = \Gamma^{\alpha}_{-}|M_{n,n'}|^2 f^{-}_{\alpha}([n-n'-\lambda^2]\omega_c) \\ \Gamma^{2\Pi_+}_{n,n':\alpha} = \Gamma^{\alpha}_{-}|M_{n,n'}|^2 f^{-}_{\alpha}([n-n'-\lambda^2]\omega_c) \\ \Gamma^{2\Pi_-}_{n,n':\alpha} = \Gamma^{\alpha}_{+}|M_{n,n'}|^2 f^{-}_{\alpha}([n-n'-\lambda^2]\omega_c). \end{cases} \tag{5.22}$$

Here $\Gamma^{AB}_{n,n':a}$ stands for the transition rate from state $|n, A\rangle$ to state $|n', B\rangle$ through lead a, n and n' being the photon numbers and A and B molecular states. $|\Pi_\pm\rangle = d^\dagger_\pm|0\rangle$.

$$M_{n_1,n_2} = [sgn(n_2-n_1)]^{n_1-n_2}\lambda^{N-n}e^{-\lambda^2/2}\sqrt{\frac{n!}{N!}}L^{N-n}_n(\lambda^2), \tag{5.23}$$

where $N = max\{n_1, n_2\}$, $N = min\{n_1, n_2\}$ and L^q_α is the generalized Laguerre polynomial and finally $\Gamma^\alpha_\pm = \pi\sum_k(t_{\alpha ke} \pm t_{\alpha kg})^2\delta(\varepsilon - \varepsilon_{\alpha k})$.

Our system behaves at high coupling as a two-level Franck–Condon system. Fig. 5.10 shows the current characteristic for the two-electronic level junction in the ultra strong coupling regime with $\lambda = 2.5$. We recover exactly the expected behaviour corresponding to the Franck–Condon physics from the energy shift $\lambda^2 = 6.25$ to the current suppression at low bias voltage and the quantization of the current. Of course one can notice some small side peaks in the conductance since it is not exactly a charge coupling and λ is not far from the photon energy.

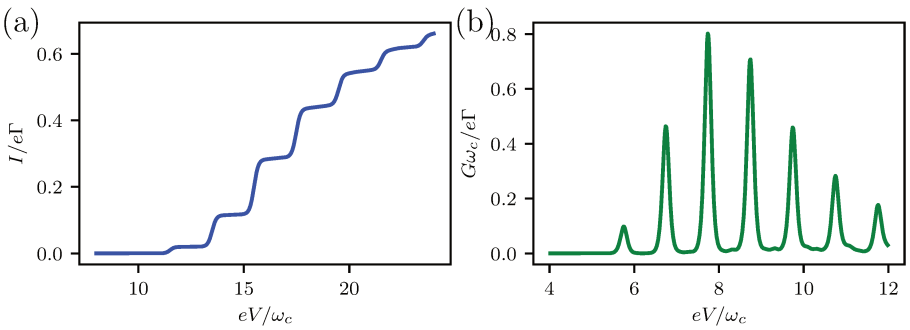

Figure 5.10: (a) electronic current as a function of the voltage drop in a two-electronic level tunnel junction coupled to a cavity with dipolar coupling $\lambda = 2.5$ at $k_BT = 5.10^{-3}\omega_c$ and $\kappa = 0$. (a) for a symmetrically biased junction $eV_L = -eV_R = eV$. (b) shows the corresponding conductance $G = dI/dV_L$.

5.3 Light emission

First of all we already noticed that the average number of photons in the cavity at $eV_L = eV_R = 0$ depends on the coupling strength. Indeed Fig. 5.11 shows the dependence of $\langle a^\dagger a\rangle$ with the coupling strength λ in this case. The average number of photons in the cavity is compared to

λ^2, shown by the dashed black curve. We separated Fig. 5.11 into three regions.

Region (a) corresponds to the weak coupling. The average number of photons is λ^2. This value of λ^2 is found from perturbation theory in the coupling λ. We call $V = \lambda\omega_c(a^\dagger + a)(d_g^\dagger d_e + d_g^\dagger d_e)$. The energies E of the perturbed system are given by

$$E = E_n + \langle n|V|n\rangle + \sum_{k\neq n} \frac{|\langle k|V|n\rangle|^2}{E_n - E_k} + ... \tag{5.24}$$

where $|n\rangle$ and $|k\rangle$ are eigenstates of the unperturbed Hamiltonian and E_n and E_k are their respective energies. Since V does not conserve the charge nor the photonic states, the first order term $\langle n|V|n\rangle$ vanishes. At $eV_L = eV_R = 0$ the only two states that should be populated are $|0,0\rangle$ and $|S_0\rangle = |g,0\rangle$ and only the latter is impacted by the coupling Hamiltonian V. At first order in λ we find

$$|\tilde{S}_0\rangle = |S_0\rangle - \frac{\Lambda}{\Delta + \omega_c}|e,1\rangle, \tag{5.25}$$

where $|\tilde{S}_0\rangle$ is the eigenstate of the perturbed Hamiltonian of energy ε_0. Thus the only two states possible for the system are $|0,0\rangle$ and $|\tilde{S}_0\rangle$. Then the average number of photons in the cavity is $\langle a^\dagger a\rangle = \left(\frac{\Lambda}{\omega_c+\Delta}\right)^2 P(|\tilde{S}_0\rangle)$.

Region (b) in Fig. 5.11 shows an intermediate regime in which the average number of photons deviates from λ^2. This region corresponds to the transition between the weak coupling and the strong coupling shown in region (c), where the system behaves like two single–level dot and the average number of photons is λ^2 as we predicted in the previous section due to the renormalization of the energies.

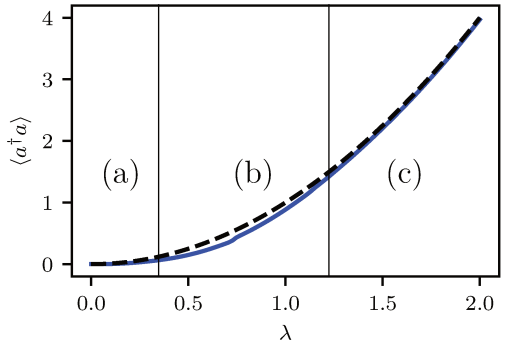

Figure 5.11: Average number of photons $\langle a^\dagger a\rangle$ at 0 voltage drop ($eV_L = eV_R = 0$) as a function of the coupling strength λ at $k_BT = 10^{-3}\omega_c$. The dashed black curve shows λ^2.

We are mostly interested in the small coupling regime in which $\lambda \ll 1$ since it is the most relevant case for experiments. Fig. 5.12 shows the average number of photons in the cavity as a function of the left and right voltage drops for three different values of the coupling strength. We see

that between $\lambda = 0.002$ and $\lambda = 0.02$ there is only an increase in $\langle a^\dagger a \rangle$ by a factor 10, but the structure remains the same.

We can see a large blue area where there are almost no photons in the cavity. In this region it seems than the electronic current does not affect the state of the cavity. This 2D maps can be compared to the map of the electronic current Fig. 5.6, we see that the red regions in Fig. 5.12 correspond to the strong blue and strong red regions in the electronic current map. Therefore, the light blue and light red regions have disappeared in Fig. 5.12.

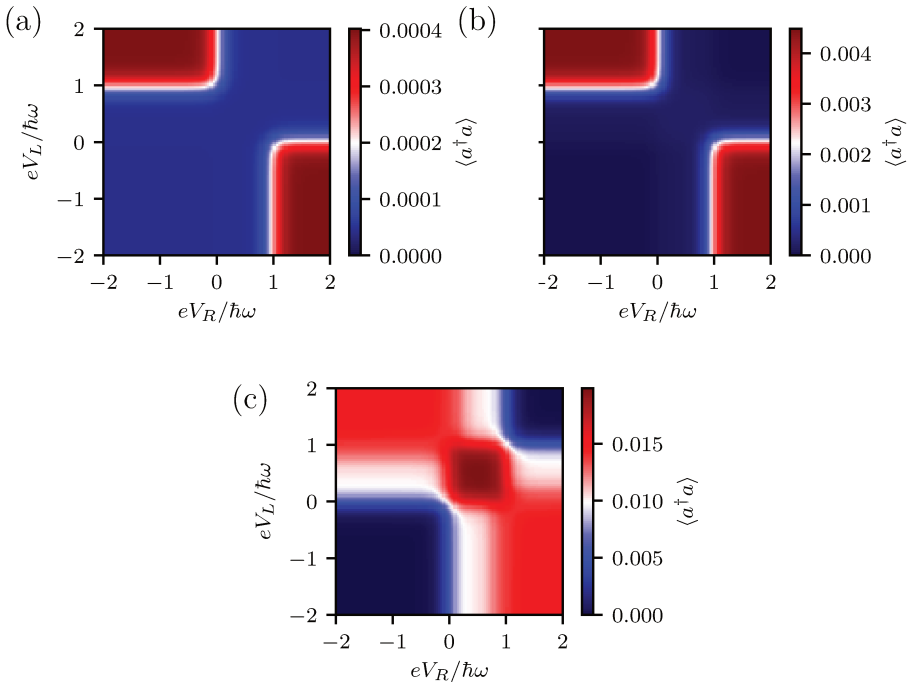

Figure 5.12: Average number of photons in the cavity $\langle a^\dagger a \rangle$ as a function of the left and right voltage drops $eV_{L/R}$ for three values of the coupling strength in the "weak" coupling regime (a) $\lambda = 0.002$, (b) $\lambda = 0.02$ and (c) $\lambda = 0.2$ in a strongly damped cavity $\kappa = 0.1\omega_c$ and weakly coupled tunnel junction $\Gamma_L = \Gamma_R = 10^{-3}\omega_c$ at temperature $k_B T = 10^{-1}\omega_c$.

First let us focus on the red regions in Fig. 5.12. The red regions are delimited by the energy thresholds corresponding to the transitions between states $|S_1\rangle$, $|A_1\rangle$ and $|0,0\rangle$. These transitions are responsible for the emission of a photon in the cavity. In fact half a photon on average at $eV = \omega_c \pm \Lambda$. With the states $|S_1\rangle$ and $|A_1\rangle$ being populated it also authorizes a bunch of other transitions between states $|S_1\rangle$ and $|A_1\rangle$ with states $|0,1\rangle$, $|2,0\rangle$ and $|2,1\rangle$. Among these transitions some correspond to emission and others to absorption. However, those transitions are less probable, since they are weighted by the population of the symmetric and anti-symmetric states which remains weak as Γ is very small and $\kappa \gg \Gamma$. Therefore, the average number of photons increases due to the population of states containing at least a photon.

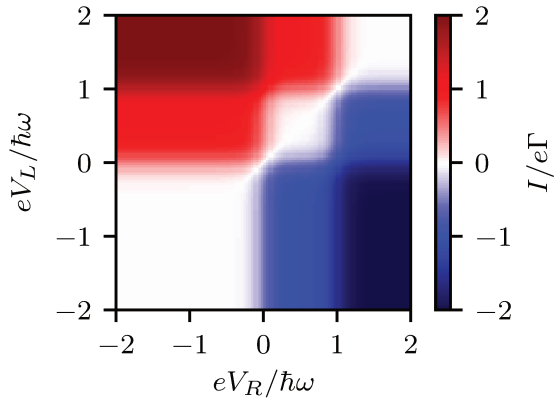

Figure 5.6: Current through the dot as a function of the left and right voltage drops eV_L and eV_R at temperature $k_BT = 10^{-1}\omega_c$ for a coupling strength $\lambda = 0.2$.

In the light red and light blue region in Fig. 5.6 we do not see any excitation of the cavity and $\langle a^\dagger a\rangle \simeq 0$. For $eV_R, eV_L < \omega_c - \Lambda$ the energy conservation condition on the voltage is not fulfilled to allow $|S_1\rangle$ and $|A_1\rangle$ to be populated. Therefore, the junction can't emit any photon.

For $eV_L > \omega_c - \Lambda$ and $eV_R < \omega_c - \Lambda$, the emission of photons is still suppressed, despite the fact that there are non vanishing transition rates that allow the population of $|S_1\rangle$ from $|0,0\rangle$. However, due to concurrent processes, the system can't populate $|S_1\rangle$ nor $|0,0\rangle$ in this window in the stationary regime. To show that, let us have a look on the electronic tunneling rates. For $\Lambda < eV_\alpha < \omega_c - \Lambda$ (dark red region in panel (c) Fig. 5.12) there is no transition in the gap between the two electrodes' potentials. The non-vanishing tunneling rates are $\Gamma^1_{L/R\rightarrow}$, $\bar{\Gamma}^1_{L/R\rightarrow}$, $\bar{\Gamma}^{1+}_{L/R\leftarrow}$, $\Gamma^{1+}_{L/R\leftarrow}$. In this case there is no current on average. The rate $\Gamma^1_{\rightarrow}$ corresponds to transitions from $|0,1\rangle$ to $|S_1\rangle$ and from $|A_1\rangle$ to $|2,0\rangle$ (during both these transitions on average $1/2$ photon is absorbed since $\langle X_1|a^\dagger a|X_1\rangle = 1/2$, with $X \in \{A,S\}$). $\bar{\Gamma}^1_{L/R\rightarrow}$ corresponds to transitions from $|0,1\rangle$ to $|A_1\rangle$ and from $|S_1\rangle$ to $|2,0\rangle$ (during both these transitions $1/2$ photon is absorbed on average). $\bar{\Gamma}^{1+}_{L/R\leftarrow}$ corresponds to transitions from $|2,1\rangle$ to $|S_1\rangle$ and from $|A_1\rangle$ to $|0,0\rangle$ (which involve the absorption of $1/2$ photon on average). Finally, $\Gamma^{1+}_{L/R\leftarrow}$ corresponds to transitions from $|S_1\rangle$ to $|0,0\rangle$ and from $|2,1\rangle$ to $|A_1\rangle$ (responsible for the absorption of $1/2$ photon on average).

Fig. 5.13 shows an oriented graph representing the tunneling processes for the states with 0 and 1 excitation. An arrow from state x to state y means that a rate for the transition from x to y is non zero. All other transitions involving states with higher numbers of excitation are represented by a dashed arrow going down since only transitions reducing the number of excitation are possible in the voltage range we are looking at. Therefore the upper part of the graph can be viewed as a source only (the upper part of the graph also connects the left and right graphs represented in Fig. 5.13).

From Fig. 5.13 only the state $|S_0\rangle$ should be significantly populated

in this case since it is at the extremity of any path in the two graphs. Therefore any random walker on the graphs ends at some point on $|S_0\rangle$ and can't leave. Hence in the stationary regime $P(|S_0\rangle) = 1$.

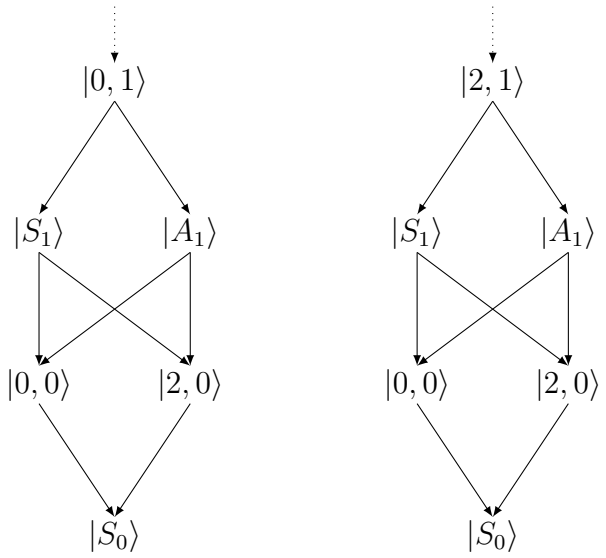

Figure 5.13: Graph of the transitions allowed for $\Lambda < eV_\alpha < \omega_c - \Lambda$ by electron tunneling.

Increasing V_L, for $\Lambda < eV_R < \omega_c - \Lambda$ and $eV_L > \omega_c - \Lambda$ (light red region in the upper left region in Fig. 5.6), the tunneling rates that are not vanishing are: $\Gamma^1_{L/R\rightarrow}$, $\overline{\Gamma}^1_{L/R\rightarrow}$, $\overline{\Gamma}^{1+}_{R\leftarrow}$, $\Gamma^{1+}_{R\leftarrow}$ and $\Gamma^{1+}_{L\rightarrow}$, $\overline{\Gamma}^{1+}_{L\rightarrow}$. $\Gamma^{1+}_{L\rightarrow}$ corresponds to transitions from $|0,0\rangle$ to $|S_1\rangle$ and from $|A_1\rangle$ to $|2,1\rangle$ (emission of $1/2$ photons). $\overline{\Gamma}^{1+}_{L\rightarrow}$ corresponds to transitions from $|0,0\rangle$ to $|A_1\rangle$ and from $|S_1\rangle$ to $|2,1\rangle$ (emission of $1/2$ photons).

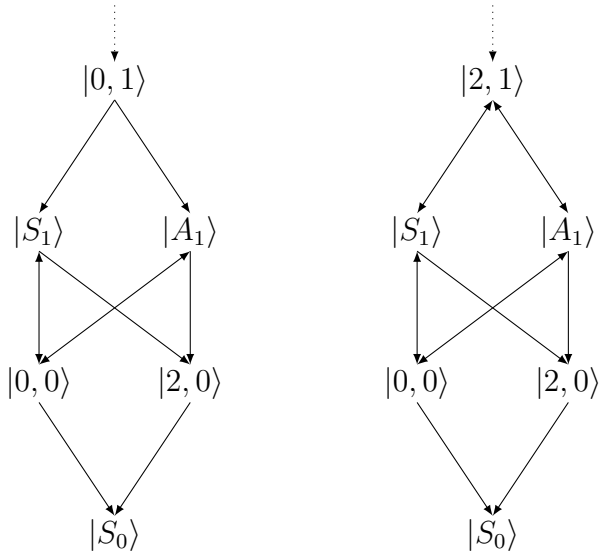

Figure 5.14: Graph of the transitions allowed for $\Lambda < eV_R < \omega_c - \Lambda$ and $\omega_c > eV_L > \omega_c - \Lambda$ by electron tunneling.

Even though more path are allowed compared to the previous regime

we explored ($\Lambda < eV_\alpha < \omega_c - \Lambda$), $|S_0\rangle$ is still the only possible end of any path in the graphs (see Fig. 5.14). Therefore, the stationary population can still only be $P(|S_0\rangle) = 1$ and $|S_0\rangle$ has no photon.

This remains true until one of the voltage drops reach ω_c, then electrons can go back and forth between $|S_0\rangle$ and $|2,0\rangle$ and the stationary population is distributed between those two states depending on the ratio Γ_{Le}/Γ_{Re} (see Fig. 5.15). Anyway none of these two states include a photon therefore the cavity is empty in this region.

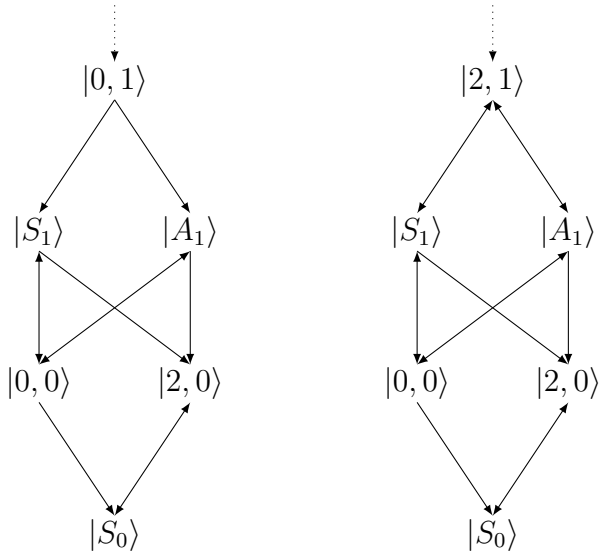

Figure 5.15: Graph of the transitions allowed for $\Lambda < eV_R < \omega_c - \Lambda$ and $\omega_c > eV_L > \omega_c - \Lambda$ by electron tunneling.

We conclude that in an experimental case, unless one of the electronic leads is tuned the energy of the ground state of the dot $|S_0\rangle$, we expect from our model, that the number of photons in the cavity should not be affected by the electronic current going through a two-electronic level quantum dot.

Now let's focus panel (c) in Fig. 5.12. As the coupling strength increases, the average number of photons in the cavity also increases in the region where electronic current is allowed, however we see that the top left and bottom right red regions of the 2D map are getting bigger as their thresholds are moved from $eV_\alpha = \omega_c - \Lambda$ to $eV_\alpha = -\Lambda$. Also, an island of large intensity appears around $eV_L = eV_R = 0$. In fact this Island corresponds to the highest light intensity in the cavity where light behave coherently from our prediction of $\langle a^\dagger a \rangle = \lambda^2$.

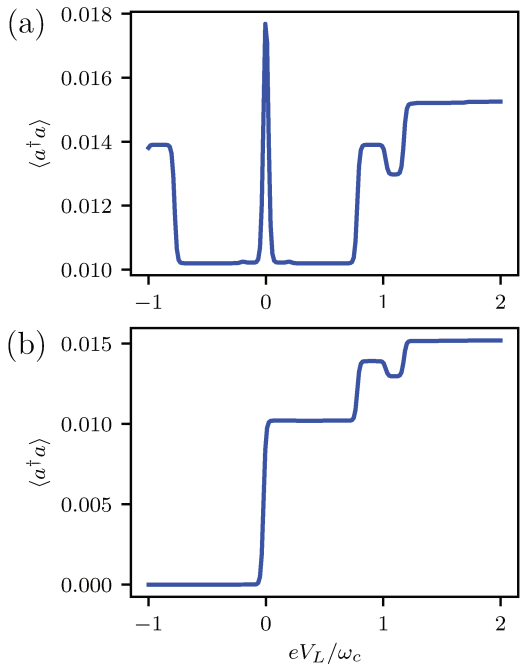

Figure 5.16: Average number of photons in the cavity $\langle a^\dagger a \rangle$ as a function of the left voltage drops eV_L for $\lambda = 0.2\omega_c$ in a strongly damped cavity $\kappa = 0.1\omega_c$ and weakly coupled tunnel junction $\Gamma_L = \Gamma_R = 10^{-3}\omega_c$ at room temperature $k_BT = 10^{-2}\omega_c$. Panel (a) shows the average number of photons for a symmetrically biased junction ($eV_L = -eV_R$) while panel (b) shows the average number of photons for $eV_R = -\omega_c$.

Fig. 5.16 shows a cut in Fig. 5.12 panel (c) along the line $eV_L = -eV_R$ in panel (a) corresponding to the symmetrically biased junction and along the line $eV_R = -\omega_c$. In the case of the symmetrically biased junction, we see that at 0 bias voltage the average number of photons is close to 0.02. Furthermore, as soon as the bias voltage deviates from 0 there is a sudden decrease of the average number of photons.

Using perturbation theory, we have already shown that the ground state of the molecule is modified by the interaction with the photons in the cavity. The ground state can be approximated by $|\tilde{S}_0\rangle = |S_0\rangle - \frac{\Lambda}{\Delta+\omega_c}|1, e\rangle$ giving the average number of photons $\langle a^\dagger a \rangle = \left(\frac{\Lambda}{\Delta+\omega_c}\right)^2 P(|\tilde{S}_0\rangle)$. At $eV = 0$, $P(|\tilde{S}_0\rangle) \simeq 1$ (see Fig. 5.13) while for $eV \gg k_BT$, $P(|\tilde{S}_0\rangle) \simeq 1/2$ leading to the decrease of $\langle a^\dagger a \rangle$.

The average number of photons then increases at the threshold $eV = \omega_c - \Lambda$ as the electrons can tunnel through the dot to populate the state $|S_1\rangle$. At the threshold $eV = \omega_c$ the average number of photons decreases due to the possibility for the electron to populate $|0, 2\rangle$ which decreases the number of photons in the cavity. Finally, the last threshold is at $eV = \omega_c + \Lambda$. At this threshold $|A_1\rangle$ can be populated from $|0, 0\rangle$ and $|S_1\rangle$ can be populated from $|2, 0\rangle$ increasing then the number of photons in the cavity.

In the case where the right voltage drop is tuned to $eV_R = -\omega_c$,

the cavity is in its ground state $|0,0\rangle$. As soon as $eV_L > 0$ the average number of photons in the cavity increases. So, while in the case of the symmetrically biased junction at $eV_R = eV_L = 0$, $P(|S_0\rangle) \simeq 1$, in the case shown in Fig. 5.16 panel (b), the system can't reach this value and the average number of photons is lower. However the plateau for $0 < eV_L < \omega_c - \Lambda$ is obtained in both cases. We then see the exact same structure in the two cases.

Hence, as the coupling strength grows, its effect on the ground state of the molecule $|S_0\rangle$ (in other words the HOMO) can greatly modify the emission spectrum. Indeed, not only $|S_1\rangle$ and $|A_1\rangle$ corresponds to light emission, but also $|S_0\rangle$ in this case.

Fig. 5.17 shows the second order correlation function of the field of the cavity corresponding to the same three cases shown in Fig. 5.16 [110]. We see that panel (a) and (b) of Fig. 5.17 and Fig. 5.16 have the same structure. In the regions where the electronic current does not affect the photonic population of the cavity, the cavity should remain in its thermal equilibrium. Therefore, the photons are bunched and $g^{(2)}(0) \geq 1$. But when the electronic current starts to affect the field of the cavity at the thresholds $eV = \omega_c - \Lambda$, the second order degree of coherence suddenly decreases. This can be understood from the fact that only single photon processes are involved, since only transitions between states $|n,0\rangle$ or $|n,2\rangle$ and $|S_{n\pm1}\rangle$ or $|A_{n\pm1}\rangle$ produce a photon exchange. Therefore on a time scale given by Γ at most one photon can be produced in the cavity. It then appears that anti-bunching is far more easier to obtain with two electronic levels than with one since there is no multi-photon process with a dipolar coupling assuming the system is not in the ultra-strong coupling regime. However panel (c) shows that when the coupling strength become high enough the anti-bunching is killed and the electronic current even produces strong bunching with $g^{(2)}(0) \sim 10$.

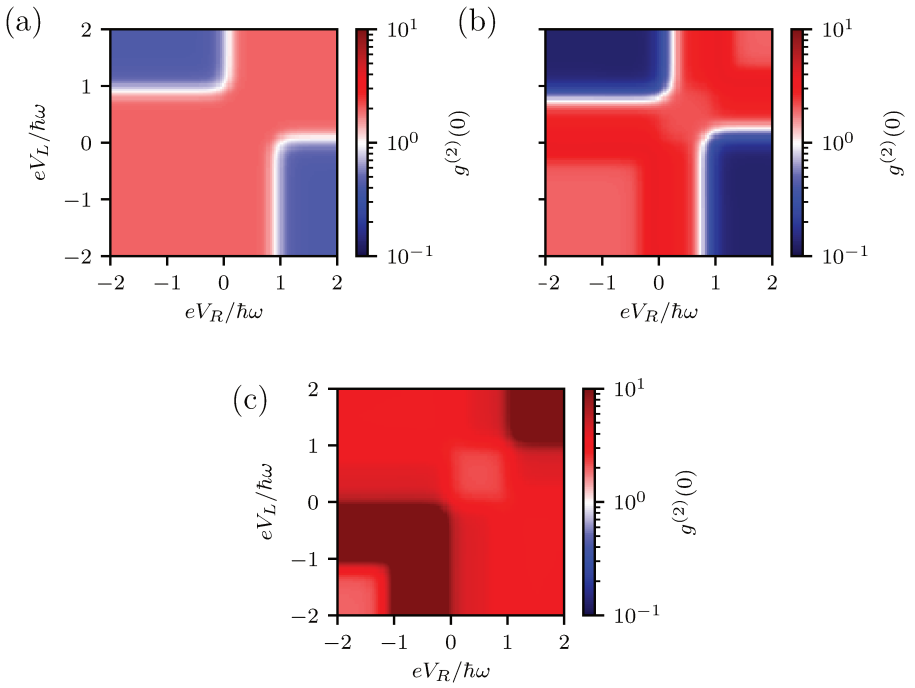

Figure 5.17: Degree of coherence $g^{(2)}(0)$ as a function of the left and right voltage drops $eV_{L/R}$ for three values of the coupling strength in the "weak" coupling regime (a) $\lambda = 0.002$, (b) $\lambda = 0.02$ and (c) $\lambda = 0.2$ in a strongly damped cavity $\kappa = 0.1\omega_c$ and weakly coupled tunnel junction $\Gamma_L = \Gamma_R = 10^{-3}\omega_c$ at temperature $k_B T = 10^{-1}\omega_c$.

Chapter 6

Conclusions

6.1 Summary

Electron-light coupling as long been studied in quantum optics and using microwave cavities. These kinds of experiments have shown the effect of the hybridization of the dipole of a molecule and the electric field of the cavity and the well known Rabi-splitting. However more recently physicists have tried to couple the electric field of the cavity to electronic transport as a way to control the light emitted from the molecule. In parallel, as microwave cavities are confined to single-molecule weak coupling and knowing that the coupling inversely scales with the volume of the cavity, physicists have designed plasmonic cavities at the nanoscale in which they hopped to observe the strong-coupling regime at the nanoscale. The mix of those two results is found in STM experiments where the STM act as a nanoplasmonic cavity and as the electronic leads of a nanocircuit.

This thesis proposes a theoretical framework for studying the coupling between electronic transport and the electric field in a cavity. Our results are applicable for nanoplasmonic cavities such as STM cavities as well as microwave cavities coupled to a nanocircuit. One major effect of the coupling between an electronic current is that not only the cavity electric field couples to the dipolar momentum of the molecule inside the cavity, but it also couples to the charge fluctuations on the molecule. This leads to a "monopolar" coupling that is similar to the coupling between phonons and electrons that has long been studied in molecular electronics. The electron–phonon coupling has been studied in the Franck–Condon physics. As in the experiments we are interested in, typically $\Gamma \ll k_B T$ and we were interested in studying the effect of the coupling strength on our model, we use a density matrix approach to solve our model in the sequential tunneling regime. This allows us to treat any regime of coupling however we are restricted to sequential tunneling of electrons and neglect any co-tunneling event. By first limiting the system to a single electronic level for the molecule in the junction, we show some specificity of that comes with the coupling the the charge fluctuations on the molecule and we clearly demonstrate the equivalence with the Franck–Condon physics. Hence we showed that the electronic current for a single level exhibits steps at each multiple of the photon en-

ergy that corresponds to the inelastic tunneling of the electrons leading to the emission or absorption of some photons in the cavity. Moreover we also incorporated the effect of a bosonic environment to our model as plasmonic cavities are known, due to their small size, to have small quality factors ($Q < 10^3$). Hence we developed a way to compute the current that take into account the broadening due to the large damping rate of the cavity. As we are interested in the photonic response of the cavity, our method does not require any assumption on the photons distribution in the cavity. As the electronic current shows photons are emitted in the cavity due to the electron tunneling, we show that the average number of photons in the cavity displays the exact same behaviour as the electronic current depending on the voltage that is imposed to the electronic leads. Then studying the photon correlation functions we show that the single electronic-level junction shows very unusual behaviour for the emitted light: Super-bunching at large voltage, where multi-photon emission is dominant. Anti-bunching at the first inelastic threshold where only one photon can be emitted in a single electron tunneling event. Of course the existence of the anti-bunching depends on the electron-photon coupling strength. We show that the condition of its existence is mainly found in the Franck–Condon overlap. That is the overlap between a wave function of the bare cavity mode and of the cavity mode displaced by Λ due to the coupling with an electron on the molecule. This overlap affects the photon-assisted electron tunneling rates and we were able to show that around $\lambda = \sqrt{2}$ the tunneling rate responsible for the emission of a second photon in the cavity is suppressed.

As mostly the two level system is studied in cavity quantum electrodynamics and it is viewed as the most probable cause of light emission in STM junctions, we then applied our model to the case of a two-level system with no "monopolar" coupling. In this case we showed that the hybridization between the molecule and the cavity electric field was measurable in the current even in plasmonic cavities. The signature of the hybridization is shown in the conductance where two side peaks appear around the peak that correspond to the tunneling through the second electronic level. These side peaks are separated in energy by the Rabi-frequency 2Λ where Λ is now the "dipolar" coupling. It is to be expected that to these two new peaks correspond light emission processes and this is shown in the light emission spectrum. It is interesting to emphasize that the monopolar and dipolar coupling are both responsible for light emission. However in the case of the monopolar coupling many transitions could result in light emission whereas for the dipolar coupling mainly two transitions are responsible for light emission. This comes from the fact that for the dipolar weak coupling regime, only single-electronic states can emit one photon in the cavity. The light $g^{(2)}$ correlation function shows that in the case of the dipolar coupling antibunching is seen as soon as the hybridized states are involved in the electronic transport as only single-photon emission is possible in this case. Thus antibunching is seen at weak coupling strength, which means that the design of a single-photon source should be easier using the dipolar coupling only

compared to the monopolar case. Interestingly as the dipolar coupling strength increases the model starts to deviate towards an equivalent of the monopolar coupling for two electronic levels and we lose the anti-bunching in the strong coupling regime.

6.2 Outlook

While we were able to answer some questions about the effect of the electronic transport on the light emission, a lot more remains to be done. One major addition we can do is to include both the monopolar and the dipolar coupling, and see what are the resulting current and photon statistics. From the experimental point of view, for the two-level system, they both are present.

For our work we developed a python library that we can use to study more complex Systems. We could take into account vibrational effects on the molecule, adding phonons in our model.

Another interesting case is the study of the super radiance in which the light emission is enhanced by the collective interaction of several identical molecules. Regarding the effect of the driving of the electric field on the electronic current, We only partially answered this question, studying the strong drive regime where the photons field becomes classical.

Finally on the method we used, it would be interesting to study the limitations of the Markov approximation that is no more valid for damping rates of the cavity $\kappa > k_B T$. The dynamics become non-Markovian and require a different approach.

Appendices

Appendix A

Numerical methods

As mentioned through the manuscript, a lot of results have been obtained numerically when analytical calculation was not possible. To this end we developed a python package named `cavity` implementing the various approached we used for our calculations. Our package is based on the use of the python libraries `numpy`, `scipy` and `netCDF4` for data storage. The package is build around four modules. The first module implements the Hamiltonians used through our work. It makes use of the package `secondquant` developed by T. Frederiksen, implementing general second quantization operators. The Hamiltonians are returned in matrix representation. Then the three other modules implement the rate equation approach, the full Liouvillian approach and the time-dependent approach used to solve section 3.8. The latter three modules have a similar implementation.

Algorithm 1: How to compute ρ_S.

Build the Hamiltonian of the system H_s;
From H_s build the Liouvillian Eq. (3.50) or its secular approximation Eq. (3.57) as a matrix;
Replace a line in L with the matrix representation of $\mathrm{Tr}(X)$;
Solve $L\rho = B$ where B ensures that $\mathrm{Tr}(\rho) = 1$;
Convert ρ into a matrix;
Result: Compute the density matrix ρ

In Algorithm 1, the reduced density matrix is computed from the Liouvillian operator. Once this is done, ρ can be used to compute any physical quantity $\langle O \rangle$. In the simplest case, corresponding to the Fermi golden rule approach, only the diagonal part of the density matrix is computed. Then any physical quantity can be computed.

Algorithm 2: How to compute $\langle O \rangle$ as a function of the voltage drops

Initialize a 2D voltage map $V = (V_L, V_R)$;
Initialize the matrix representation of O;
for μ_L, μ_R *in* V **do**
    Compute $\rho_S(\mu_L, \mu_R)$;
    Compute $\mathrm{Tr}(O\rho)$;
end
Result: Compute $\langle O \rangle$ as a function of voltage map V

Of course the calculation of the electronic current in the case of the full density matrix implementation is a little bit more complicated as we recollect the coherent evolution of the cavity mode. In this case Algorithm 2 still applies but we use Algorithm 3 instead of computing the trace in the for loop of Algorithm 2.

Algorithm 3: How to compute the electronic current taking into account the cavity damping

Initialize the Liouvillian Eq. (3.50);
Compute ρ;
Define a grid G;
for ω *in* G **do**
    Compute the current density $i(\omega)$ in frequency space;
end
Integrate the current density;
Result: Compute the electronic current

For the integration Algorithm 3 uses numpy function trapz. Finally the time dependence of an operator is computed using the Liouvillian operator L using exponential multiplication `expm_multiply` from scipy.

Algorithm 4: How to compute time dependent correlation functions

Result: Compute a time dependent correlation function
Initialize operators O_1 and O_2;
Initialize the Liouvillian;
Compute ρ as a matrix;
if $t \geq 0$ **then**
    Compute $v = O_2\rho$ as a vector;
    Compute $S =$ `expm_multiply`(Lt, v) as a matrix;
    Compute $\mathrm{Tr}(O_1 S)$;
end
else
    Hermitian transpose O_1 and O_2;
    Compute $v = O_1\rho$ as a vector;
    Compute $S =$ `expm_multiply(-Lt,v)` as a matrix;
    Compute $\mathrm{Tr}(O_2 S)^*$;
end

Algorithm 4 separates the case of positive and negative times as the formula used to holds only for positive times. To address negative time evolution one has to Hermition transpose the expression and makes the system evolves with $-\mathcal{L}$.

Bibliography

[1] A. W. Copeland, O. D. Black, and A. B. Garrett, "The photovoltaic effect.," *Chemical Reviews*, vol. 31, pp. 177–226, 08 1942.

[2] M. A. Fox and M. T. Dulay, "Heterogeneous photocatalysis," *Chemical reviews*, vol. 93, no. 1, pp. 341–357, 1993.

[3] R. Bohning and C. A. Burnside, "The effect of light intensity on rate of apparent photosynthesis in leaves of sun and shade plants," *American Journal of Botany*, pp. 557–561, 1956.

[4] H. J. Bailes and R. J. Lucas, "Melanopsin and inner retinal photoreception," *Cellular and Molecular Life Sciences*, vol. 67, no. 1, pp. 99–111, 2010.

[5] J. Yu, Y. Zheng, and J. Huang, "Towards high performance organic photovoltaic cells: A review of recent development in organic photovoltaics," *Polymers*, vol. 6, no. 9, pp. 2473–2509, 2014.

[6] H. Haken, "Laser theory," in *Light and Matter Ic/Licht und Materie Ic*, pp. 1–304, Springer, 1970.

[7] A. Einstein, "On a heuristic viewpoint of the creation and modification of light," *Ann. d. Phys*, vol. 17, pp. 133–148, 1905.

[8] Anonymous, "Proceedings of the american physical society," *Physical Review*, vol. 69, pp. 674–674, Jun 1946.

[9] G. Barton, "Quantum-electrodynamic level shifts between parallel mirrors: analysis," *Proceedings of the Royal Society of London. A. Mathematical and Physical Sciences*, vol. 410, no. 1838, pp. 141–174, 1987.

[10] E. A. Hinds and V. Sandoghdar, "Cavity qed level shifts of simple atoms," *Physical Review A*, vol. 43, pp. 398–403, Jan 1991.

[11] M. Brune, P. Nussenzveig, F. Schmidt-Kaler, F. Bernardot, A. Maali, J. M. Raimond, and S. Haroche, "From lamb shift to light shifts: Vacuum and subphoton cavity fields measured by atomic phase sensitive detection," *Physical Review Letters*, vol. 72, pp. 3339–3342, May 1994.

[12] D. J. Heinzen and M. Feld, "Vacuum radiative level shift and spontaneous-emission linewidth of an atom in an optical resonator," *Physical review letters*, vol. 59, no. 23, p. 2623, 1987.

[13] H. Walther, B. T. Varcoe, B.-G. Englert, and T. Becker, "Cavity quantum electrodynamics," *Reports on Progress in Physics*, vol. 69, no. 5, p. 1325, 2006.

[14] E. T. Jaynes and F. W. Cummings, "Comparison of quantum and semiclassical radiation theories with application to the beam maser," *Proc. IEEE*, vol. 51, pp. 89–109, Jan 1963.

[15] T. Stievater, X. Li, D. G. Steel, D. Gammon, D. Katzer, D. Park, C. Piermarocchi, and L. Sham, "Rabi oscillations of excitons in single quantum dots," *Physical Review Letters*, vol. 87, no. 13, p. 133603, 2001.

[16] H. Kamada, H. Gotoh, J. Temmyo, T. Takagahara, and H. Ando, "Exciton rabi oscillation in a single quantum dot," *Physical Review Letters*, vol. 87, no. 24, p. 246401, 2001.

[17] H. Htoon, T. Takagahara, D. Kulik, O. Baklenov, A. Holmes Jr, and C.-K. Shih, "Interplay of rabi oscillations and quantum interference in semiconductor quantum dots," *Physical review letters*, vol. 88, no. 8, p. 087401, 2002.

[18] J. M. Martinis, S. Nam, J. Aumentado, and C. Urbina, "Rabi oscillations in a large josephson-junction qubit," *Physical review letters*, vol. 89, no. 11, p. 117901, 2002.

[19] M. Gross and S. Haroche, "Superradiance: An essay on the theory of collective spontaneous emission," *Physics Reports*, vol. 93, no. 5, pp. 301 – 396, 1982.

[20] M. Brune, F. Schmidt-Kaler, A. Maali, J. Dreyer, E. Hagley, J. M. Raimond, and S. Haroche, "Quantum rabi oscillation: A direct test of field quantization in a cavity," *Physical Review Letters*, vol. 76, pp. 1800–1803, Mar 1996.

[21] E. Hagley, X. Maître, G. Nogues, C. Wunderlich, M. Brune, J. M. Raimond, and S. Haroche, "Generation of einstein-podolsky-rosen pairs of atoms," *Physical Review Letters*, vol. 79, pp. 1–5, Jul 1997.

[22] D. Meschede, H. Walther, and G. Müller, "One-atom maser," *Physical review letters*, vol. 54, no. 6, p. 551, 1985.

[23] S. Schiller and R. L. Byer, "High-resolution spectroscopy of whispering gallery modes in large dielectric spheres," *Opt. Lett.*, vol. 16, pp. 1138–1140, Aug 1991.

[24] A. Kiraz, P. Michler, C. Becher, B. Gayral, A. Imamoğlu, L. Zhang, E. Hu, W. V. Schoenfeld, and P. M. Petroff, "Cavity-quantum electrodynamics using a single inas quantum dot in a microdisk structure," *Applied Physics Letters*, vol. 78, no. 25, pp. 3932–3934, 2001.

[25] J. Joannopoulos, P. R. Villeneuve, and S. Fan, "Photonic crystals," *Solid State Communications*, vol. 102, no. 2, pp. 165 – 173, 1997. Highlights in Condensed Matter Physics and Materials Science.

[26] C. Böckler, S. Reitzenstein, C. Kistner, R. Debusmann, A. Löffler, T. Kida, S. Höfling, A. Forchel, L. Grenouillet, J. Claudon, and J. M. Gérard, "Electrically driven high-q quantum dot-micropillar cavities," *Applied Physics Letters*, vol. 92, no. 9, p. 091107, 2008.

[27] S. Reitzenstein, C. Hofmann, A. Gorbunov, M. Strauß, S. H. Kwon, C. Schneider, A. Löffler, S. Höfling, M. Kamp, and A. Forchel, "Alas/gaas micropillar cavities with quality factors exceeding 150.000," *Applied Physics Letters*, vol. 90, no. 25, p. 251109, 2007.

[28] T. L. van den Berg and P. Samuelsson, "Charge-photon transport statistics and short-time correlations in a single quantum dot–resonator system with an arbitrarily large coupling parameter," *Physical Review B*, vol. 100, p. 035408, Jul 2019.

[29] R. Chikkaraddy, B. de Nijs, F. Benz, S. J. Barrow, O. A. Scherman, E. Rosta, A. Demetriadou, P. Fox, O. Hess, and J. J. Baumberg, "Single-molecule strong coupling at room temperature in plasmonic nanocavities," *Nature*, vol. 535, p. 127, 06 2016.

[30] C. Hood, M. Chapman, T. Lynn, and H. Kimble, "Real-time cavity qed with single atoms," *Physical review letters*, vol. 80, no. 19, p. 4157, 1998.

[31] H. Mabuchi and A. Doherty, "Cavity quantum electrodynamics: coherence in context," *Science*, vol. 298, no. 5597, pp. 1372–1377, 2002.

[32] J. McKeever, A. Boca, A. D. Boozer, J. R. Buck, and H. J. Kimble, "Experimental realization of a one-atom laser in the regime of strong coupling," *Nature*, vol. 425, no. 6955, pp. 268–271, 2003.

[33] J. P. Reithmaier, G. Sęk, A. Löffler, C. Hofmann, S. Kuhn, S. Reitzenstein, L. Keldysh, V. Kulakovskii, T. Reinecke, and A. Forchel, "Strong coupling in a single quantum dot–semiconductor microcavity system," *Nature*, vol. 432, no. 7014, pp. 197–200, 2004.

[34] B. J. van Wees, H. van Houten, C. W. J. Beenakker, J. G. Williamson, L. P. Kouwenhoven, D. van der Marel, and C. T. Foxon, "Quantized conductance of point contacts in a two-dimensional electron gas," *Physical Review Letters*, vol. 60, pp. 848–850, Feb 1988.

[35] M. Büttiker, "Quantized transmission of a saddle-point constriction," *Physical Review B*, vol. 41, pp. 7906–7909, Apr 1990.

[36] J. Krans, J. Van Ruitenbeek, V. Fisun, I. Yanson, L. De Jongh, and J, "The signature of conductance quantization in metallic point contacts," *Nature*, vol. 375, no. 6534, pp. 767–769, 1995.

[37] S. J. Tans, M. H. Devoret, H. Dai, A. Thess, R. E. Smalley, L. Geerligs, and C. Dekker, "Individual single-wall carbon nanotubes as quantum wires," *Nature*, vol. 386, no. 6624, pp. 474–477, 1997.

[38] S. De Franceschi, J. Van Dam, E. Bakkers, L. Feiner, L. Gurevich, and L. P. Kouwenhoven, "Single-electron tunneling in inp nanowires," *Applied Physics Letters*, vol. 83, no. 2, pp. 344–346, 2003.

[39] D. L. Klein, R. Roth, A. K. Lim, A. P. Alivisatos, and P. L. McEuen, "A single-electron transistor made from a cadmium selenide nanocrystal," *Nature*, vol. 389, no. 6652, pp. 699–701, 1997.

[40] T. Oosterkamp, T. Fujisawa, W. Van Der Wiel, K. Ishibashi, R. Hijman, S. Tarucha, and L. P. Kouwenhoven, "Microwave spectroscopy of a quantum-dot molecule," *Nature*, vol. 395, no. 6705, pp. 873–876, 1998.

[41] M. R. Delbecq, V. Schmitt, F. D. Parmentier, N. Roch, J. J. Viennot, G. Fève, B. Huard, C. Mora, A. Cottet, and T. Kontos, "Coupling a quantum dot, Fermionic leads, and a microwave cavity on a chip," *Physical Review Letters*, vol. 107, p. 256804, Dec 2011.

[42] L. E. Bruhat, J. J. Viennot, M. C. Dartiailh, M. M. Desjardins, T. Kontos, and A. Cottet, "Cavity photons as a probe for charge relaxation resistance and photon emission in a quantum dot coupled to normal and superconducting continua," *Physical Review X*, vol. 6, p. 021014, May 2016.

[43] A. Cottet, M. C. Dartiailh, M. M. Desjardins, T. Cubaynes, L. C. Contamin, M. Delbecq, J. J. Viennot, L. E. Bruhat, B. Douçot, and T. Kontos, "Cavity QED with hybrid nanocircuits: From atomic-like physics to condensed matter phenomena," *J. Phys.: Condens. Matter*, vol. 29, p. 433002, 09 2017.

[44] L. E. Bruhat, T. Cubaynes, J. J. Viennot, M. C. Dartiailh, M. M. Desjardins, A. Cottet, and T. Kontos, "Circuit QED with a quantum-dot charge qubit dressed by Cooper pairs," *Physical Review B*, vol. 98, p. 155313, Oct 2018.

[45] T. Cubaynes, M. R. Delbecq, M. C. Dartiailh, R. Assouly, M. M. Desjardins, L. C. Contamin, L. E. Bruhat, Z. Leghtas, F. Mallet, A. Cottet, and T. Kontos, "Highly coherent spin states in carbon

nanotubes coupled to cavity photons," *npj Quantum Information*, vol. 5, no. 1, p. 47, 2019.

[46] X. Mi, J. V. Cady, D. M. Zajac, P. W. Deelman, and J. R. Petta, "Strong coupling of a single electron in silicon to a microwave photon," *Science*, vol. 355, no. 6321, pp. 156–158, 2017.

[47] X. Mi, J. V. Cady, D. M. Zajac, J. Stehlik, L. F. Edge, and J. R. Petta, "Circuit quantum electrodynamics architecture for gate-defined quantum dots in silicon," *Appl. Phys. Lett.*, vol. 110, no. 4, p. 043502, 2017.

[48] A. Stockklauser, P. Scarlino, J. V. Koski, S. Gasparinetti, C. K. Andersen, C. Reichl, W. Wegscheider, T. Ihn, K. Ensslin, and A. Wallraff, "Strong coupling cavity QED with gate-defined double quantum dots enabled by a high impedance resonator," *Physical Review X*, vol. 7, p. 011030, Mar 2017.

[49] Y.-Y. Liu, K. D. Petersson, J. Stehlik, J. M. Taylor, and J. R. Petta, "Photon emission from a cavity-coupled double quantum dot," *Physical Review Letters*, vol. 113, p. 036801, Jul 2014.

[50] A. Wallraff, D. I. Schuster, A. Blais, L. Frunzio, R.-S. Huang, J. Majer, S. Kumar, S. M. Girvin, and R. J. Schoelkopf, "Strong coupling of a single photon to a superconducting qubit using circuit quantum electrodynamics," *Nature*, vol. 431, no. 7005, p. 162, 2004.

[51] C. Rolland, A. Peugeot, S. Dambach, M. Westig, B. Kubala, Y. Mukharsky, C. Altimiras, H. le Sueur, P. Joyez, D. Vion, P. Roche, D. Esteve, J. Ankerhold, and F. Portier, "Antibunched photons emitted by a dc-biased Josephson junction," *Physical Review Letters*, vol. 122, p. 186804, May 2019.

[52] A. Grimm, F. Blanchet, R. Albert, J. Leppäkangas, S. Jebari, D. Hazra, F. Gustavo, J.-L. Thomassin, E. Dupont-Ferrier, F. Portier, and M. Hofheinz, "Bright on-demand source of antibunched microwave photons based on inelastic Cooper pair tunneling," *Physical Review X*, vol. 9, p. 021016, Apr 2019.

[53] J. Gimzewski, J. Sass, R. Schlitter, and J. Schott, "Enhanced photon emission in scanning tunnelling microscopy," *EPL (Europhysics Letters)*, vol. 8, no. 5, p. 435, 1989.

[54] S. Enoch and N. Bonod, *Plasmonics: from basics to advanced topics*, vol. 167. Springer, 2012.

[55] A. E. Schlather, N. Large, A. S. Urban, P. Nordlander, and N. J. Halas, "Near-field mediated plexcitonic coupling and giant rabi splitting in individual metallic dimers," *Nano letters*, vol. 13, no. 7, pp. 3281–3286, 2013.

[56] G. Zengin, G. Johansson, P. Johansson, T. J. Antosiewicz, M. Käll, and T. Shegai, "Approaching the strong coupling limit in single plasmonic nanorods interacting with j-aggregates," *Scientific reports*, vol. 3, p. 3074, 2013.

[57] G. Zengin, M. Wersäll, S. Nilsson, T. J. Antosiewicz, M. Käll, and T. Shegai, "Realizing strong light-matter interactions between single-nanoparticle plasmons and molecular excitons at ambient conditions," *Physical review letters*, vol. 114, no. 15, p. 157401, 2015.

[58] K. Santhosh, O. Bitton, L. Chuntonov, and G. Haran, "Vacuum rabi splitting in a plasmonic cavity at the single quantum emitter limit," *Nature communications*, vol. 7, no. 1, pp. 1–5, 2016.

[59] R. Berndt, J. K. Gimzewski, and P. Johansson, "Inelastic tunneling excitation of tip-induced plasmon modes on noble-metal surfaces," *Physical Review Letters*, vol. 67, pp. 3796–3799, Dec. 1991.

[60] X. H. Qiu, G. V. Nazin, and W. Ho, "Vibrationally resolved fluorescence excited with submolecular precision," *Science*, vol. 299, p. 542, 2003.

[61] N. L. Schneider and R. Berndt, "Plasmonic excitation of light emission and absorption by porphyrine molecules in a scanning tunneling microscope," *Physical Review B*, vol. 86, p. 035445, July 2012.

[62] R. Zhang, Y. Zhang, Z. C. Dong, S. Jiang, C. Zhang, L. G. Chen, L. Zhang, Y. Liao, J. Aizpurua, Y. Luo, J. L. Yang, and J. G. Hou, "Chemical mapping of a single molecule by plasmon-enhanced Raman scattering," *Nature*, vol. 498, pp. 82–86, June 2013.

[63] G. Reecht, F. Scheurer, V. Speisser, Y. J. Dappe, F. Mathevet, and G. Schull, "Electroluminescence of a polythiophene molecular wire suspended between a metallic surface and the tip of a scanning tunneling microscope," *Physical Review Letters*, vol. 112, pp. 047403–, Jan. 2014.

[64] P. Merino, C. Große, A. Roslawska, K. Kuhnke, and K. Kern, "Exciton dynamics of c60-based single-photon emitters explored by hanbury brown-twiss scanning tunnelling microscopy," *Nat. Commun.*, vol. 6, p. 8461, Sept. 2015.

[65] Y. Zhang, Y. Luo, Y. Zhang, Y.-J. Yu, Y.-M. Kuang, L. Zhang, Q.-S. Meng, Y. Luo, J.-L. Yang, Z.-C. Dong, and J. G. Hou, "Visualizing coherent intermolecular dipole-dipole coupling in real space," *Nature*, vol. 531, pp. 623–627, Mar. 2016.

[66] L. Zhang, Y.-J. Yu, L.-G. Chen, Y. Luo, B. Yang, F.-F. Kong, G. Chen, Y. Zhang, Q. Zhang, Y. Luo, J.-L. Yang, Z.-C. Dong, and J. G. Hou, "Electrically driven single-photon emission from an isolated single molecule," *Nat. Commun.*, vol. 8, p. 580, Sept. 2017.

[67] H. Imada, K. Miwa, M. Imai-Imada, S. Kawahara, K. Kimura, and Y. Kim, "Single-molecule investigation of energy dynamics in a coupled plasmon-exciton system," *Physical Review Letters*, vol. 119, p. 013901, Jul 2017.

[68] B. Doppagne, M. C. Chong, H. Bulou, A. Boeglin, F. Scheurer, and G. Schull, "Electrofluorochromism at the single-molecule level," *Science*, vol. 361, no. 6399, pp. 251–255, 2018.

[69] M. C. Chong, N. Afshar-Imani, F. Scheurer, C. Cardoso, A. Ferretti, D. Prezzi, and G. Schull, "Bright electroluminescence from single graphene nanoribbon junctions," *Nano Lett.*, vol. 18, pp. 175–181, Jan. 2018.

[70] T. Neuman, R. Esteban, D. Casanova, F. J. Garcia-Vidal, and J. Aizpurua, "Coupling of molecular emitters and plasmonic cavities beyond the point-dipole approximation," *Nano Lett.*, vol. 18, no. 4, pp. 2358–2364, 2018.

[71] H. Imada, K. Miwa, M. Imai-Imada, S. Kawahara, K. Kimura, and Y. Kim, "Single-molecule investigation of energy dynamics in a coupled plasmon-exciton system," *Physical Review Letters*, vol. 119, p. 013901, Jul 2017.

[72] L. Zhang, Y.-J. Yu, L.-G. Chen, Y. Luo, B. Yang, F.-F. Kong, G. Chen, Y. Zhang, Q. Zhang, Y. Luo, *et al.*, "Electrically driven single-photon emission from an isolated single molecule," *Nature communications*, vol. 8, no. 1, pp. 1–7, 2017.

[73] C. C. Leon, O. Gunnarsson, D. G. de Oteyza, A. Rosławska, P. Merino, A. Grewal, K. Kuhnke, and K. Kern, "Single photon emission from a plasmonic light source driven by a local field-induced coulomb blockade," *arXiv:1909.08117*, 2019.

[74] D. Hagenmüller, S. Schütz, J. Schachenmayer, C. Genes, and G. Pupillo, "Cavity-assisted mesoscopic transport of Fermions: Coherent and dissipative dynamics," *Physical Review B*, vol. 97, p. 205303, May 2018.

[75] D. Hagenmüller, J. Schachenmayer, S. Schütz, C. Genes, and G. Pupillo, "Cavity-enhanced transport of charge," *Physical Review Letters*, vol. 119, p. 223601, Nov 2017.

[76] P. Goy, J. M. Raimond, M. Gross, and S. Haroche, "Observation of cavity-enhanced single-atom spontaneous emission," *Physical Review Letters*, vol. 50, pp. 1903–1906, Jun 1983.

[77] B. W. Shore and P. L. Knight, "The jaynes-cummings model," *Journal of Modern Optics*, vol. 40, no. 7, pp. 1195–1238, 1993.

[78] J. K. Gimzewski, J. K. Sass, R. R. Schlitter, and J. Schott, "Enhanced photon emission in scanning tunnelling microscopy," *Europhysics Letters (EPL)*, vol. 8, pp. 435–440, mar 1989.

[79] Y. Uehara, Y. Kimura, S. Ushioda, and K. Takeuchi, "Theory of visible light emission from scanning tunneling microscope," *Japanese journal of applied physics*, vol. 31, no. 8R, p. 2465, 1992.

[80] K. Kaasbjerg and A. Nitzan, "Theory of light emission from quantum noise in plasmonic contacts: Above-threshold emission from higher-order electron-plasmon scattering," *Physical Review Letters*, vol. 114, p. 126803, Mar 2015.

[81] F. Xu, C. Holmqvist, G. Rastelli, and W. Belzig, "Dynamical coulomb blockade theory of plasmon-mediated light emission from a tunnel junction," *Physical Review B*, vol. 94, p. 245111, Dec 2016.

[82] J. Liu and D. Segal, "Generalized input-output method to quantum transport junctions. ii. applications," *Phys. Rev. B*, vol. 101, p. 155407, Apr 2020.

[83] A. Cottet, T. Kontos, and B. Douçot, "Electron-photon coupling in mesoscopic quantum electrodynamics," *Physical Review B*, vol. 91, p. 205417, May 2015.

[84] J. R. Schrieffer, "Theory of electron tunneling," *Rev. Mod. Phys.*, vol. 36, pp. 200–204, Jan 1964.

[85] T. Neuman and J. Aizpurua, "Origin of the asymmetric light emission from molecular exciton–polaritons," *Optica*, vol. 5, pp. 1247–1255, Oct 2018.

[86] J. Koch, F. von Oppen, and A. V. Andreev, "Theory of the Franck–Condon blockade regime," *Physical Review B*, vol. 74, p. 205438, Nov 2006.

[87] R. Leturcq, C. Stampfer, K. Inderbitzin, L. Durrer, C. Hierold, E. Mariani, M. G. Schultz, F. von Oppen, and K. Ensslin, "Franck–Condon blockade in suspended carbon nanotube quantum dots," *Nat. Phys.*, vol. 5, p. 327, 04 2009.

[88] J. Koch and F. von Oppen, "Franck–Condon blockade and giant Fano factors in transport through single molecules," *Physical Review Letters*, vol. 94, no. 20, p. 206804, 2005.

[89] S. Braig and K. Flensberg, "Vibrational sidebands and dissipative tunneling in molecular transistors," *Physical Review B*, vol. 68, p. 205324, Nov 2003.

[90] B. Min, E. Ostby, V. Sorger, E. Ulin-Avila, L. Yang, X. Zhang, and K. Vahala, "High-q surface-plasmon-polariton whispering-gallery microcavity," *Nature*, vol. 457, no. 7228, pp. 455–458, 2009.

[91] D. A. Ryndyk *et al.*, "Theory of quantum transport at nanoscale," *Springer Series in Solid-State Sciences*, vol. 184, 2016.

[92] C. Cohen-Tannoudji, J. Dupont-Roc, and G. Grynberg, *Photons and Atoms: Introduction to Quantum Electrodynamics*. Wiley, 1989.

[93] Q. Schaeverbeke, R. Avriller, T. Frederiksen, and F. Pistolesi, "Single-photon emission mediated by single-electron tunneling in plasmonic nanojunctions," *Physical Review Letters*, vol. 123, p. 246601, Dec 2019.

[94] M. Lax, "Quantum noise. x. density-matrix treatment of field and population-difference fluctuations," *Phys. Rev.*, vol. 157, pp. 213–231, May 1967.

[95] C. Cohen-Tannoudji, J. Dupont-Roc, and G. Grynberg, *Atom-Photon Interactions: Basic Processes and Applications*. Wiley, 1998.

[96] C. Bruder and H. Schoeller, "Charging effects in ultrasmall quantum dots in the presence of time-varing fields," *Physical Review Letters*, vol. 72, pp. 1076–1079, Feb 1994.

[97] R. J. Glauber, "Coherent and incoherent states of the radiation field," *Physical Review*, vol. 131, pp. 2766–2788, Sep 1963.

[98] D. F. Walls and G. J. Milburn, *Quantum optics*. Springer Berlin, 2nd ed. ed., 2008.

[99] X. T. Zou and L. Mandel, "Photon-antibunching and sub-poissonian photon statistics," *Physical Review A*, vol. 41, pp. 475–476, Jan 1990.

[100] W. H. Louisell, *Quantum statistical properties of radiation*. Wiley, 1973.

[101] B. W. Shore and P. L. Knight, "The jaynes-cummings model," *Journal of Modern Optics*, vol. 40, no. 7, pp. 1195–1238, 1993.

[102] J. M. Fink, M. Göppl, M. Baur, R. Bianchetti, P. J. Leek, A. Blais, and A. Wallraff, "Climbing the jaynes–cummings ladder and observing its nonlinearity in a cavity qed system," *Nature*, vol. 454, no. 7202, pp. 315–318, 2008.

[103] E. K. Irish, "Generalized rotating-wave approximation for arbitrarily large coupling," *Physical Review Letters*, vol. 99, p. 173601, Oct 2007.

[104] J. Larson, "Dynamics of the jaynes–cummings and rabi models: old wine in new bottles," *Physica Scripta*, vol. 76, pp. 146–160, jul 2007.

[105] D. Zueco, G. M. Reuther, S. Kohler, and P. Hänggi, "Qubit-oscillator dynamics in the dispersive regime: Analytical theory beyond the rotating-wave approximation," *Physical Review A*, vol. 80, p. 033846, Sep 2009.

[106] S. Ashhab and F. Nori, "Qubit-oscillator systems in the ultrastrong-coupling regime and their potential for preparing nonclassical states," *Physical Review A*, vol. 81, p. 042311, Apr 2010.

[107] J. M. Fink, R. Bianchetti, M. Baur, M. Göppl, L. Steffen, S. Filipp, P. J. Leek, A. Blais, and A. Wallraff, "Dressed collective qubit states and the tavis-cummings model in circuit qed," *Phys. Rev. Lett.*, vol. 103, p. 083601, Aug 2009.

[108] T. Brandes, "Coherent and collective quantum optical effects in mesoscopic systems," *Physics Reports*, vol. 408, no. 5, pp. 315 – 474, 2005.

[109] W. G. van der Wiel, S. De Franceschi, J. M. Elzerman, T. Fujisawa, S. Tarucha, and L. P. Kouwenhoven, "Electron transport through double quantum dots," *Rev. Mod. Phys.*, vol. 75, pp. 1–22, Dec 2002.

[110] R. Sánchez, G. Platero, and T. Brandes, "Resonance fluorescence in transport through quantum dots: Noise properties," *Phys. Rev. Lett.*, vol. 98, p. 146805, Apr 2007.

[111] E. Orgiu, J. George, J. A. Hutchison, E. Devaux, J. F. Dayen, B. Doudin, F. Stellacci, C. Genet, J. Schachenmayer, C. Genes, G. Pupillo, P. Samorì, and T. W. Ebbesen, "Conductivity in organic semiconductors hybridized with the vacuum field," *Nat. Mater.*, vol. 14, p. 1123, 09 2015.

[112] M. Galperin and A. Nitzan, "Current-Induced Light Emission and Light-Induced Current in Molecular-Tunneling Junctions," *Physical Review Letters*, vol. 95, p. 206802, Nov. 2005.